



Norwegian University  
of Life Sciences

Master's Thesis 2017 30 ECTS  
Faculty of Science and Technology

# **Assessment of overstrength factor for seismic design of cross laminated timber structures: research and experimental investigation**

Dag Pasquale Pasca  
Structural Engineering and Architecture

## ABSTRACT

In the perspective of seismic engineering the adoption of Capacity Design principles requires that ductile failure mechanism take place before the failure of brittle members. This work investigates the causes and implications of the hidden reserve of strength that could compromise this behaviour for Cross Laminated Timber structures.

In the first chapter an introduction to the basic concepts behind Capacity Design philosophy and how these apply to timber buildings is presented. Furthermore, an overview on how the Capacity Design principles are treated by the building codes of Europe, Canada and New Zealand is presented and discussed.

In the second chapter, the methods and results on how the overstrength factor has been so far calculated in the literature for timber building are reported and discussed. A comparison has also been made between the techniques used to evaluate the overstrength factor for other common building materials and timber.

The third chapter treats the planning and the execution of the experimental tests performed in the university's laboratory. After a description of the material, equipment and methods used for the tests, the outcomes of the investigation are presented and discussed.

Finally, in the concluding chapter the implications of the results are critically discussed and a suggestion on how to assume the overstrength factor is presented. Moreover, some suggestion on how future research could further investigate the matter are also given.



## ACKNOWLEDGEMENTS

I wish to express my gratitude to professor Roberto Tomasi for giving me the opportunity to widen my knowledge of wooden structures and for his precious suggestions and tutoring during the preparation of this work.

This work has been carried out in collaboration with the exchange student Mariano Fiorencis from the University of Trento, to whom goes a special thanks for the shared experience and the profitable cooperation.

Many thanks to Rothoblaas for providing much of the equipment needed for the experimental testing and to the staff at NMBU for their technical support.

Finally I am extremely grateful to my loving parents, who have unceasingly encouraged my studies and supported me both with moral and financial backing, and to my family in Norway, who always make me feel at home, despite the thousands of miles that separate me from Florence, the city where I was born.



# CONTENTS

<b>1 INTRODUCTION.....</b>	<b>15</b>
1.1 INTRODUCTION TO CAPACITY DESIGN AND OVERSTRENGTH .....	17
1.2 DESIGN OF EARTHQUAKE RESISTANT TIMBER STRUCTURES .....	20
1.2.1 Ductility.....	20
1.2.2 Ductility in timber buildings .....	22
1.2.3 Behaviour Factor .....	23
1.2.4 Behaviour factor for timber buildings .....	25
1.3 SEISMIC REGULATORY FRAMEWORK FOR TIMBER STRUCTURES.....	27
1.3.1 Europe and EC8.....	27
1.3.2 Switzerland and SIA 265.....	30
1.3.3 New Zealand and NZS 3603/ NZS 3604.....	30
1.3.4 Canada and CSA O86.....	31
1.3.5 New version of chapter 8 of Eurocode 8 – draft of 01.02.2017.....	31
<b>2 OVERSTRENGTH.....</b>	<b>35</b>
2.1 RESERVE OF STRENGTH .....	36
2.2 OVERSTRENGTH FACTOR FOR OTHER STRUCTURAL MATERIALS .....	38
2.3 OVERSTRENGTH FACTOR FOR TIMBER STRUCTURES .....	41
<b>3 EXPERIMENTAL INVESTIGATION .....</b>	<b>53</b>
3.1 TESTS OVERVIEW .....	54
3.2 MATERIALS AND EQUIPMENT .....	56
3.2.1 Material gathering .....	56
3.2.2 CLT.....	57
3.2.3 Screws .....	61
3.2.4 Steel holding system.....	64
3.2.5 Testing machine .....	66
3.2.6 Displacement transducers.....	67
3.3 SPECIMEN SETUP .....	69
3.4 CONNECTION RESISTANCE .....	72
3.4.1 Minimum distances .....	72
3.4.2 Embedding strength and withdrawal capacity.....	74
3.4.3 Yielding moment of the fasteners .....	76
3.4.4 Fasteners shear resistance.....	77
3.4.5 Overall connection strength capacity .....	80

3.5 LOADING PROTOCOL .....	82
3.6 TEST RESULTS.....	84
3.6.1 <i>Data processing</i> .....	84
3.6.2 <i>Results</i> .....	87
3.6.3 <i>Discussion of the results</i> .....	100
<b>4 CONCLUSIONS .....</b>	<b>103</b>
<b>5 REFERENCES.....</b>	<b>105</b>

## LIST OF TABLES

TABLE 1: DENSITY 120MM PANELS. ....	58
TABLE 2: DENSITY 100MM PANELS. ....	59
TABLE 3: DENSITY 80MM PANELS. ....	60
TABLE 4: VGZ SCREWS GEOMETRICAL DATA. ....	62
TABLE 5: WT SCREWS GEOMETRICAL DATA. ....	63
TABLE 6: SCREWS SPECIFICATIONS. ....	70
TABLE 7: MINIMUM DISTANCES. ....	72
TABLE 8: MINIMUM DISTANCES FOR EACH FASTENER. ....	73
TABLE 9: EMBEDDING STRENGTH ....	75
TABLE 10: WITHDRAWAL CAPACITY. ....	76
TABLE 11: FASTENERS YELDING MOMENT. ....	77
TABLE 12: VGZ7-80 AND VGZ7-100 FAILURE MODES. ....	79
TABLE 13: VGZ7-120 AND VGZ9 FAILURE MODES. ....	79
TABLE 14: W6 AND W8 FAILURE MODES. ....	80
TABLE 15: CONNECTIONS RESISTANCE FINAL VALUES. ....	81
TABLE 16: V7-80 MECHANICAL PROPERTIES. ....	88
TABLE 17: V7-100 MECHANICAL PROPERTIES. ....	90
TABLE 18: V7-120 MECHANICAL PROPERTIES. ....	92
TABLE 19: V9 MECHANICAL PROPERTIES. ....	94
TABLE 20: W6 MECHANICAL PROPERTIES. ....	96
TABLE 21: W8 MECHANICAL PROPERTIES. ....	98
TABLE 22: OVERSTRENGTH FACTORS RESULTS. ....	99



# LIST OF FIGURES

FIGURE 1: THREE UNDAMAGED MODERN WOOD FRAME BUILDINGS (BACKGROUND) NEXT TO AN OLDER BUILDING (FOREGROUND) WHOSE GROUND FLOOR HAS COLLAPSED COMPLETELY.....	15
FIGURE 2: IMAGES FROM SHAKING TABLE TESTS PERFORMED IN JAPAN FOR THE SOFIE PROJECT. ....	16
FIGURE 3: CAPACITY DESIGN CONCEPT. ....	18
FIGURE 4: OVERSTRENGTH CONCEPT. ....	19
FIGURE 5: DUCTILITY AND ENERGY DISSIPATED THROUGH PLASTIC DEFORMATIONS. ....	21
FIGURE 6: DUCTILITY TYPES, FIGURE FROM (GIONCU V., 2000) <sup>8</sup> .....	22
FIGURE 7: LOAD-SLIP CURVE FROM EN12512. ....	23
FIGURE 8 ELASTIC AND DESIGN RESPONSE SPECTRA. ....	24
FIGURE 9: RELATIONSHIP BETWEEN BEHAVIOUR FACTOR Q, OVERSTRENGTH $\Omega$ AND INTRINSIC REDUCTION FACTOR $Q_0$ , FIGURE FROM (CECCOTTI ET AL, 2016) <sup>15</sup> . ....	25
FIGURE 10: PROCEDURES FOR Q-FACTOR EVALUATION.....	26
FIGURE 11: TABLE 8.1 FROM EN 1998-1 <sup>6</sup> . ....	29
FIGURE 12: TABLE 8.2 FROM NEW CHAPTER 8 OF EC8 DRAFT PROPOSAL.....	32
FIGURE 13: FACTORS INFLUENCING OVERSTRENGTH, FIGURE FROM (MITCHELL D. & PAULTRE P., 1994) <sup>24</sup> .....	36
FIGURE 14: STEEL STRUCTURE DETAIL TO ENSURE COLUMN AND JOINT OVERSTRENGTH. ....	38
FIGURE 15: CONCEPT OF OVERSTRENGTH. ....	41
FIGURE 16: OVERSTRENGTH VALUES FOR THE CONFIGURATIONS TESTED IN <sup>12</sup> . ....	42
FIGURE 17: CYCLIC TEST RESULTS FROM (FRAGIACOMO ET AL, 2011) <sup>32</sup> .....	43
FIGURE 18: OVERSTRENGTH VALUES FOR THE CONFIGURATIONS TESTED IN (FRAGIACOMO ET AL, 2011) <sup>32</sup> .....	43
FIGURE 19: OVERSTRENGTH VALUES FOR THE CONFIGURATIONS TESTED IN (GAVRIC ET AL, 2012) <sup>33</sup> .....	44

FIGURE 20: OVERSTRENGTH VALUES FOR THE CONFIGURATIONS TESTED IN (GAVRIC ET AL, 2015) <sup>34</sup> .....	45
FIGURE 21: OVERSTRENGTH VALUES FOR THE CONFIGURATIONS TESTED IN (GAVRIC ET AL, 2015) <sup>34</sup> .....	46
FIGURE 22: CONCEPT OF OVERSTRENGTH. ....	47
FIGURE 23: INPUT VARIABLES, FIGURE TAKEN FROM (BRÜHL ET AL, 2014) <sup>37</sup> .....	48
FIGURE 24: LIMIT STATE FUNCTION AND FAILURE LINE.....	48
FIGURE 25: FACTOR KCS FOR DIFFERENT RELIABILITY INDEX, FIGURE TAKEN FROM (BRÜHL ET AL, 2014) <sup>37</sup> .....	49
FIGURE 26: SEGMENTED SHEAR WALL. ....	54
FIGURE 27: POSSIBLE WAYS OF CONNECTING TWO ADJACENT PARALLEL PANELS.....	54
FIGURE 28: SPECIMEN SETUP AND LOADING DIRECTION.....	55
FIGURE 29: MAKING OF THE SPECIMENS. ....	56
FIGURE 30: CLT PANEL.....	57
FIGURE 31: WOODEN SPECIMENS. ....	57
FIGURE 32: 5 LAYERS, 120MM THICK SPECIMEN.....	58
FIGURE 33: 5 LAYERS, 100MM THICK SPECIMEN.....	59
FIGURE 34: 3 LAYERS, 80MM THICK SPECIMEN.....	60
FIGURE 35: SCREWS USED TO JOIN THE SPECIMENS. ....	61
FIGURE 36: VGZ SCREW DETAIL.....	62
FIGURE 37: VGZ SCREWS MECHANICAL CHARACTERISTICS.....	62
FIGURE 38: WT SCREW DETAIL.....	63
FIGURE 39: WT SCREW MECHANICAL CHARACTERISTICS.....	63
FIGURE 40: FRONT VIEW. ....	64
FIGURE 41: 3D VIEW AND EXPLODED VIEW. ....	65
FIGURE 42: STEEL PLATES DETAILS.....	65
FIGURE 43: TESTING MACHINE.....	66
FIGURE 44: DISPLACEMENT TRANSDUCERS DATA FROM PRODUCER.....	67

FIGURE 45: DISPLACEMENT TRANSDUCERS DATA FROM PRODUCER.....	67
FIGURE 46: VIEW OF THE TRANSDUCERS MOUNTED ON THE SPECIMEN. ....	68
FIGURE 47: SPECIMEN SET UP.....	69
FIGURE 48: READY MADE SPECIMEN. ....	70
FIGURE 49: A VIEW OF ALL CONFIGURATIONS.....	71
FIGURE 50: MINIMUM DISTANCES. ....	72
FIGURE 51: NARROW AND LATERAL FACES.....	73
FIGURE 52: DISTANCES BETWEEN THE SCREWS.....	74
FIGURE 53: T <sub>1</sub> AND T <sub>2</sub> DISTANCES.....	78
FIGURE 54: POSSIBLE FAILURE MODES ACCORDING TO JOHANSEN’S THEORY. ....	78
FIGURE 55: LOADING PROTOCOL, IMAGE FROM EN26891.....	82
FIGURE 56: DETAIL OF THE INITIAL PART OF THE LOADING PROTOCOL. ....	83
FIGURE 57: SCREENSHOT TAKEN FROM THE COMPUTER THAT CONTROLS THE TESTING MACHINE, WITH A DETAIL OF THE SCATTERING OF THE LOAD-SLIP CURVE. ....	84
FIGURE 58: A VIEW ON HOW THE MECHANICAL CHARACTERISTICS WAS CALCULATED. ...	85
FIGURE 59: IMAGE TAKEN FROM EN14358 THAT SHOWS HOW THE VALUES WERE CALCULATED .....	86
FIGURE 60: LOAD-SLIP CURVE FOR EACH CONFIGURATION. ....	87
FIGURE 61: OVERLAPPED LOAD-SLIP CURVES. ....	87
FIGURE 62: LOAD-SLIP CURVE FOR EACH CONFIGURATION. ....	89
FIGURE 63: OVERLAPPED LOAD-SLIP CURVES. ....	89
FIGURE 64: LOAD-SLIP CURVE FOR EACH CONFIGURATION. ....	91
FIGURE 65: OVERLAPPED LOAD-SLIP CURVES. ....	91
FIGURE 66: LOAD-SLIP CURVE FOR EACH CONFIGURATION. ....	93
FIGURE 67: OVERLAPPED LOAD-SLIP CURVES. ....	93
FIGURE 68: LOAD-SLIP CURVE FOR EACH CONFIGURATION. ....	95
FIGURE 69: OVERLAPPED LOAD-SLIP CURVES. ....	95

FIGURE 70: LOAD-SLIP CURVE FOR EACH CONFIGURATION. ....	97
FIGURE 71: OVERLAPPED LOAD-SLIP CURVES. ....	97
FIGURE 72: YIELDED SCREWS AFTER TESTING.....	100

## LIST OF ABBREVIATIONS AND ACRONYMS

CD	Capacity design
CLT	Cross laminated timber
COV	Covariance
d	Diameter of the fastener
D	Ductility ratio
DCL	Low ductility class
DCM	Medium ductility class
DCH	High ductility class
EC8	Eurocode 8
EC5	Eurocode 5
ETA	European Technical Approval document
$f_{ax,k}$	Characteristic withdrawal capacity
$f_{h,k}$	Characteristic embedding strength
F	Force
$F_y$	Yielding force
$F_{max}$	Maximum force
$F_u$	Ultimate force
$F_{v,Rk}$	Characteristic shear resistance
k	Stiffness
$k_{el}$	Elastic stiffness
$k_{pl}$	Plastic stiffness
$M_{y,Rk}$	Characteristic yielding moment of the fastener
OSF	Overstrength factor
q	Behaviour factor
R	Action reduction factor (behaviour factor North America)

$R_{0.05}$	5 <sup>th</sup> percentile resistance value
$R_{0.95}$	95 <sup>th</sup> percentile resistance value
$R_{b,Rd}$	Design resistance brittle element
$R_{d,Rd}$	Design resistance ductile element
SLS	Serviceability limit state
$t$	Penetration length
$u / v$	Displacement
$u_y / v_y$	Yielding displacement
$u_u / v_u$	Ultimate displacement
ULS	Ultimate limit state
$\beta$	Reliability index
$\gamma_{an}$	Overstrength difference model-experimental results
$\gamma_m$	Material safety factor
$\gamma_{Rd}$	Overstrength factor
$\gamma_{sc}$	Overstrength 95 <sup>th</sup> to 5 <sup>th</sup> percentile ratio
$\delta$	Displacement
$\delta_y$	Ultimate displacement
$\delta_u$	Yielding displacement
$\varepsilon$	Strain rate
$\varepsilon_u$	Ultimate strain rate
$\varepsilon_y$	Yielding strain rate
$\theta$	Rotation
$\mu$	Ductility ratio
$\rho$	Density
$\sigma$	Stress
$\sigma_y$	Yielding stress

$\sigma_u$	Ultimate stress
$\chi$	Curvature
$\Omega$	Over-strength / Over-design

# 1 INTRODUCTION

It is now internationally recognized that a well-designed and -manufactured timber building can provide high levels of seismic safety. This because, among other reason, wood is much lighter than other building materials. The forces acting on a building in case of earthquake are proportional to the mass of the building itself; this means that wooden constructions are subjected to lower seismic loads in comparison to other types of buildings. These statements are widely proven by the fact that wooden buildings have traditionally been very common in areas known for the high frequency of seismic phenomena as Japan and northern America, and responded very well under severe events like Northridge 1994 and Kobe 1995



**Figure 1: Three undamaged modern wood frame buildings (background) next to an older building (foreground) whose ground floor has collapsed completely.**



Furthermore, several research projects have been carried out in the last years to test the performance of the relatively new construction systems made by Cross Laminated Timber panels. Probably the most important has been the SOFIE (Sistema Costruttivo Fiemme) project<sup>1</sup>, where a joint research programme between CNR-IVALSA (Trees and Timber Institute – Italian National Research Council) and Building Research Institute and National Institute for Earth Science and Disaster Prevention (NIED) of Japan on the earthquake behaviour of multi-storey CLT buildings was undertaken. The project began with wall tests and pseudo-dynamic test on single panels<sup>2</sup>, continued with a shaking table test on a CLT-three story building<sup>3</sup> and was concluded in 2007 with an additional shaking table test on a CLT-seven story building<sup>4</sup>. The results were extremely positive and definitively showed the reliability and safety of this kind of building system even for mid-rise buildings in earthquake prone areas.

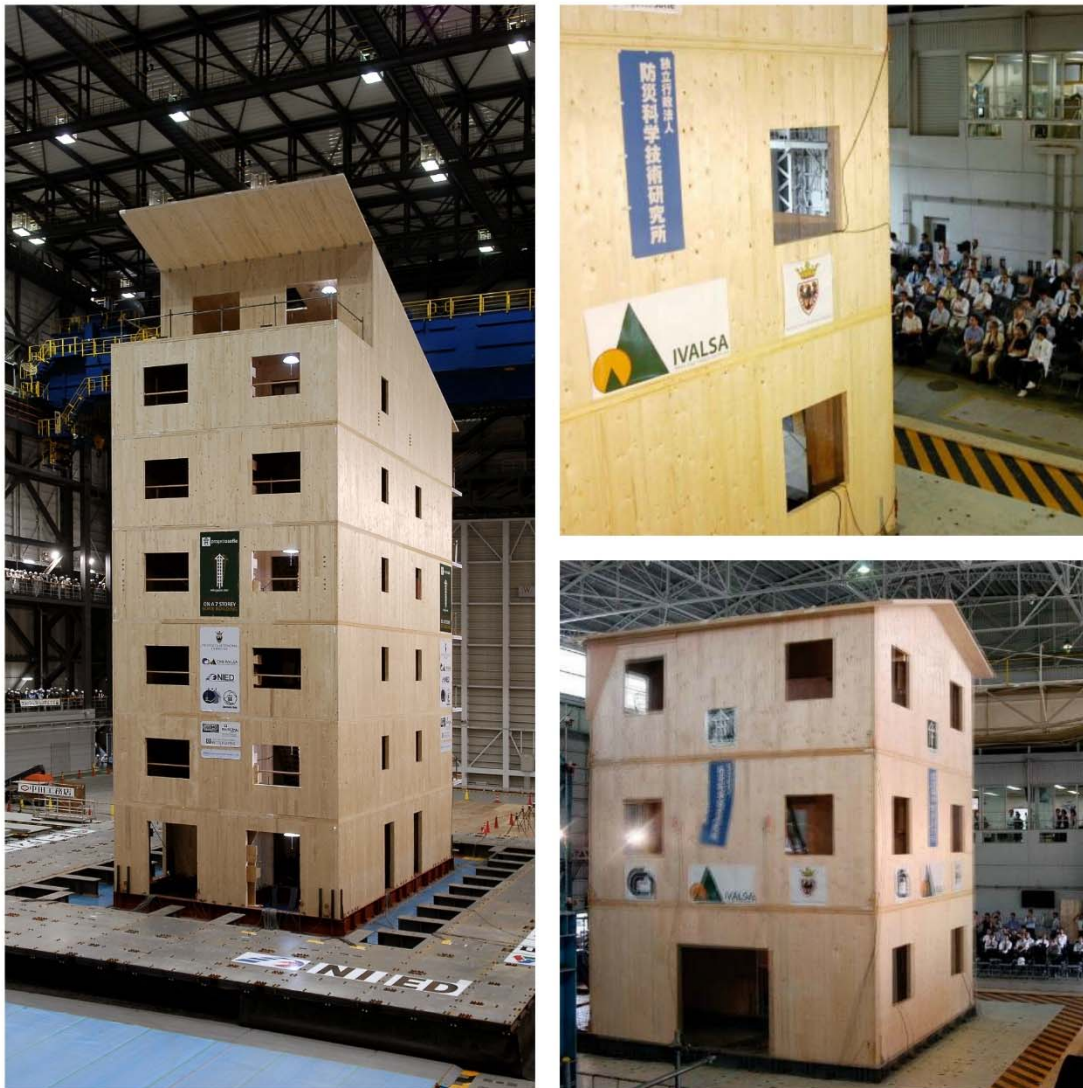


Figure 2: Images from shaking table tests performed in Japan for the SOFIE project.

## 1.1 Introduction to Capacity Design and Overstrength

The study of the catastrophic events caused by earthquakes have led to assert a fundamental concept in earthquake engineering: any structures must be able to dissipate the energy transmitted from earthquakes. This is the only viable way to avoid the recurrence of catastrophic events in terms of loss of human lives.

Structures designed according to recent seismic regulations possess resistance margins that allow them to withstand, accepting significant damage but preventing collapse, seismic loads of a level well above the design ones. These margins come substantially from the application, during the design phase, of principles that aim at obtaining a properly highly dissipative plasticization mechanism, e.g. Capacity Design.

This design procedure is a practical application of the more general concept of “Performance Based Design”. A building designed in this way is required to meet certain measurable or predictable performance requirements, in other word, instead of designing a building that could resist any load condition, one should try to maximize the overall response, getting the best results possible in terms of operativity of the building and occupant protection.

Capacity Design was developed in New Zealand during the nineteen seventies for the seismic design of reinforced concrete structures<sup>5</sup>, and is the most common way of ensuring a dissipative behaviour. The definition of CD according to Eurocode 8<sup>6</sup> is: *“design method in which elements of the structural system are chosen and suitably designed and detailed for energy dissipation under severe deformations while all other structural elements are provided with sufficient strength so that the chosen means of energy dissipation can be maintained”*.

A common way to explain the concept behind CD is the chain analogy (Figure 3): if we imagine having a chain made of several links, some brittle and some ductile, and apply a tension force to it, then the overall behaviour of the chain will be ductile (large deformation after yielding, and before failure) - if the resistance of the ductile links is lower than the resistance of the brittle links. Otherwise the behaviour of the chain will be brittle (sudden failure after yielding) - if the resistance of the brittle elements is lower than the ductile links. It is then obvious that the designer shall aim to obtain an overall ductile behaviour, by ensuring that the ductile failure mechanisms will activate before the brittle ones do.

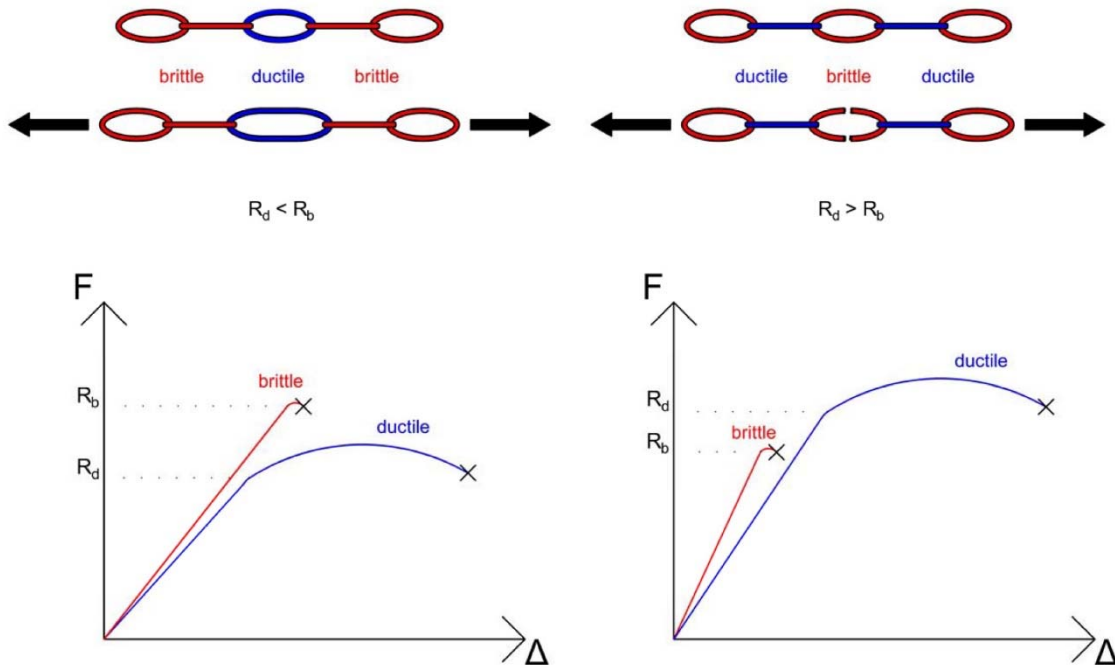


Figure 3: Capacity design concept.

The procedure aims to achieve a controlled damage by selecting proper lateral load resisting systems and proper detailing of individual members, and can be summarized as follows:

- A process in which it is decided which objects within a structural system will be permitted to yield (ductile components) and which objects will remain elastic (brittle components).
- Ductile components are designed with sufficient deformation capacity to withstand the earthquake impact.
- Brittle components are designed to achieve sufficient strength levels in comparison to the ductile ones.

This is ensured by the application of eq. (1):

$$R_{b,Rd} \geq \gamma_{Rd} \cdot R_{d,Rd} \quad (1)$$

Where  $R_{b,Rd}$  and  $R_{d,Rd}$  stand for the design resistance of the brittle and the ductile components respectively, whereas  $\gamma_{Rd}$  is the overstrength factor (OSF).

The overstrength factor represents the amount by which the actual strength of the element may exceed the design strength. It depends on several factors, among which one of the most important is the difference between the 5<sup>th</sup> percentile (characteristic) strength used for the design of the yielding components and the 95<sup>th</sup> percentile strength value which

could be present. Since in fact with the CD the resistance of the ductile element acts as a load on the brittle one, this difference needs to be considered, otherwise the resistance of the brittle element could be lower than the ductile one, resulting in a sudden collapse.

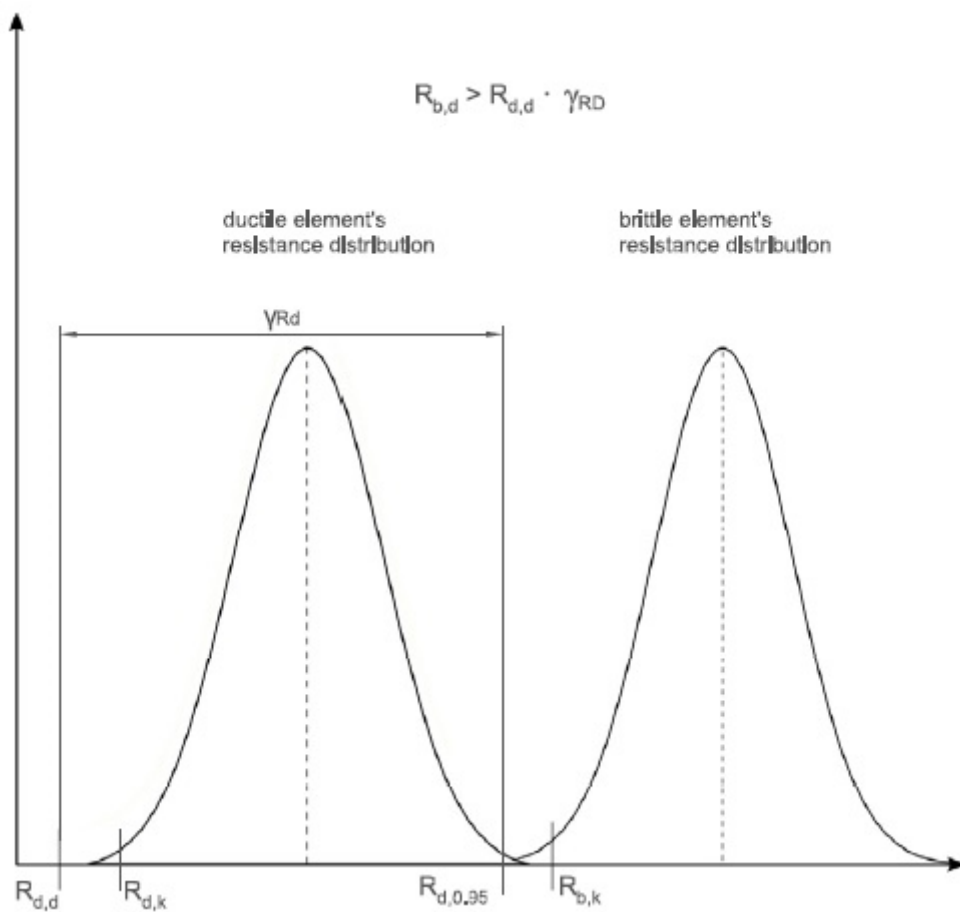


**Figure 4: Overstrength concept.**

## 1.2 Design of earthquake resistant Timber Structures

In EC8<sup>6</sup> the satisfaction of the Ultimate Limit State asks for the verification that the structural system have simultaneously lateral resistance and energy-dissipation capacity, so as to be able to survive design earthquakes without a complete collapse. The fulfilment of the no-collapse requirement does not require that the structure remains elastic under the design seismic action. On the contrary, it allows and accepts the development of significant inelastic deformations in the structural members, provided that the integrity of the structure is maintained. Even though EC8<sup>6</sup> opens for the possibility of using displacement-based approaches as alternative design methods, the reference method adopted is force-based. In reality, seismic actions correspond to the application of rapidly changing displacements at the base of the structures and not to the application of forces, but the use of force-based design is well established, since most of the other actions with which structural engineers have to deal, are forces acting on the structures. The basic concept is the possible trade-off between resistance and ductility that is at the base of the introduction of Ductility Classes, and the use of behaviour factors<sup>7</sup>. In this framework, to better understand the approach to a correct seismic design, the concept of ductility and the meaning of the behaviour factor will be briefly addressed.

### 1.2.1 Ductility

Ductility is a very important property in earthquake engineering and for the CD approach. At material level, it is the mechanical property of a solid, that indicates its ability to plastically deform before reaching failure, i.e. the capability of the material to get itself stretched beyond the elastic zone. Ductility is defined as the ratio of ultimate strain to yield strain of the material (Figure 5 a). The opposite property to ductility is brittleness, namely the tendency of some material to break abruptly without showing significant permanent deformations. It should be underlined that ductility does not consider the strength of the material, but only defines the ratio of the inelastic and elastic areas (Figure 5 b). The term is commonly used nowadays in structural engineering to indicate the quantity of energy which may be dissipated through plastic deformations and the degree to which a structure that is damaged can undergo large deformations without collapsing.

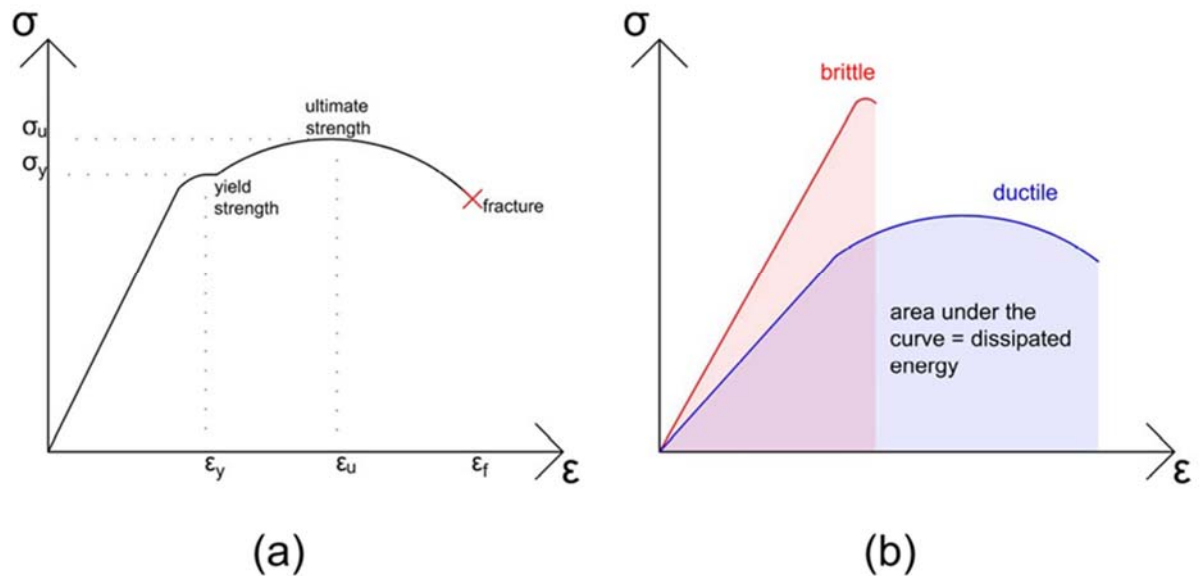


**Figure 5: Ductility and energy dissipated through plastic deformations.**

Since ductility is related to the possibility of achieving large displacements without losing too much strength it is universally recognized as a very important requirement. Among other reasons this ensure that the failure will occur with large deformations, so that the occupants will get a clear warning. Furthermore, allowing for energy dissipation the effect of the earthquake is reduced.

For steel and reinforced concrete buildings the following ductility types are widely used in literature<sup>8</sup>:

- material ductility, or axial ductility, which characterizes the material plastic deformations;
- cross-section ductility, or curvature ductility, which refers to the plastic deformations of cross-sections, considering the interaction between the parts composing the cross-section itself;
- member ductility, or rotation ductility, when the properties of members are considered;
- structure ductility, or displacement ductility, which considers the behaviour of the whole structure.

These definitions are summarized in Figure 6 from (Gioncu V., 2000)<sup>8</sup>

Ductility types	Schematic representation	Definition
Material (axial) ductility		$\mu_\epsilon = \frac{\epsilon_u}{\epsilon_y}$
Cross-section (curvature) ductility		$\mu_\chi = \frac{\chi_u}{\chi_y}$
Member (rotation) ductility		$\mu_\theta = \frac{\theta_u}{\theta_y}$
Structure (displacement) ductility		$\mu_\delta = \frac{\delta_u}{\delta_y}$

Figure 6: Ductility types, figure from (Gioncu V., 2000)<sup>8</sup>.

### 1.2.2 Ductility in timber buildings

Since wood is an inherently brittle material, specially under tensile loads, timber elements exhibit almost no potential for energy dissipation. Thus, in a timber structure the only elements that provide ductility, and consequently exhibit hysteretic dissipation of energy under cyclic loading, are the metal connection systems.

Although a definition of ductility is given in EN12512<sup>9</sup>, a lot of different definitions exist in literature and no widely accepted definition of the term is established<sup>10 11</sup>. In general, the definitions of ductility can be divided into two categories: one that compares strains or deformations at different load levels and the other which is based on energy<sup>11</sup>. The definition adopted by CEN is the relative definition given by the relation:

$$D_u = \frac{u_u}{u_y} \quad (2)$$

In (Jorissen A. & Fragiaco M., 2011)<sup>12</sup> and (Muñoz et al, 200)<sup>13</sup> the authors discuss the implications of ductility in design of timber structures under static and dynamic loading. One of the problems in the definition of ductility is the identifying of the so-called yield slip  $u_y$ . The procedure for the evaluation of this quantity is suggested in different documents and is treated in depth in (Muñoz et al, 200)<sup>13</sup> where six different methods commonly used all around the world for the determination of  $u_y$  are presented. From these studies arises the fact that the utilisation of different methods for assessing the yield point could give very different results in the calculation of the ductility ratio.

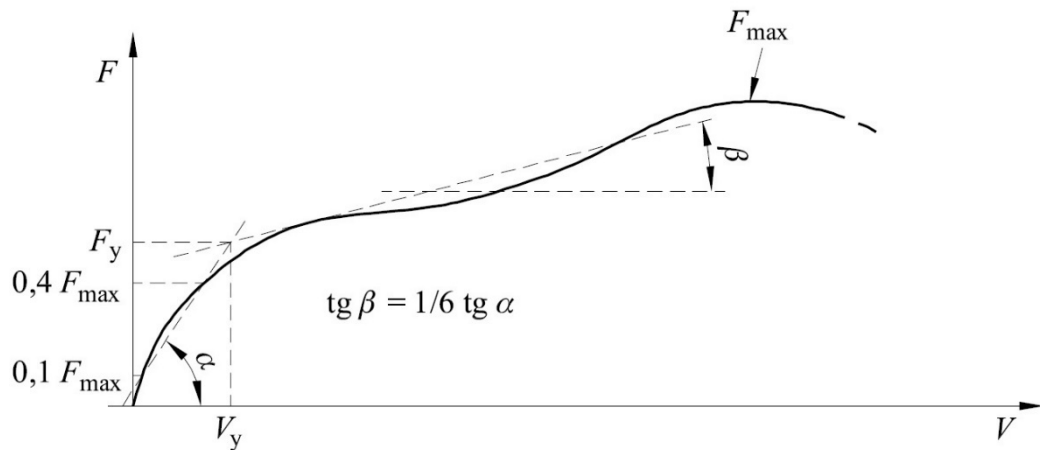


Figure 7: Load-slip curve from EN12512.

The importance of ductility in the design of earthquake resistant timber buildings is reflected by the introduction in EC8<sup>6</sup> of Ductility Classes that reflect the ductile behaviour and energy dissipation capacity of the building. Namely: Low Ductility Class (DCL); Medium Ductility Class (DCM) and High Ductility Class (DCH). The importance of a proper design of the dissipative zones is clearly pointed out and some specific indications concerning the wood elements and the fasteners' characteristics are given.

### 1.2.3 Behaviour Factor

Most design codes contain action reduction factors in order to evaluate the design forces that will be used for a simplified linear elastic analysis. These factors are called behaviour factor ( $q$ -factor) in Europe and response modification factor ( $R$ ) in North America, and takes into account the capacity of the structure to exploit energy dissipation through an inelastic behaviour, the presence of force reducing effects, such as stiffness degradation



and soil structure interaction. In fact, in EC8<sup>6</sup> is stated that “*The resistance and energy-dissipation capacity to be assigned to the structure are related to the extent to which its non-linear response is to be exploited. In operational terms such balance between resistance and energy-dissipation capacity is characterised by the values of the behaviour factor  $q$  and the associated ductility classification...*”. The behaviour factor is then defined as “... *an approximation of the ratio of the seismic forces that the structure would experience if its response was completely elastic with  $\xi = 5\%$  viscous damping, to the seismic forces that may be used in the design, with a conventional elastic analysis model, still ensuring a satisfactory response of the structure*”.

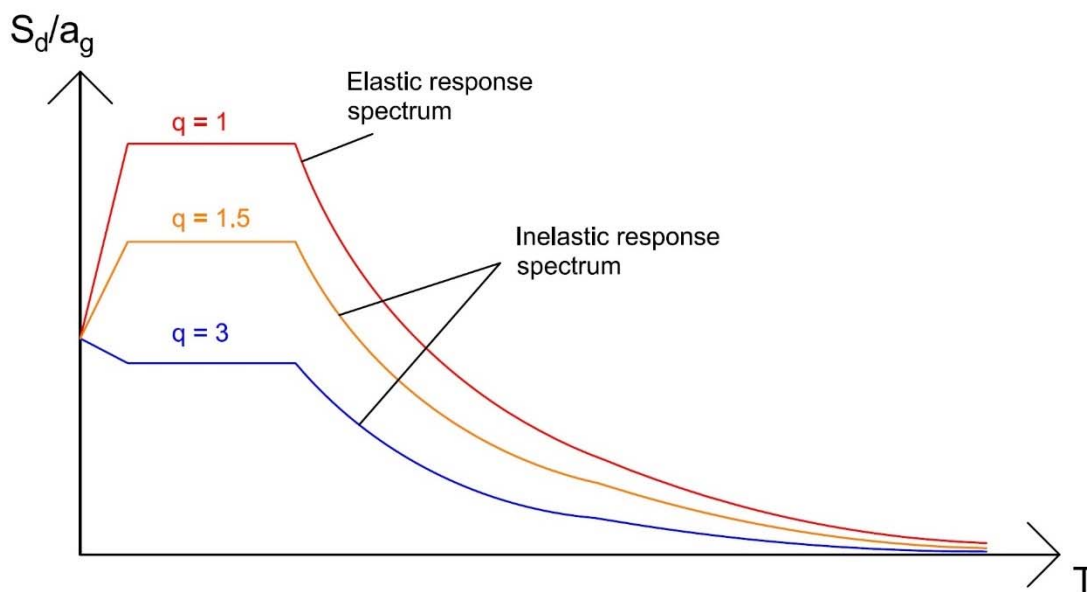


**Figure 8 Elastic and design response spectra.**

So ultimately the behaviour factor is the value by which the elastic response spectrum has to be divided in order to get the design forces, and depends on:

- The construction material used, as different materials present different capacities to withstand plastic deformation before failure.
- The structural type, because different systems have different abilities to dissipate energy before giving rise to liability.
- The global level of ductility of the structure
- The intrinsic over-resistance possessed by the structure
- The plan and elevation regularity

### 1.2.4 Behaviour factor for timber buildings

Since the higher the q-factor, the lower the seismic base shear, a proper definition of the most suitable behaviour factor for timber building systems is a fundamental issue of the codes for structural seismic design<sup>14</sup>. In fact, available seismic codes provide the q-factor only for standard building typologies, and refer to the outcomes from specific experimental cyclic tests to give an estimation of the ductility class and therefore of the most suitable q-factor range<sup>15</sup>.

According to (Pozza L., 2013)<sup>14</sup>, the behaviour factor q can be estimated as the product between an intrinsic part  $q_0$ , accounting for the total dissipative capacity and all intrinsic over-resistances and the design over-strength  $\Omega$  accounting for the code's partial safety factor and for the differences between the design resistance and the applied external force, as showed in equation 3 and Figure 9 from (Ceccotti et al, 2016)<sup>15</sup>.

$$q = q_0 \cdot \Omega \tag{3}$$

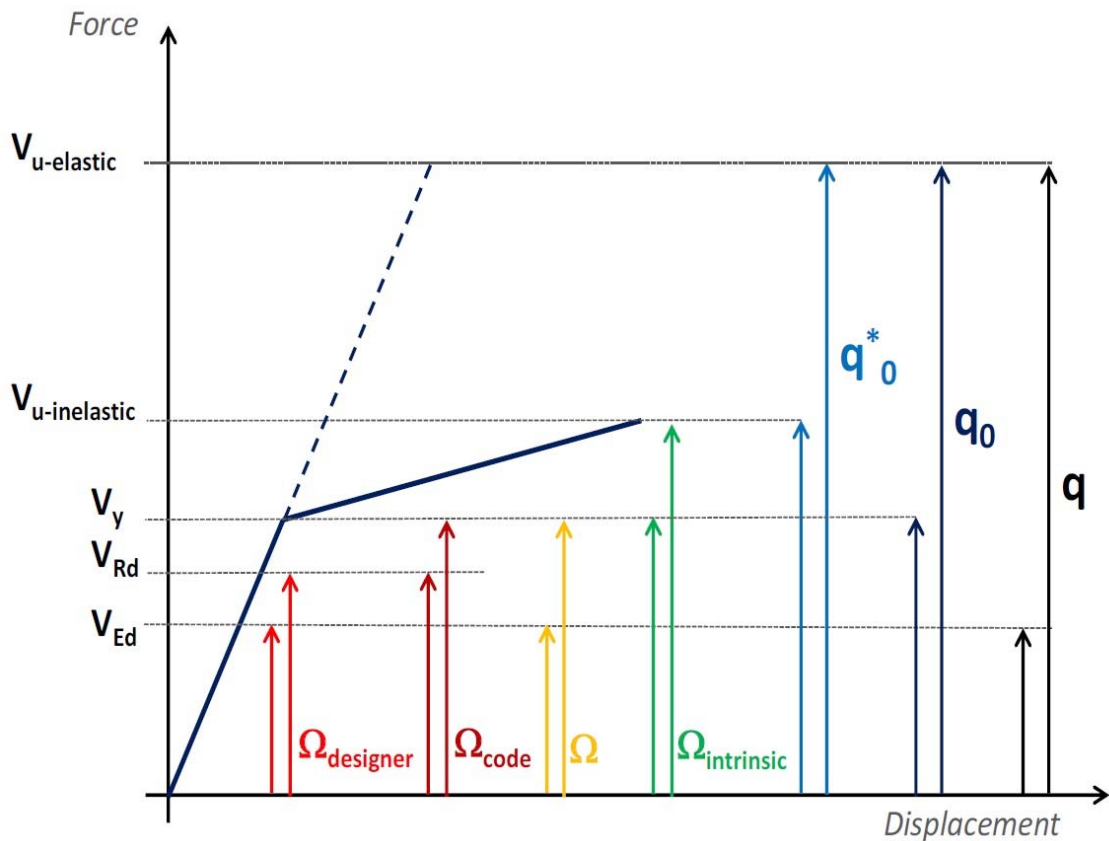
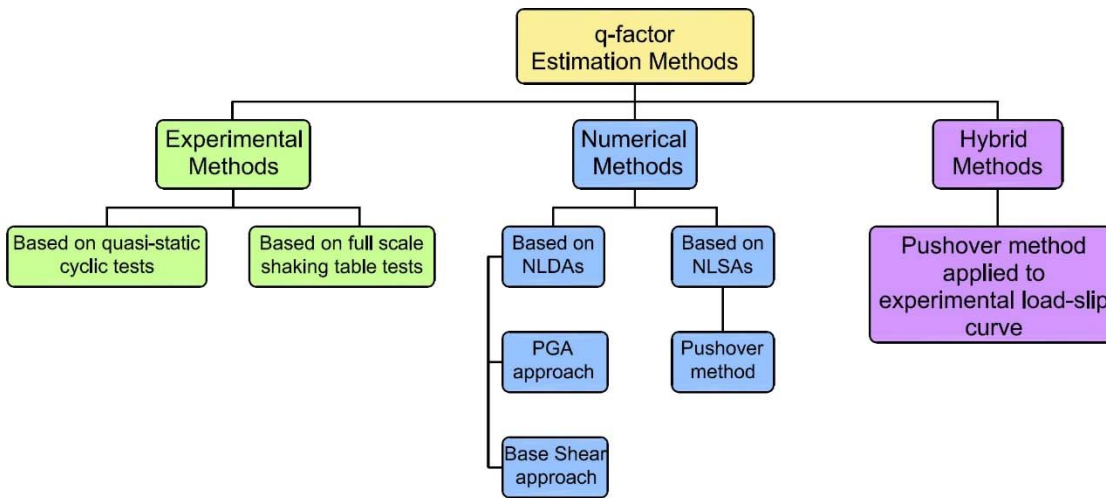


Figure 9: Relationship between behaviour factor q, overstrength  $\Omega$  and intrinsic reduction factor  $q_0$ , figure from (Ceccotti et al, 2016)<sup>15</sup>.

In (Ceccotti et al, 2016)<sup>15</sup> three different methods (experimental methods, numerical methods, hybrid experimental-analytical method) for the q-factor evaluation are discussed. A scheme of the methods is presented in Figure 10.



**Figure 10: Procedures for q-factor evaluation.**

### 1.3 Seismic regulatory framework for timber structures

Even though building codes permit the employment of any material as long as the prescribed performances are met, there are some limitations to the use of wooden based products which need to be addressed. The extraordinary advancements of timber technologies and construction techniques of the past years has as a consequence that modern timber engineering codes are struggling to keep up to date. A typical example is the lack of regulations regarding CLT products. Another regulatory limitation to the enhanced use of wood-based products in residential construction relates to the fire performance and sound insulation specifications, especially in multi-storey residential constructions<sup>14</sup>. From the seismic point of view the lack of regulation, at least in Europe, is even more evident. In EC 8<sup>6</sup> the sections that treat concrete, steel, composite concrete-steel and timber buildings have 58, 23, 26 and 6 pages respectively. If the importance of a construction material was measured by its number of pages in the standard, timber will not come out well from this comparison. This undeniable lack of prescriptions and guidelines could limit the diffusion of building systems that have proven themselves reliable and safe under earthquake loads, and a viable alternative to more common construction materials, even for mid to high-rise buildings. The following section contains a brief overview of the current seismic codes valid in Europe, Switzerland, New Zealand and Canada that apply to timber buildings, with particular attention to the provided values for the overstrength factor by these codes. Finally, the main features of the draft proposal for the new chapter 8 of the Eurocode are analysed.

#### 1.3.1 Europe and EC8

Eurocode 8<sup>6</sup> is the reference standard in Europe for the design of seismic resistant structures, and its composed of 10 Sections. Beside the introductory Section 1, Section 2 and 3 contain the basic performance requirements and compliance criteria and give the rules for the representation of seismic actions, Section 4 contains general design rules relevant specifically to buildings, and Sections 5 through 9 give specific rules for the most common structural materials, namely: concrete, steel, composite concrete-steel, timber and masonry, while section 10 gives provisions for base isolation.

The code identifies two fundamental performance requirements:

- The no-collapse requirement: *“the structure shall be designed and constructed to withstand the design seismic action defined in Section 3 without local or global*

*collapse, thus retaining its structural integrity and a residual load bearing capacity after the seismic events*". Which represents the Ultimate Limit State.

- The damage limitation requirement: *"the structure shall be designed and constructed to withstand a seismic action having a larger probability of occurrence than the design seismic action, without the occurrence of damage and the associated limitations of use, the costs of which would be disproportionately high in comparison with the costs of the structure itself"*. Which represents the Serviceability Limit State.

As already seen in §1.2 the importance of designing structures able to dissipate energy through inelastic displacements is clearly pointed out in the code, and the Capacity Design philosophy is exposed.

Section 8 deals with the specific rules for timber structures and the provisions therein included are considered additional to those present in Eurocode 5<sup>16</sup>. The section is composed of 7 different parts:

- 8.1 General: This introductory part contains some general information, the definition of specific terms related to timber structures and information about the design concepts.
- 8.2 Materials and properties of dissipative zones: This part gives provisions for material and properties of dissipative zones when a dissipative structural behaviour is adopted.
- 8.3 Ductility classes and behaviour factors: Here different structural types are listed and the relevant ductility class and behaviour factors are defined depending on their ductile behaviour and energy dissipation capacity.
- 8.4 Structural analysis: in this brief part, some general information regarding the slip of joints, the elasticity modulus and rules on rigid diaphragms are given.
- 8.5 Detailing rules: This part provides detailing rules for connections and horizontal diaphragms.
- 8.6 Safety verifications: This part provides some provisions for the  $k_{mod}$  and  $\gamma_M$  values to be used in the safety verifications. Provisions are also given for the structural elements to which overstrength requirements apply, even though no value of the overstrength factor is given. In addition, some indications on detailing rules for carpentry joints to avoid brittle failure are given.

- 8.7 Control of design and construction: The last section gives provisions for how the structural elements should be detailed and identified in the design drawings.

**Table 8.1: Design concept, Structural types and upper limit values of the behaviour factors for the three ductility classes.**

Design concept and ductility class	$q$	Examples of structures
Low capacity to dissipate energy - DCL	1,5	Cantilevers; Beams; Arches with two or three pinned joints; Trusses joined with connectors.
Medium capacity to dissipate energy - DCM	2	Glued wall panels with glued diaphragms, connected with nails and bolts; Trusses with doweled and bolted joints; Mixed structures consisting of timber framing (resisting the horizontal forces) and non-load bearing infill.
	2,5	Hyperstatic portal frames with doweled and bolted joints (see 8.1.3(3)P).
High capacity to dissipate energy - DCH	3	Nailed wall panels with glued diaphragms, connected with nails and bolts; Trusses with nailed joints.
	4	Hyperstatic portal frames with doweled and bolted joints (see 8.1.3(3)P).
	5	Nailed wall panels with nailed diaphragms, connected with nails and bolts.

**Figure 11: Table 8.1 from EN 1998-1<sup>6</sup>.**

At the current state, Section 8 cannot be considered exhaustive due to several reasons. One of the first critical issues concerns the clear and univocal definition and identification of the different structural systems. This is a critical aspect if we consider the importance of the correct choice of the ductility class and the relevant behaviour factor  $q$  according to the Capacity Based Design<sup>17</sup>. Some of the structural types listed in table 8.1 refer to old buildings (e.g. mixed structures consisting of timber framing and non-load bearing infill) but no longer in use, while other structural types that are rapidly growing in popularity, such as CLT, are not treated.

Another aspect highlighted in (Follesa et al, 2011)<sup>17</sup> are the ductility provisions given for the dissipative zones which are based on simplified rules on the diameter of dowel type fasteners and on the thickness of connected members. According to the authors such rules on the characteristics of joints should be superseded by requiring a failure mode characterized by the formation of one or two plastic hinges in the mechanical fastener, which can be easily checked using the Johanssen's equations prescribed by the EC 5<sup>16</sup>.

Finally, despite the fact that the standard embrace the capacity design principle and states at 8.6 (4)p that non-dissipative zones shall be designed with sufficient over-strength, it

fails to provide any values that quantify this over-strength, making de facto the Capacity Design approach not applicable to any kind of timber structure, not only the CLT ones.

### 1.3.2 Switzerland and SIA 265

In the context of harmonized European standards, SIA (Swiss Society of Engineers and Architects) has published a new generation of structural standards based on the Eurocodes. For wooden structures the reference standard is the SIA 265-2012<sup>18</sup>. Even though the influence of the Eurocodes is evident, one difference is that instead of producing an independent seismic document (as Eurocode 8), the seismic regulations in Switzerland are directly integrated into the different material related codes (SIA 265 deals with the design for seismic loads at §4.6). Other differences are present in the models adopted for the calculations of timber connections, with the swiss code adopting simpler and more empirical models in comparison to EC5. Unfortunately, not even the Swiss code has a set of specific rules for CLT buildings, but unlike EC8 it gives an indication on the overstrength that the non-dissipative zones shall be designed for; specifically stating at point 4.6.3.1 that the brittle elements shall be overdesigned by 20% ( $\gamma_{Rd} = 1.2$ ) with respect to the ductile zones.

### 1.3.3 New Zealand and NZS 3603/ NZS 3604

If we move outside of Europe, New Zealand has always been a reference point with respect to seismic design, being the place where Capacity Design principles were invented<sup>5</sup>. Although CLT arrived in the region later than in Europe, it is quickly gaining popularity within the engineering community. However, this delay had, as consequence, that New Zealand too lacks a set of specific rules for the designing of CLT structures.

In New Zealand light timber frame building is a familiar system to many builders and designers because the widespread history of use and observations following the 2010 and 2011 Canterbury earthquakes have provided ample evidence that this construction type provides more than adequate resistance to earthquake loading. The design and construction of timber frame buildings in New Zealand are described primarily by prescriptive means using NZS 3604:2011<sup>19</sup> or, for timber structural solutions requiring specific engineering design, using NZS 3603:1993<sup>20</sup> Timber structures standard<sup>21</sup>.

With regard to overstrength factors NZS 3603 at C4.2.2 states: *“The average ultimate strength of nailed connections in single shear is approximately 1.6 times the characteristic strength given in table 4.3. Hence for capacity design, an overstrength*

*factor of 1.6/  $\varphi = 2.0$  should be used*". It should however be noted though that resistance values for nailed connections are derived from other methods than the ones used in Europe.

#### 1.3.4 Canada and CSA O86

The National Building Code of Canada (NBCC) is the model building code of Canada and sets out technical provisions for the design and construction of new buildings. Housing and small buildings can be built without a full structural design using prescriptive requirements found in Part 9 of the NBCC, due to the extensive experience with small wood-frame buildings in the country. Buildings that fall outside the prescriptive boundaries must be designed in accordance with Part 4 of the Code by design professionals. Structural resistance to Part 4 loads is specified in the material standard for engineering design, which for wood is CSA Standard O86 "*Engineering Design in Wood*"<sup>22</sup>.

Canada is the only nation so far to have directly implemented criteria for the design of CLT structures in their national timber standard. The standard deals with specific verification rules for CLT walls/slab in chapter 8, and with seismic design consideration for CLT structures in chapter 11.9. With regard to overstrength factor it is stated that non-dissipative connections and CLT panels shall be designed for forces that are induced in them when the energy dissipative connections reach the 95<sup>th</sup> percentile of their ultimate resistance, with the limitation that the design force needs not exceed the force determined using a behaviour factor of 1.3 ( $R_d \cdot R_o = 1.3$ ).

#### 1.3.5 New version of chapter 8 of Eurocode 8 – draft of 01.02.2017

Given the worldwide raising interest for timber structures several research projects have been carried out all around Europe in the last years. The proposals to improve the current regulatory framework for the design of earthquake resistant timber structures are, in fact, based on the outcomes of these investigations.

The draft proposal for the new version of section 8 of EC8<sup>23</sup> maintains the same structure as the old one, but addresses many of the deficiency previously seen.

The entire part 8.3 has undergone significant improvement. The issue with the uncertainty of the choice of the correct structure type has been addressed, and more indication concerning the requirement for the dissipative zones are given. Table 8.1 is completely new with respect to the current version of Eurocode 8. New structural systems as the CLT



system and the Log House system have been introduced. The table gives also an example figure, in order to further clarify and help in the choice of the correct structural type. Structural type and upper limit values of the behaviour factors are then given in table 8.2, while the indications on the required ductility values of dissipative zones tested according to EN 12512 are given in table 8.3.

Structural type	DCM	DCH
1. CLT buildings	2,0	3,0
2. Light-Frame buildings	2,5	4,0
3. Log House buildings	2,0	-
4. Moment resisting frames	2,5	4,0
5. Post and beam timber buildings with dowel type connections	2,0	-
6. Timber framed walls with carpentry connections	-	-
7. Timber framed walls with carpentry connections and masonry infill	2,0	-
8. Large span arches with two or three hinged joints	-	-
9. Large span trussed frames with nailed, screwed, doweled and bolted joints	-	-
10. Vertical cantilever systems made with glulam or CLT wall elements	1,5	-

**Figure 12: Table 8.2 from new chapter 8 of EC8 draft proposal.**

Given the importance of Capacity design principles a paragraph dedicated to this has been added. Two values for the overstrength factor have been proposed based on the structural type. Namely 1.3 for: CLT buildings, Light-Frame buildings, Log House buildings, High ductility moment resisting frames with expanded tube fasteners, Timber framed walls with masonry infills. While 1.6 has been proposed for: Moment resisting frames (except for high ductility moment resisting frames with tube fasteners and Densified Veneer Wood), Post and beam timber buildings, Vertical cantilever systems made with glulam or CLT wall elements.

Specific rules for each structural type are then presented. A quite comprehensive description on CLT structures has been introduced, and specific rules for the capacity design of structures in medium and high ductility class are given, with the identification of the structural elements that shall provide energy dissipation, and those that instead shall be designed with sufficient overstrength.

Keeping in mind that this is anyway still a draft, in the opinion of the writer, there are still some aspects that should be further clarified, and others that perhaps should be treated in

a slightly different way. For example at §8.4.1.3.1.(2)p the vertical connection between parallel panels, within the segmented shear wall, is indicated as the connection that shall be designed as dissipative for CLT buildings in DCH, but it is also stated that this provision should be added to those presented for buildings in DCM, where hold-downs and angle brackets are indicated as the dissipative connections. This seems to mean that both vertical joints, and hold-downs and angle brackets should be considered as dissipative zones, but this could compromise the intended behaviour of the building if there is not a hierarchy of resistance between these systems. A proposal to address some of these inconsistencies will be presented in the conclusive chapter.



## 2 OVERSTRENGTH

The term overstrength usually defines the ratio between the actual resistance of whichever material/component/structure and the design resistance. In the framework of structural engineering, this concept has, in most cases, a positive meaning since it is indicative of a reserve of strength, not considered at the stage of design, which further decreases the failure probability. In case of earthquake loads, instead the overstrength of some element of the structure may instead lead to negative outcomes. This possible overcapacity of the structure has thus to be considered, so that the specific hierarchy of resistances shall follow the order planned by the designer.

A survey of the literature has allowed to find out how the OSF is evaluated for timber buildings, with particular attention to CLT structures. These methods and the results of some of the researches on the subject are presented in the following chapter, but first an introduction is made on the possible causes for the reserve of strength that structures usually possess, and also a brief overview on how the OSF is evaluated for other materials.

## 2.1 Reserve of strength

A great quantity of scientific research has been conducted in order to identify and assess the sources of reserve of strength and to study the influence of ductility and structural overstrength in seismic design of reinforced concrete and steel structures, the ones used as reference for this study were (Mitchell D. & Paultre P., 1994)<sup>24</sup> and (Humar J. & Rahgozar M., 1996)<sup>25</sup>.

That structures possess an overstrength is clearly noticeable in the event of earthquakes of high intensity, with the observation that most of the structures of new conception are able to sustain, without or with little damage, seismic actions considerably higher than those they were designed for.

In fact, regulations usually take into account the reserve of strength that a structure possesses, with the definition of a behaviour factor through which the seismic load is reduced, and with the introduction of overstrength factors. It is necessary to promptly underline that not each of the resources of overstrength can be unambiguously and clearly identified, and thus relied upon. Some of these factors involve uncertainty, or cannot be accounted for since they are difficult to quantify because of the complexity of the behaviour and/or the lack of knowledge.

TABLE 4. Factors influencing overstrength

Factors that increase overstrength	Factors that limit overstrength
Participation of nonstructural elements	Nonstructural elements (e.g., short columns)
Code-calculated period and related base shear, $V$	Code-calculated period and related base shear, $V$
Load combinations	Improper design and detailing according to older codes
Minimum size and reinforcement	Shear failure
Design controlled by drift consideration	Bond failure
Limited bar sizes and arrangement	Deterioration
Importance of building	Poor structural system (soft storey, setbacks)
Increased resistance due to confinement	Lack of confinement
Reduced stiffness due to cracking	Consideration of redistribution in design
Assumed lateral load distribution	Assumed lateral load distribution
Slab participation	Slab participation
Material overstrength	Material understrength
Capacity design	
Design controlled by other loading case (e.g., wind)	

Figure 13: Factors influencing overstrength, figure from (Mitchell D. & Paultre P., 1994)<sup>24</sup>.

A first relevant factor is the gap between the effective strength of the material and the design one. This takes into account both the discrepancy between the actual value of resistance and the characteristic one and the reduction of the strength applied by the partial safety factors suggested by the standards.

A second factor comes from the difference between the actual dimensions of the elements and those required by the design since the structural components are available in limited

and discrete commercial dimensions. In addition, often building codes prescribe some minimum requirements.

Other reserves of strength arise from the redistribution of internal forces in the inelastic range, from the strain hardening of material modelled as elastic-perfectly plastic in design. Redistribution allows, in fact, the structure to resist forces that are significantly higher than those causing first yield.

Another simplification is the use of single degree-of-freedom spectra along with assumed load distribution to estimate the demand on multi-degree-of-freedom systems.

Further contributions come from the use of conservative models for predicting member capacities, from the effect of non-structural elements, such as for example, infill walls, and from the effect of structural elements that are not included in the prediction of lateral load capacity.

## 2.2 Overstrength factor for other structural materials

The definition for the factor  $\gamma_{Rd}$  is not univocally established yet and may result from different approaches. If data are available from real experimental tests, the overstrength factor is usually calculated as the ratio between the value of the effective strength (at 95<sup>th</sup> or 50<sup>th</sup> percentile) and the nominal/design one.

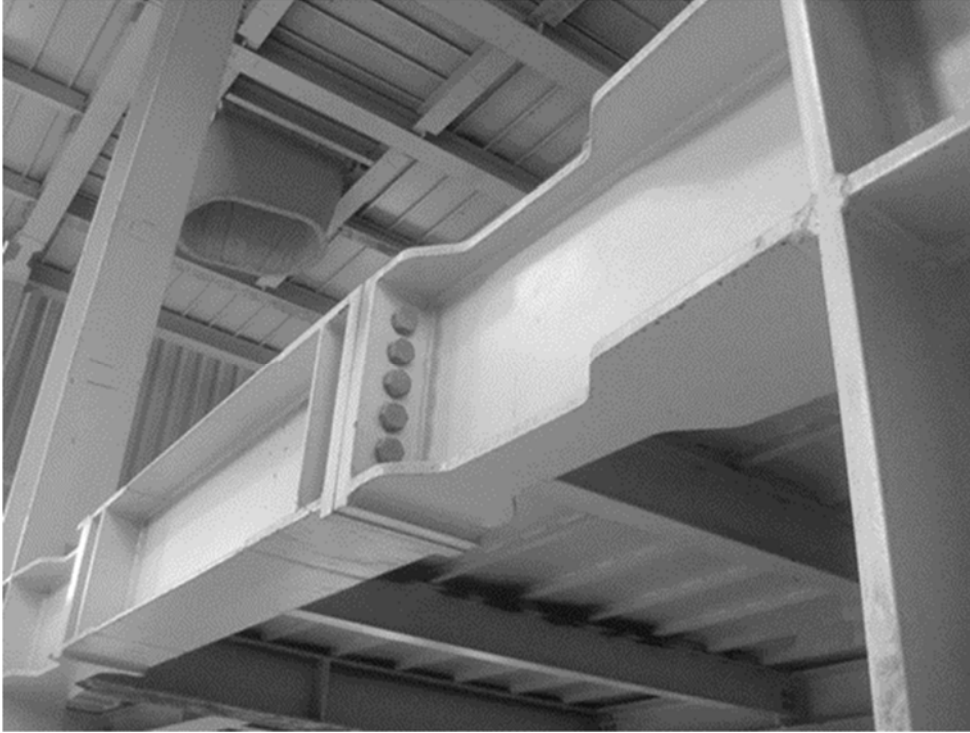


**Figure 14: Steel structure detail to ensure column and joint overstrength.**

The rules implemented for capacity design in case of steel structures are different from those implemented for other materials. In case of steel structures, capacity design of non-dissipative parts is regulated by a unique format applicable to all the different structural types covered by the code<sup>26</sup>, namely the expression:

$$R_{b,Ed,i} = R_{Ed,G,i} + 1,1 \cdot \gamma_{ov} \cdot \Omega \cdot R_{Ed,E,i} \quad (4)$$

The earthquake-induced effects are increased by the factor 1.1,  $\gamma_{ov}$  and  $\Omega$ , where  $\gamma_{ov}$  is the material overstrength factor (suggested value 1.25, in case of lack of better evaluations), which accounts for the possibility that the actual yield strength of steel is higher than the nominal yield strength,  $\Omega$  is the minimum value of  $\Omega_i = R_{pl,Rd,i} / R_{Ed,i}$ , where  $R_{pl,Rd,i}$  is the design strength of the  $i$ -th plastic zone and  $R_{Ed,i}$  is the required strength.  $R_{b,Ed}$  is the design load on the brittle component while subscripts “G” and “E” indicate the effect of gravity and earthquake loads. 1.1 is a coefficient that considers other effects such as the strain

hardening of steel<sup>27</sup> and presumably the redistribution of forces after the formation of the first plastic hinge<sup>26</sup>.

It can be noticed that both  $\gamma_{ov}$  and  $\Omega$  are only applied to the lateral seismic input and not to the gravitational one.

On the other hand, a frequently employed method is based on the Monte Carlo simulation method. Starting from the statistical distributions of the fundamental properties of the resistant elements, a deterministic analytical model is applied to randomly chosen values from these distributions. The procedure is then repeated until a sufficiently regular distribution of results is achieved. In literature, several variants of this approach can be found. Some authors implement methods based on reliability analysis by using limit state functions whereas other ones directly refer to the obtained distribution and usually focus on its 95<sup>th</sup> percentile. Some research takes into account the variability in the strength of the brittle component and some neglects it.

An application of this Monte Carlo procedure can be found in the investigation on reinforced concrete beams<sup>28</sup>. The fundamental material and geometrical properties are defined through their statistical distribution (normal distributions described by their mean and covariance value) in accordance with a specific testing programme, previous studies and data from the producers. From each distribution, a value at random is picked and each value is used to calculate the capacity of the cross-section  $M_{R,i}$ . This process is repeated for a large number of samples (5000) and for different configurations of the cross-section. Finally the resultant values of  $\gamma_i = M_{R,i} / M_{Rd,i}$  are aggregated in the resulting statistical distribution. From this distribution of overstrength factors, the authors focus on the 90<sup>th</sup> and 50<sup>th</sup> percentiles to make a comparison with the regulations and to draw their conclusions. It has to be noted that in this application no reference has been made to the possible overstrength of the brittle element and that the conclusions have been directly drawn on the resulting distribution without exploiting any limit state function.

Another interesting application of the Monte Carlo method is the one implemented in the investigation on steel-concrete composite structures<sup>29</sup>. In this case the resistance of both the ductile and the brittle components is simulated through the previously presented procedure. Afterwards, the resulting cross-sectional characteristics are applied to a dynamic non-linear analysis of a whole 3D structure. The process of sampling and analysing the structure is then repeated 500 times and a distribution of overstrength factors is so generated. More specifically, the overstrength factor is calculated as the value



that, if applied to the design seismic demand, would generate the maximum simulated action on the brittle members as resulted from the dynamic non-linear analysis. Finally, the authors take as a reference the value of the 95th percentile of the resulting distribution of overstrength factors.

To conclude, one more variant to the implementation of the Monte Carlo simulation to evaluate the overstrength factor is presented in (Leslie et al, 2009)<sup>30</sup>. Here, once the samples are generated through the Monte Carlo simulation, both for the ductile and the brittle member, a limit state function is implemented. The authors compare the resistance distribution of the ductile element with the distribution of the brittle one multiplied by an overstrength factor. The failure probability of the system is then evaluated as a function of the value of the overstrength factor. Consequently, once the target reliability index is chosen, the overstrength factor is immediately calculable.

### 2.3 Overstrength factor for timber structures

Several work of research address the problem of the lack of information about the OSF for timber structures in the EC8. In the following a review of the methods presented in a series of scientific papers is discussed.

The first proposal for the evaluation of the overstrength factor for timber structures can be found in (Jorissen A. & Fragiacommo M., 2011)<sup>12</sup>. In this paper, a general overview on ductility and over-strength factor for timber structures is presented using the results on previous work of Jorissen on dowelled connections. The overstrength factor is here defined as:

$$\gamma_{Rd} = \frac{R_{d,0.95}}{R_{d,0.05}} \cdot \frac{R_{d,0.05}}{R_{d,k}} \cdot \frac{R_{d,k}}{R_{d,d}} = \gamma_{sc} \cdot \gamma_{an} \cdot \gamma_M \quad (5)$$

Where  $R_{d,0.95}$  and  $R_{d,0.05}$  are respectively the 95<sup>th</sup> and 5<sup>th</sup> percentile of the ductile component strength distribution;  $R_{d,k}$  and  $R_{d,d}$  are respectively the characteristic and the design values of the analytical prediction of the ductile element strength. The coefficient  $\gamma_{sc} = R_{d,0.95} / R_{d,0.05}$  then express then the scatter of the experimental connection strength properties and, therefore, gives an indication on the reliability of the connection. The coefficient  $\gamma_{an} = R_{d,0.05} / R_{d,k}$  express instead the approximation of the analytical formula used to evaluate the strength property, which will tend to one in case of an exact prediction. Finally,  $\gamma_M$  is the partial material factor that, for verifications of structures designed in accordance with the concept of dissipative structural behaviour (DCM, DCH), should be taken from the accidental load combinations (equal to one).

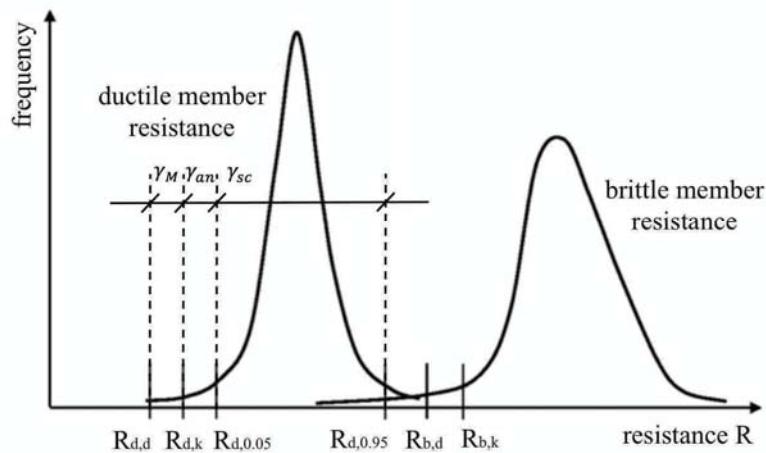


Figure 15: Concept of overstrength.

The experimental investigation was carried out on dowelled timber to timber connection loaded monotonically up to failure in shear parallel to the grain. 14 configurations, varying dowel diameter, number of fastener, spacing between fastener and thickness of the wooden elements, were tested. For each configuration 10 to 25 specimens were considered. The average values and standard deviations of the connection strength distribution were calculated according to EN 14358<sup>31</sup> using a lognormal distribution. From the previously defined formulas the values for  $\gamma_{an}$ ,  $\gamma_{sc}$  and  $\gamma_{Rd}$  were calculated. The values for  $\gamma_{an}$  was found ranging between 0.79 and 1.63 with a mean value of 1.18, while  $\gamma_{sc}$  between 1.03 and 2.14 with a mean value of 1.39.  $\gamma_{Rd}$  had instead values ranging from 1.2 to 2.1, the authors proposed as a consequence the use of the mean value 1.6 as overstrength factor for a ductile design.

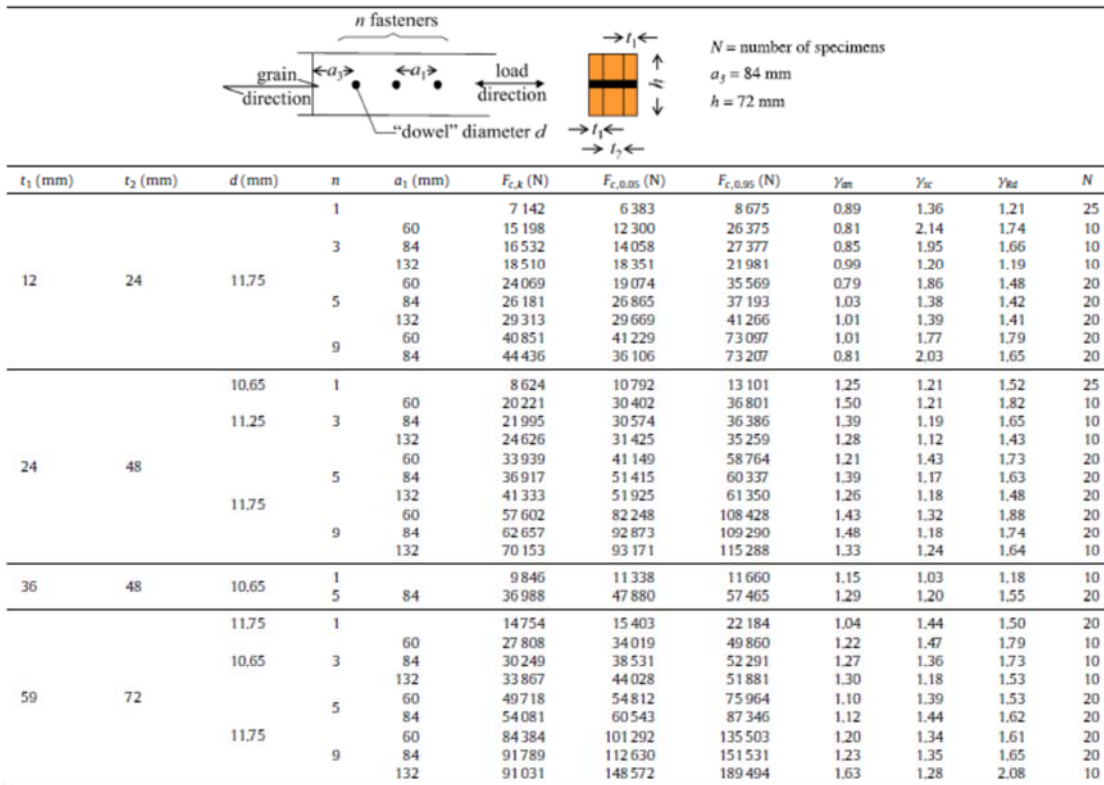


Figure 16: Overstrength values for the configurations tested in <sup>12</sup>.

In (Fragiacomo et al, 2011)<sup>32</sup> the authors discuss the seismic design of multi-storey buildings made from CLT, paying particular attention to analysis methods, issues on the modelling of crosslam wall and connections, and evaluating the values for the OSF for some kinds of connections. The same procedure as in <sup>12</sup> is, in fact, applied to the results of experimental cyclic tests performed by Dujic and Zarnic on timber connections made of angular brackets and screwed connections between perpendicular panels. The difference with (Jorissen A. & Fragiaco M., 2011)<sup>12</sup> is that here the 5<sup>th</sup> and 95<sup>th</sup> percentiles were evaluated using a student's t distribution, due to limited experimental data available (only 2 to 5 specimens for configuration), and without considering the contribution of  $\gamma_{an}$ . The overstrength factor was, in fact, calculated as  $\gamma_{Rd} = R_{d,0.95}/R_{d,0.05}$ . As a consequence, the discrepancy between the analytical prediction of resistance and the actual one is neglected. The configuration using angle brackets with 40mm nails showed a rather brittle behaviour giving as results an overstrength factor of 2.12 in shear and 1.85 in uplift, hence the recommendation is given to use nails at least 60mm long so that the brittle failure can be avoided. Instead, the configuration with 60mm nails gives much lower values for the overstrength, namely 1.26 in shear and 1.18 in uplift. The tests performed on the screwed connection between perpendicular panels shows that due to a larger scatter of the results the overstrength factor calculated was 1.63.

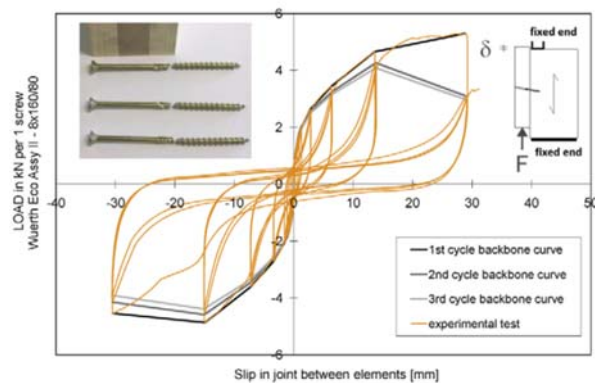


Figure 17: Cyclic test results from (Fragiacomo et al, 2011)<sup>32</sup>.

		Number of specimens tested	Mean value of peak force ( $F_{max}$ )	Standard deviation $\sigma$ of peak force	5th percentile $F_{0.05}$	95th percentile $F_{0.95}$	Overstrength factor $\gamma_{Rd}$ (Eq. (1))
BMF 105 angular brackets with ten 40 mm nails	Shear	3	13.5	1.73	8.4	18.5	2.12
	Uplift	3	14.8	1.51	10.4	19.3	1.85
BMF 105 angular brackets with ten 60 mm nails	Shear	3	15.0	0.59	13.3	16.8	1.26
	Uplift	2	23.1	0.31	21.2	25.0	1.18
Wuerth Assy II 8 x 160/80 self-tapping screws	Shear	5	4.7	0.52	3.6	5.8	1.63

Figure 18: Overstrength values for the configurations tested in (Fragiacomo et al, 2011)<sup>32</sup>.

In (Gavric et al,2012)<sup>33</sup> and (Gavric et al, 2015)<sup>34</sup> the results from an experimental programme conducted by CNR IVALLSA is presented. The tests were carried out on hold-downs, angle brackets and screwed connections between panels, for a total of 20 different configurations. These different set-ups were based on the typical connections used within the buildings tested for the SOFIE project.

In (Gavric et al,2012)<sup>33</sup> the results of the tests performed on 12 different configurations of screwed connections between CLT panels are presented. The configurations vary so that the capacity of the screw could be assessed for both a lateral and a withdrawal load. For each of the configurations at least one monotonic and six cyclic tests were performed. Also here the overstrength factor is defined as the ratio between 95<sup>th</sup> percentile of the connection strength distribution and the analytical prediction of the design connection strength. However, the final values for the OSF,  $\gamma_{Rd}$  were calculated neglecting the contribution of  $\gamma_{an}$ . The 5<sup>th</sup> and 95<sup>th</sup> strength values were calculated assuming three different distributions, namely normal, log-normal and the procedure prescribed by the EN14358 standard. A comparison between the three different approaches was then made showing that with the normal and log-normal distribution the factor was ranging from 1.15 to 1.7, with the exception of one configuration that gives a value of 2.3 due to a brittle failure mode (shear plug), so that the high scatter gives a much higher value. The average OSF value calculated was 1.46. On the other hand, using the approach given in EN14358 leads to higher values, that range from 1.2 to 1.9, and 3.3 for the configuration that was characterized by a brittle failure mode. The average calculated value was 1.74.

Type of distribution	Test configuration											
	9	10	11	12	13	14	15	16	17	18	19	20
<b>Normal</b>												
$F_{0.05}$ [kN]	4.12	5.95	2.94	5.51	6.69	5.78	6.90	6.07	7.53	7.06	9.39	7.93
$F_{0.95}$ [kN]	6.39	7.97	6.89	7.00	8.38	10.07	8.77	9.67	9.53	9.14	10.81	11.73
$\gamma_{ov}$ [-]	1.55	1.34	2.34	1.27	1.25	1.74	1.27	1.59	1.27	1.29	1.15	1.48
<b>Log-Normal</b>												
$F_{0.05}$ [kN]	4.20	6.00	3.18	5.52	6.74	5.97	6.95	6.20	7.55	7.14	9.42	7.99
$F_{0.95}$ [kN]	6.48	8.02	7.21	7.05	8.40	10.29	8.79	9.83	9.58	9.15	10.81	11.95
$\gamma_{ov}$ [-]	1.54	1.34	2.27	1.28	1.25	1.72	1.26	1.59	1.27	1.28	1.15	1.50
<b>EN14358</b>												
$F_{0.05}$ [kN]	3.81	5.62	2.64	5.23	6.41	5.27	6.59	5.59	7.16	6.75	9.13	7.30
$F_{0.95}$ [kN]	7.14	8.56	8.67	7.45	8.83	11.63	9.27	10.91	10.11	9.67	11.16	13.08
$\gamma_{ov}$ [-]	1.88	1.52	3.28	1.42	1.38	2.21	1.41	1.95	1.41	1.43	1.22	1.79

Figure 19: Overstrength values for the configurations tested in (Gavric et al, 2012)<sup>33</sup>.

In (Gavric et al, 2015)<sup>34</sup> the results from the tests performed on hold-down and angle brackets connectors loaded in both tension and shear are presented. The 8 configurations investigated recreate CLT-foundation and CLT-CLT (wall-floor) connection types. Here as well one monotonic and six cyclic tests were performed, while the 5<sup>th</sup> and 95<sup>th</sup> percentile values were evaluated according to EN14358. The OSF average value for hold-down loaded in tension were found to be 1.3, while in shear the ratios were found to be 1.25 and 1.38, depending on the configuration (CLT-CLT and CLT-foundation respectively). For angle brackets connecting foundation to CLT wall panel, the overstrength factors range from 1.16 to 1.23 depending on the direction of loading (tension and shear respectively). Angle brackets connecting CLT wall to CLT floor were found to have higher overstrength ratios, namely 1.44 in tension and 1.40 in shear, due to the larger scatter of the experimental results.

**Table 2** Mechanical properties of hold-down connections according to EN 12512 [11] with overstrength factors ( $\gamma_{Rd}$ )

Mechanical property	Test configuration no.							
	1		2		3		4	
	$x_{mean}$	COV	$x_{mean}$	COV	$x_{mean}$	COV	$x_{mean}$	COV
$k_{cl}$ (kN/mm)	4.51	14.31	2.65	19.27	3.40	33.25	1.56	16.20
$k_{pl}$ (kN/mm)	0.75	14.24	0.44	19.13	0.28	7.27	0.21	5.43
$F_y$ (kN)	40.46	8.11	32.21	4.52	3.61	35.59	2.72	28.13
$v_y$ (mm)	8.81	21.76	11.91	19.83	1.13	42.30	1.71	17.23
$F_{max}$ (kN)	48.33	5.37	36.21	5.45	–	–	–	–
$F_{max(3rd)}$ (kN)	41.33	7.53	31.27	7.68	–	–	–	–
$v_{max}$ (mm)	20.30	14.17	21.52	11.00	–	–	–	–
$F_u$ (kN)	38.79	5.31	30.22	12.80	–	–	–	–
$v_u$ (mm)	23.75	13.82	22.99	9.51	–	–	–	–
$D$ [–]	2.76	16.21	1.97	13.75	–	–	–	–
$F_{30}$ (kN)	–	–	–	–	9.98	7.03	7.88	4.78
$D_{30}$ (–)	–	–	–	–	31.26	43.50	18.73	20.00
$\Delta F_{1-3}$ (%)	15.90	34.59	66.30	9.05	12.45	25.48	10.98	20.18
$v_{eq(1st)}$ (%)	8.50	5.70	8.11	9.98	19.84	13.91	21.38	6.93
$v_{eq(3rd)}$ (%)	2.78	17.29	3.60	24.40	14.63	17.79	16.09	14.86
$F_{0.05}$ (kN)	42.40	–	31.59	–	8.48	–	7.04	–
$F_{0.95}$ (kN)	54.95	–	41.40	–	11.70	–	8.80	–
$\gamma_{Rd}$ (–)	<b>1.30</b>	–	<b>1.31</b>	–	<b>1.38</b>	–	<b>1.25</b>	–

**Figure 20:** Overstrength values for the configurations tested in (Gavric et al, 2015)<sup>34</sup>.

Mechanical property	Test configuration no.							
	5		6		7		8	
	$x_{\text{mean}}$	COV	$x_{\text{mean}}$	COV	$x_{\text{mean}}$	COV	$x_{\text{mean}}$	COV
$k_{cl}$ (kN/mm)	2.53	9.72	2.98	22.05	2.09	16.41	1.10	12.34
$k_{pl}$ (kN/mm)	0.42	10.11	0.50	22.01	0.35	16.56	0.18	11.95
$F_y$ (kN)	19.22	2.73	11.12	9.69	22.98	5.19	16.61	7.46
$v_y$ (mm)	7.26	9.04	3.97	28.12	11.74	5.87	13.73	7.27
$F_{\text{max}}$ (kN)	23.47	4.32	12.57	7.71	26.85	3.15	19.91	6.95
$F_{\text{max}(3rd)}$ (kN)	18.59	9.72	10.96	7.80	18.80	10.25	14.26	9.75
$v_{\text{max}}$ (mm)	17.69	9.62	7.10	10.62	28.51	14.75	29.09	7.01
$F_u$ (kN)	18.74	4.32	10.06	7.68	21.48	3.15	15.86	7.59
$v_u$ (mm)	23.19	6.14	20.01	46.39	31.86	0.33	52.26	2.21
$D$ (-)	3.21	6.86	5.40	54.20	2.63	6.03	3.97	10.81
$\Delta F_{1-3}$ (%)	22.85	32.43	9.26	9.32	32.59	9.31	28.20	6.79
$v_{\text{eq}(1st)}$ (%)	12.33	5.43	7.40	11.71	22.75	5.93	17.49	5.59
$v_{\text{eq}(3rd)}$ (%)	7.07	19.17	1.74	10.90	14.01	6.84	11.17	14.15
$F_{0.05}$ (kN)	21.16		10.45		24.89		16.80	
$F_{0.95}$ (kN)	26.00		15.05		28.93		23.49	
$\gamma_{Rd}$ (-)	<b>1.23</b>		<b>1.44</b>		<b>1.16</b>		<b>1.40</b>	

Figure 21: Overstrength values for the configurations tested in (Gavric et al, 2015)<sup>34</sup>.

The authors in both (Gavric et al, 2012)<sup>33</sup> and (Gavric et al, 2015)<sup>34</sup> underline the fact that for connections that were not experimentally tested, higher values that take into account the difference between the analytical prediction (Johansen formulas) and the actual experimental values, should be used for the OSF.

A formally different approach is presented in (Schick et al, 2013)<sup>35</sup> and (Vogt et al, 2014)<sup>36</sup>. Here the overstrength factor is determined through the following equation:

$$\gamma_{Rd} = \gamma_{mat} \cdot \gamma_{mech} \cdot \gamma_{0.95} = \frac{R_m^*}{R_k} \cdot \frac{R_{exp,m}}{R_m^*} \cdot \frac{R_{exp,0.95}}{R_{exp,m}} \quad (6)$$

Where  $R_k$  is the design value according to code provisions,  $R_m^*$  is the mean value of resistance calculated with the mean values of material properties (instead of the characteristic ones),  $R_{exp,m}$  is the mean value of strength capacity according to test results and  $R_{exp,0.95}$  is the 95% quantile of the experimental distribution of strength.

The partial coefficient  $\gamma_{mat}$  then takes into account the spread between the characteristic resistance calculated according to design provisions and the one calculated using mean values for the material properties.  $\gamma_{mech}$  considers the “hidden reserves” that is present from the difference between calculated and experimental values. Finally,  $\gamma_{0.95}$  is defined as the ratio between the 95<sup>th</sup> percentile and the mean value from testing.

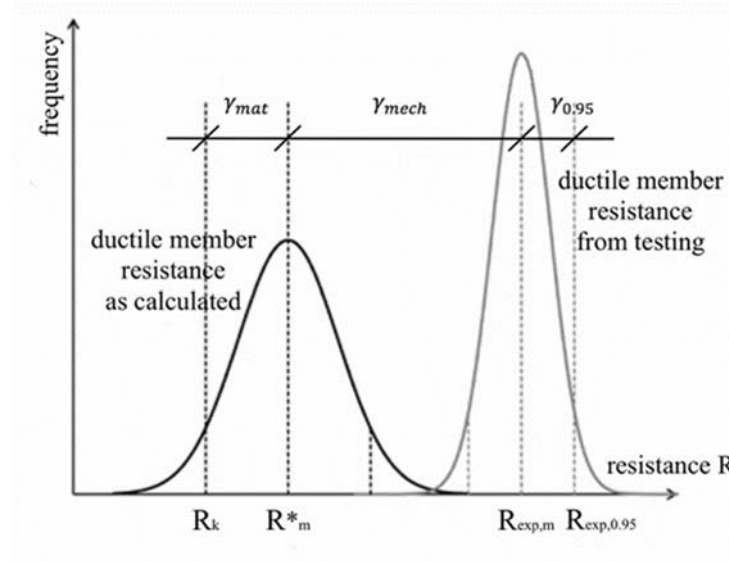


Figure 22: Concept of overstrength.

A closer look at the equation (6) reveals that the differences with the definition found in (Jorissen A. & Fragiacomio M., 2011)<sup>12</sup> is only in how the various contributions to evaluate  $\gamma_{Rd}$  are defined. Ultimately in fact, in both the procedures  $\gamma_{Rd}$  depends ultimately only on the ratio  $R_{c,0.95}/R_k$ .

Relying on data obtained by experimental investigation on light-frame timber shear walls, the authors calculated the partial factor above explained for every configuration tested and derived the final overstrength factor as the product of the mean values of the partial factors. The mean value for  $\gamma_{mat}$  was found to be 1.30, while  $\gamma_{mech}$  had instead a mean value of 1.33 and  $\gamma_{0.95}$  a mean value of 1.28.

Multiplication of partial over-strength factors leads to:

$$\gamma_{Rd} = 1.3 \cdot 1.33 \cdot 1.28 \cong 2.20$$

The authors then state that if the same mechanical over-strength is expected for the wall element and connection then the over-strength factor  $\gamma_{mech}$  can be decreased to 1.0 reducing thus  $\gamma_{Rd}$  to:

$$\gamma_{Rd} = 1.3 \cdot 1.0 \cdot 1.28 \cong 1.65$$



Finally, an alternative approach to determine the overstrength factor is presented in (Brühl et al, 2014)<sup>37</sup>. The purely experimental approach is here replaced by a probabilistic analysis conducted with a Monte Carlo simulation.

The investigated connection is a moment-resisting joint in the middle of a GL24h beam that the authors had already experimentally tested. The bending resistance is split in a compression force acting on the wood through an interposed steel plate and in a tensile force transferred via steel fasteners. Three different geometrical configurations of dowels (S235, 12 mm diameter) have been tested.

		tensile strength $f_u$ [MPa]	diameter [mm]	timber density $\rho$ [kg/m <sup>3</sup> ]	bending strength $f_m$ [MPa]	width [mm]	height [mm]	model uncertainty [-]
distribution		log-normal [21]	normal	normal [22]	log-normal [22]	normal	normal	log-normal [21]
test	2x4 mean value	581 ↑	12 ↑	441.7	33.8	180 ↑	320 ↑	1 ↑
	3x3 mean value	581 ↓	12 ↓	449.6	33.9	180 ↓	320 ↓	1 ↓
	5x2 mean value	581 ↓	12 ↓	440.3	33.4	180 ↓	320 ↓	1 ↓
	COV	0.04 [21]	0.001	0.1 [22]	0.15 [22]	0.0025	0.0015	0.1 [21]

Figure 23: Input variables, figure taken from (Brühl et al, 2014)<sup>37</sup>.

The simulation is built on the distributions (normal and log-normal) of the basic material and of the geometrical properties taken from previous tests or from literature. The model uncertainty is also taken into account with a log-normal distribution with mean value of 1 and coefficient of variation set at 0.1 according to (Köhler, 2006)<sup>38</sup>.

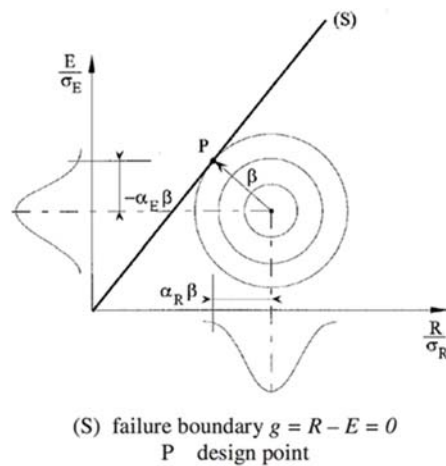


Figure 24: Limit state function and failure line.

A reliability analysis was conducted by defining the limit state function  $g$ :

$$g = R - E \tag{7}$$

The two terms R and E, that usually represent the resistance and the effect on the system, in this case are set respectively as the resistance of the brittle element (moment resistance of the wooden beam) and the strength capacity of the ductile one (resistance of the dowelled connection) multiplied by an overstrength factor. The limit state function then becomes:

$$g = W_{net} \cdot f_m - X_M \cdot \kappa_{cs} \cdot n \cdot F_{v,Rk} = M_{beam} - X_M \cdot \kappa_{cs} \cdot M_{joint} \quad (8)$$

Where the factor  $\kappa_{cs}$  is the inverse of the overstrength factor  $\gamma_{Rd}$

The outcomes of the limit state function  $g$  can then be processed by sampling the basic variables (tensile strength of the connector, geometrical data, timber density, bending strength, model uncertainty) at random according to their distribution functions (normal and lognormal). The outcomes might be in the failure domain ( $g < 0$ ) or in the safe domain ( $g > 0$ ). The reliability index  $\beta = \mu_g / \sigma_g$  is determined from the statistical distribution of  $g$  obtained by 108 calculations, for each input values of  $\kappa_{cs}$ .

The authors derive therefore the normalized overstrength factor  $k_{cs}$  through the relation:

$$k_{cs} = \kappa_{cs} \cdot \frac{M_{joint,design}}{M_{cs,design}} \quad (9)$$

The expression for the reliability line is then calculated as:

$$\beta = 7.65 - 7.65 \cdot k_{cs} \quad (10)$$

The verification of the reliability line shows a reliability index  $\beta$  of zero (failure probability of 0.5, indifferent condition) for a  $k_{cs}$  value of one.

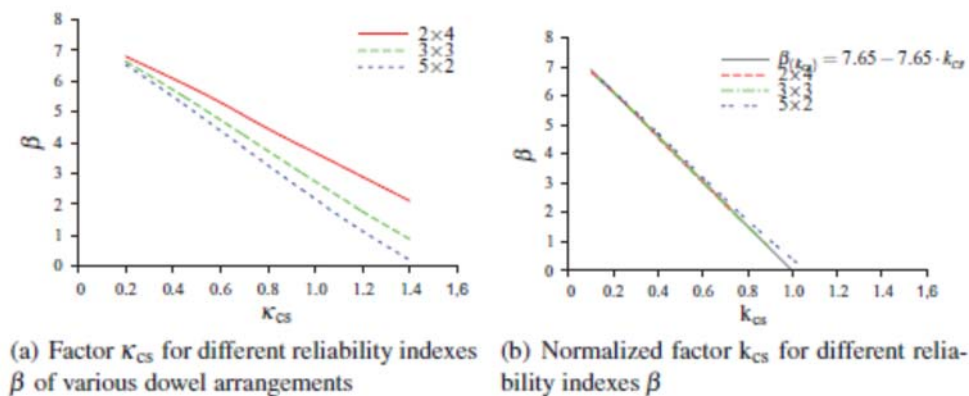


Figure 25: Factor  $k_{cs}$  for different reliability index, figure taken from (Brühl et al, 2014)<sup>37</sup>.

Several suggestions for a correct application of the CD principles are given throughout all the previously presented papers and in (Follesa et al, 2011)<sup>17</sup>, where the authors sum these up in a set of indications that will be used as basis for the draft proposal for the new section 8 of EC8.

A summary of these suggestion is also presented in (Gavric et al, 2013)<sup>39</sup>. Here the author uses the results of several previous experimental tests, and critically discusses the typical failure mechanisms of connections and wall systems, the influences of different types of wall behaviour on mechanical properties and energy dissipation, and provides a guideline on how the CD approach should be used for a proper seismic design.

The importance of the developing a ductile failure mode at connection level is underlined, and a guideline on how to achieve such failure mode is presented. First of all, the designer shall ensure that the failure mode of the fastener is of the ductile type, corresponding to either one or two plastic hinge formations. This is achieved once again by applying equation (1):

$$R_{b,Rd} \geq \gamma_{Rd} \cdot R_{d,Rd} \quad (1)$$

Where  $R_{d,d}$  is the lowest design shear resistance associated with the ductile failure mode (modes b), d) and e) for steel to timber connections, and modes d), e) and f) for timber to timber connections) and  $R_{b,d}$  is the lowest resistance associated with the brittle failure mode (modes a) and c) for steel to timber connections, and modes a), b) and c) for timber to timber connections). In addition, other possible brittle failure mode as shear plug, splitting of timber, tear out, resistance of net section of the metal plate, or withdrawal of the fastener and pull-through resistance of bolts shall be avoided as well by the application of eq (1).

Once the ductility at the connection level is ensured, it is suggested that, at the wall level, the plasticization should occur in the hold-downs and angle brackets loaded in tension, rather than in angle brackets loaded in shear. This because in this way there will be no residual slip at the end of the seismic event, and the self-weight can act as stabilizing load and re-centre the building. This behaviour can be ensured again using eq (1), hence ensuring that the total shear resistance of the angle brackets is larger than 1.3 times the design value of the uplift resistance of hold-downs and angle brackets. Nevertheless, still at the wall level, the CLT panel resistance should be larger than 1.3 times the connection resistance.

At the building level, some other suggestions are given. In order to ensure a proper uniform distribution of lateral forces from the slabs to the wall panels below, the floor panels should act as non-dissipative rigid diaphragms, and therefore any floor to floor connection should be over-designed according the same principle. Similarly, floor to wall connections should also be over-designed to guarantee an efficient transmission of forces. Furthermore, in order to ensure a box-type behaviour perpendicular wall to wall connections should as well be designed in accordance to eq(1).



# 3 EXPERIMENTAL INVESTIGATION

This chapter presents the experimental programme carried out at the laboratory of Norges miljø og biovitenskapelige universitet (NMBU). The aim is to evaluate the overstrength factor for the different types of connection tested. In-plane monotonic shear tests were performed on screwed connections between adjacent CLT panels.

After a brief description of the testing, the material and equipment used is listed and explained. The setting up of the specimens is then presented, describing the method and type of work realised. Attention has been paid to the analytical prediction of the connection resistance. Then the results of the testing programme are listed, and after a description on how the data has been processed a discussion of these follows.

### 3.1 Tests Overview

Several researches have pointed out that in order to ensure an overall higher ductile behaviour in CLT buildings, seismic resistant shear walls, in each perpendicular direction, shall be segmented. Segmented walls (Figure 26) are composed of more than one panel connected with joints made with mechanical fasteners inserted perpendicular to the shear plane. The testing programme carried out is based on push-out tests employed to evaluate the shear resistance of such type of connections.

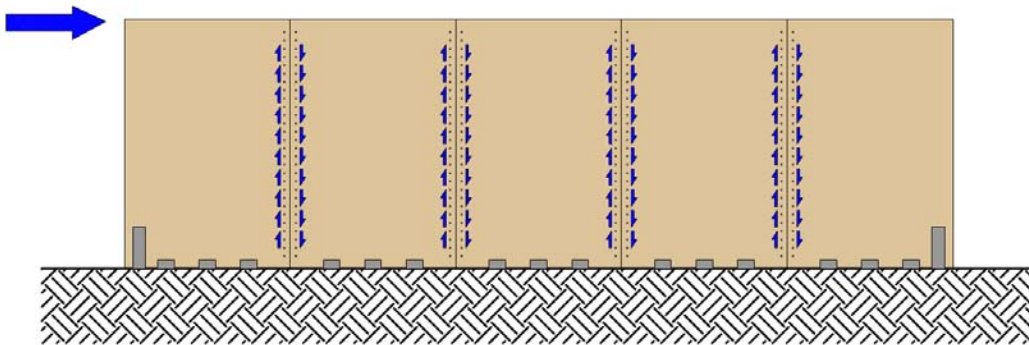


**Figure 26: Segmented shear wall.**

The connection between two adjacent parallel panels can be made in several ways, the most common ones are shown in Figure 27. The cuts on each end of the panels needed to make a spline joint (Figure 27 a) and a lap joint (Figure 27 b) are made during the manufacturing process. One of the great advantages of building with CLT is, in fact, the high degree of prefabrication. The panels arrive on site finished, and for the most are here just assembled together, allowing in this way to spare a lot of time during the construction phase. These cuts are easily made in the production line, but to obtain such cuts with the machinery at disposal was not possible, therefore configuration c) was chosen.

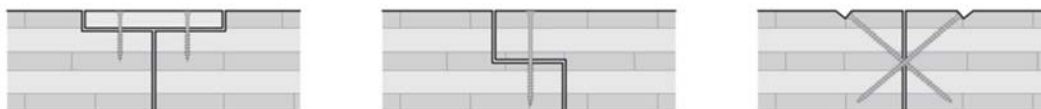


**Figure 27: Possible ways of connecting two adjacent parallel panels.**

These connections are not only used to join vertical wall panels, but are also employed as connections between adjacent floor panels. In these circumstances the joints are obviously placed along a direction parallel to the floor's span direction. The connections between

floor panels, however, shall never be regarded as dissipative, but rather be designed with sufficient overstrength.

Although it could seem that the screws are inserted with a 45° angle, such angle has no influence on the connection resistance, in fact, relatively to the shear plane and the force direction the screws are inserted with a 90° angle, and thus subjected only to a shear load.

Three specimens with a size of 350 mm x 200 mm are connected to each other along their longer narrow side through pairs of crossed fully-threaded screws, both inserted perpendicularly to the direction of the grain of the outer layer. A configuration composed by three specimens was preferred to a configuration composed by two because of the eccentricity that would have arisen during the loading process in the latter.



**Figure 28: Specimen setup and loading direction.**

The two side elements are held down through specifically designed steel constraints while the middle element is loaded through a load cell.

Several configurations have been tested ranging between three different CLT panel thickness (80, 100 and 120 mm) and different length, diameter and type of screws.

The experimental programme should have included both monotonic and cyclic tests, but unfortunately, the software through which the machine is controlled did not allow to set up the necessary input to perform cyclic tests.



## 3.2 Materials and equipment

### 3.2.1 Material gathering

Originally a set of ready-made wooden specimens were supposed to be delivered by a CLT producer, but unfortunately, far beyond the agreed deadline, they told us that they were not able to do so, and therefore an alternative solution was necessary.

The wooden specimens are, in fact, made from left-over CLT boards that were collected from two different building sites. Two panels, with a thickness of 80mm and with a size of approximately 1m x 1.5m delivered by Cross Timber System, were taken from the construction site of the new Bjørkelangen school. The remaining panels of various size ranging from 0.5m x 0.5m up to 1.8m x 1.8m with a thickness of 100mm and 120mm, were picked up from the construction site for the student housing project at Kringsjø Student Village in Oslo, in this case the supplier was Mayr Melnhof Holz.



**Figure 29: Making of the specimens.**

The boards were cut first into smaller parts with a chain saw and then further cut down into the final size using a circular saw for the 80mm panels and a band saw for the 100mm and 120mm ones. Maximizing the exploitation of the material was among the criteria for the choice of the size of the specimens.

The specimens were then stored in a controlled environment with 20°C and 65% of relative humidity.

### 3.2.2 CLT

CLT or Cross Laminated Timber is defined in EN 16351:2015<sup>40</sup> as structural timber consisting of at least three layers of which a minimum of three are orthogonally bonded.

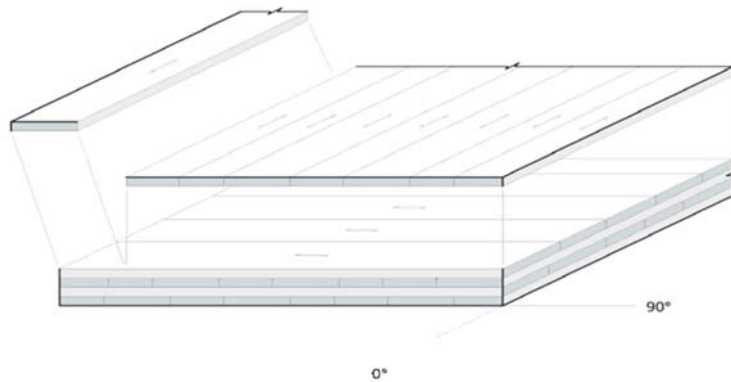


**Figure 30: CLT panel.**

The softwood boards of the individual layers are strength graded, technically dried and planed. They are connected to each other in the longitudinal direction by means of finger joint whereas in transversal direction the boards may be edge bonded or non-edge bonded. The panels are intended to be used in service class 1 and 2 according to EN 1995-1-1<sup>16</sup>. Specification and regulations for CLT may be taken from EN 16351:2015<sup>40</sup> and from European Technical Approvals (ETA) documents provided by the producers.

In this experimental programme three different types of CLT panel have been tested. The five layer panels with thickness of 100 and 120 mm are produced by Mayr-Melnhof Holz and the three layer panels with a thickness of 80 mm produced by Cross Timber Systems SIA.



**Figure 31: Wooden specimens.**

### 3.2.2.1 MM crosslam - 5 layers, 100 mm

This type of panel is made by 5 layers, each one with a thickness of 20 mm, and has an overall thickness of 100 mm. The relevant material properties are either taken from the technical approval document ETA-09/0036 of 30.06.2015 or directly measured in the lab.



**Figure 32: 5 layers, 120mm thick specimen.**

Sample	Density [kg/m <sup>3</sup> ]
1	513.7
2	461.5
3	477.6
4	496.9
5	465.2
Mean value	483.0

**Table 1: Density 120mm panels.**

The boards are strength graded as C24 according to EN 338<sup>41</sup>. To be more precise, as stated in the ETA, the cover layers are graded as C24 while in the inner layers more than 90% of the boards should be at least C24 and less than 10% of them should be at least C16.

### 3.2.2.2 MM crosslam - 5 layers, 120 mm

This type of panel is made by 5 layers, the outer layers have a thickness of 30 mm whereas the three inner layers have a thickness of 20mm. The overall thickness is 120 mm. The relevant material properties are either taken from the technical approval document ETA-09/0036 of 30.06.2015 or directly measured in the lab.

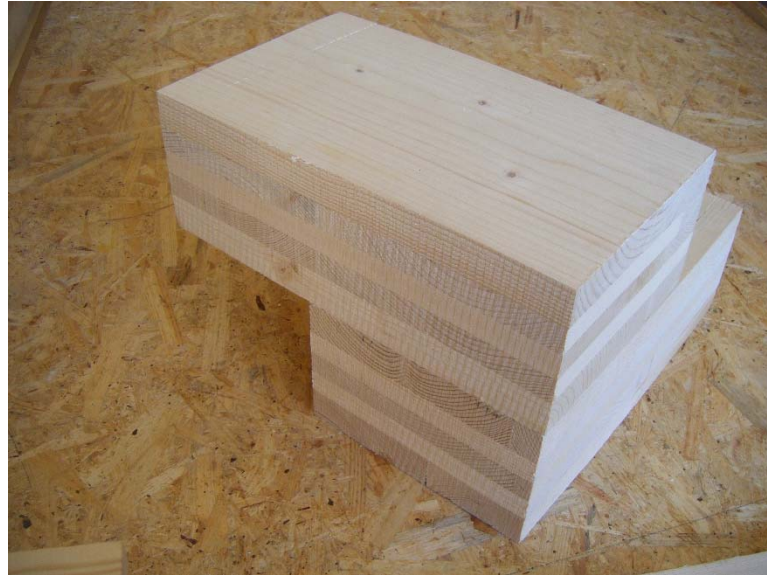


**Figure 33: 5 layers, 100mm thick specimen.**

<b>Sample</b>	<b>Density [kg/m<sup>3</sup>]</b>
1	456.5
2	492.4
3	457.7
4	511.0
5	481.1
Mean value	479.8

**Table 2: Density 100mm panels.**

The boards are strength graded as C24 according to EN 338<sup>41</sup>. To be more precise, as stated in the ETA, the cover layers are graded as C24 while in the inner layers more than 90% of the boards should be at least C24 and less than 10% of them should be at least C16.

### 3.2.2.3 Cross Timber System CLT - 3 layers, 80 mm

This type of panel is made by 3 layers, the outer layers have a thickness of 30 mm whereas the inner one has a thickness of 20mm. The overall thickness is 80 mm. The relevant material properties are either taken from the technical approval document ETA-15/0906 of 24.02.2016 or directly measured in the lab.



**Figure 34: 3 layers, 80mm thick specimen.**

Sample	Density [kg/m <sup>3</sup> ]
1	532.0
2	497.3
3	471.6
4	508.5
5	503.9
Mean value	502.7

**Table 3: Density 80mm panels.**

The boards are strength graded as C24 according to EN 338<sup>41</sup>. To be more precise, as stated in the ETA, the cover layers are graded as C24 while in the inner layers more than 90% of the boards should be at least C24 and less than 10% of them should be at least C16.

### 3.2.3 Screws

For the kind of connection analysed, the usually employed type of fasteners is a fully-threaded self-tapping screw. These screws provide a similar withdrawal resistance in both sides of the connection thanks to the full-length thread and the negligible contribution of the small diameter head.

In this testing programme, two main types of self-tapping screws have been employed: VGZ screws produced by Rothoblass that have a constant thread through their length and WT screws produced by SFS that have two different and separated threads through their length.

The maximum length for the fasteners was calculated by multiplying the panel thickness by the square root of 2. Then the commercial screws length was chosen with the purpose of getting as close as possible to the theoretical maximum length without overcome it. The diameter of the screws ranges between 6,2 to 9 mm and their length between 100 and 160 mm.



**Figure 35: Screws used to join the specimens.**

### 3.2.3.1 Rothoblaas – VGZ

This fully-threaded self-tapping type of screw is produced by Rothoblaas from carbon steel with a characteristic yield strength of  $f_{y,k} = 1000 \text{ N/mm}^2$ . The relevant mechanical properties of the screws are taken from the technical approval document ETA-11/0030 of 2016-04-07. For the testing programme 3 different sizes of screws have been employed accordingly with the thickness of the panels connected.

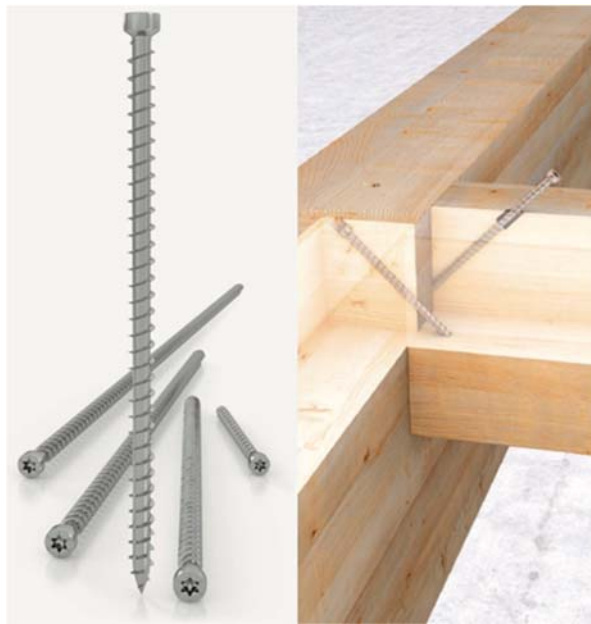


Figure 36: VGZ screw detail.

Name	Diameter [mm]	Length [mm]	Panel thickness [mm]
VGZ7100	7	100	80
VGZ7140	7	140	100/120
VGZ9160	9	160	120

Table 4: VGZ screws geometrical data.

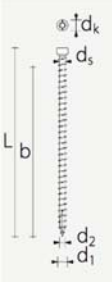
	VGZ CONNECTOR		
	Nominal diameter	$d_1$ [mm]	7
Head diameter	$d_k$ [mm]	9,50	11,50
Tip diameter	$d_2$ [mm]	4,60	5,90
Shank diameter	$d_s$ [mm]	5,00	6,50
Pre-bored hole diameter	$d_1$ [mm]	4,0	5,0
Characteristic yield moment	$M_{y,k}$ [Nmm]	14174,2	27244,1
Characteristic extraction-resistance parameter	$f_{ex,k}$ [N/mm <sup>2</sup> ]	11,7	11,7
Characteristic tensile strength	$f_{tens,k}$ [kN]	15,4	25,4
Characteristic yield strength	$f_{y,k}$ [N/mm <sup>2</sup> ]	1000	1000

Figure 37: VGZ screws mechanical characteristics.

3.2.3.2 SFS – WT

This self-tapping screw is produced by SFS from special carbon steel. The special feature of this screw is that the thread is divided into three sections: threaded length (close to the drill tip), non-threaded shaft and clamping thread (close to the head). As a result, this configuration is able to apply a compression between the two elements connected. The relevant mechanical properties of the screws are taken from the technical approval document ETA-12/0063 of 2012-06-18. For this testing programme 2 different sizes of screws have been employed accordingly with the thickness of the panels connected.



Figure 38: WT screw detail

Name	Diameter [mm]	Length [mm]	Panel thickness [mm]
WT-T-6.5	6.5	160	120
WT-T-8.2	8.2	160	120

Table 5: WT screws geometrical data.

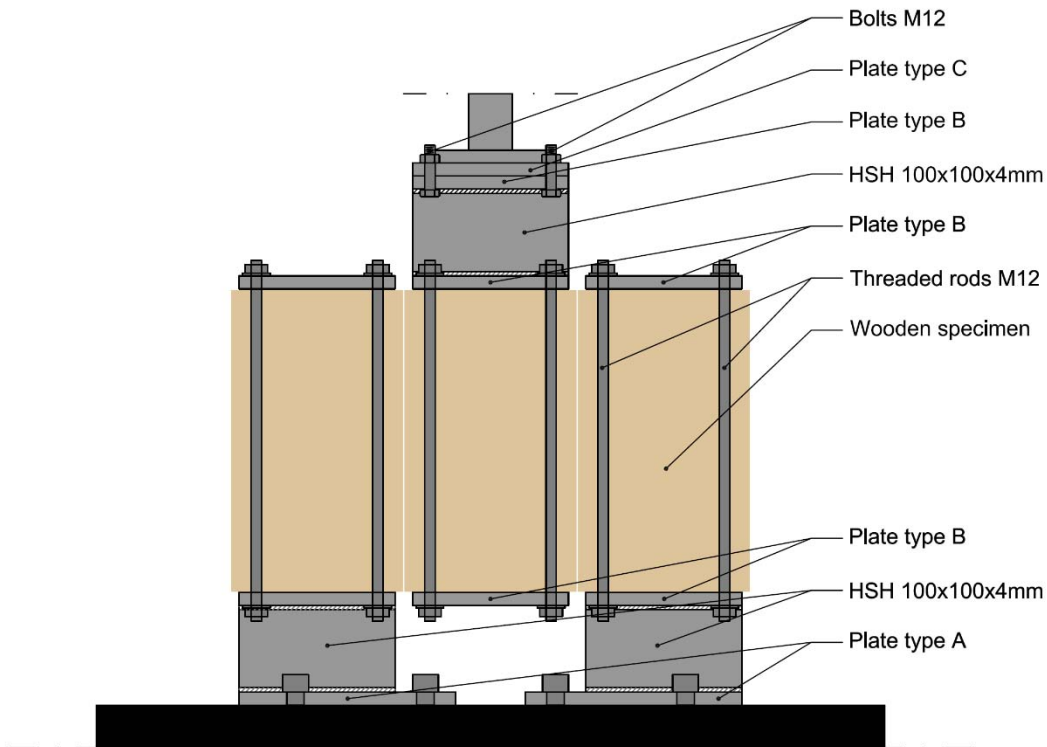
	WT CONNECTOR		
	Parameter	Value	Value
Nominal diameter	$d_1$ [mm]	6,5	8,2
Locking thread diameter	$d_3$ [mm]	6,50	8,90
Head diameter	$d_4$ [mm]	8,00	10,00
Tip diameter	$d_2$ [mm]	4,00	5,40
Shank diameter	$d_5$ [mm]	4,60	6,30
Characteristic yield moment	$M_{yk}$ [Nmm]	12700	19500
Characteristic extraction-resistance parameter	$f_{ex,k}$ [N/mm <sup>2</sup> ]	12,9	13,35
Characteristic tensile strength	$f_{tens,k}$ [kN]	14,4	28,6
Characteristic yield strength	$f_{yk}$ [N/mm <sup>2</sup> ]	990	870

Figure 39: WT screw mechanical characteristics.



### 3.2.4 Steel holding system

To support the wooden specimens, giving enough room to the middle piece to deform downward, and transfer the load coming from the load cell, a steel holding system was designed. The system is composed of two supports that can be fixed to the base of the hydraulic machine, and a part that can be connected to the load cell. The former are made by a hollow-square profile to which a bottom steel plate (type A) and a top steel plate (type B) are welded, the latter is also made by a hollow-square profile with two plates of the same type (type B) welded over and under. The upper plate is then connected through M12 bolts to another plate (type C) which is connected to the load cell via a set of countersunk bolts. The system was designed to be able to permit cyclic loadings. If needed the specimens can in fact, be held together with a set of plates (type B) connected to the opposite one through threaded steel rods, allowing so to apply both tension and compression loads. In addition, all the steel elements were designed to remain elastic during the testing. The elongation in the threaded rods and the deflection of the steel plates were checked according to the rules of mechanics and the size chosen accordingly.



**Figure 40: Front view.**

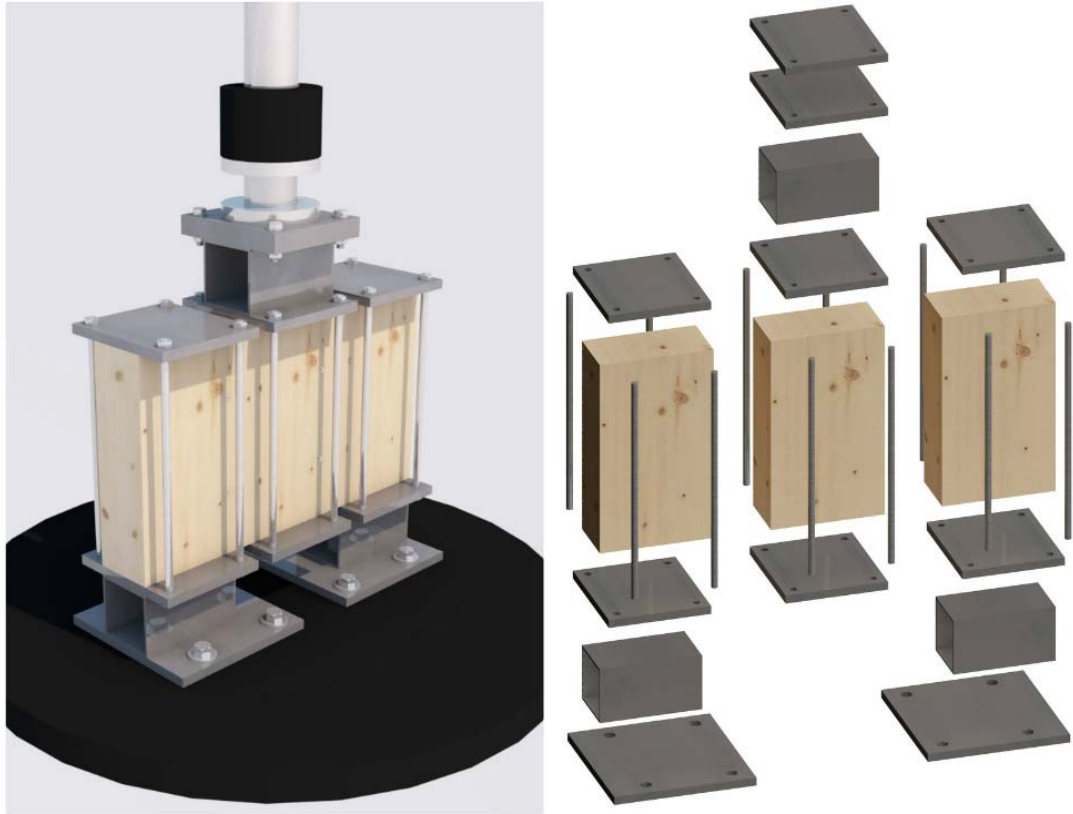


Figure 41: 3D view and exploded view.

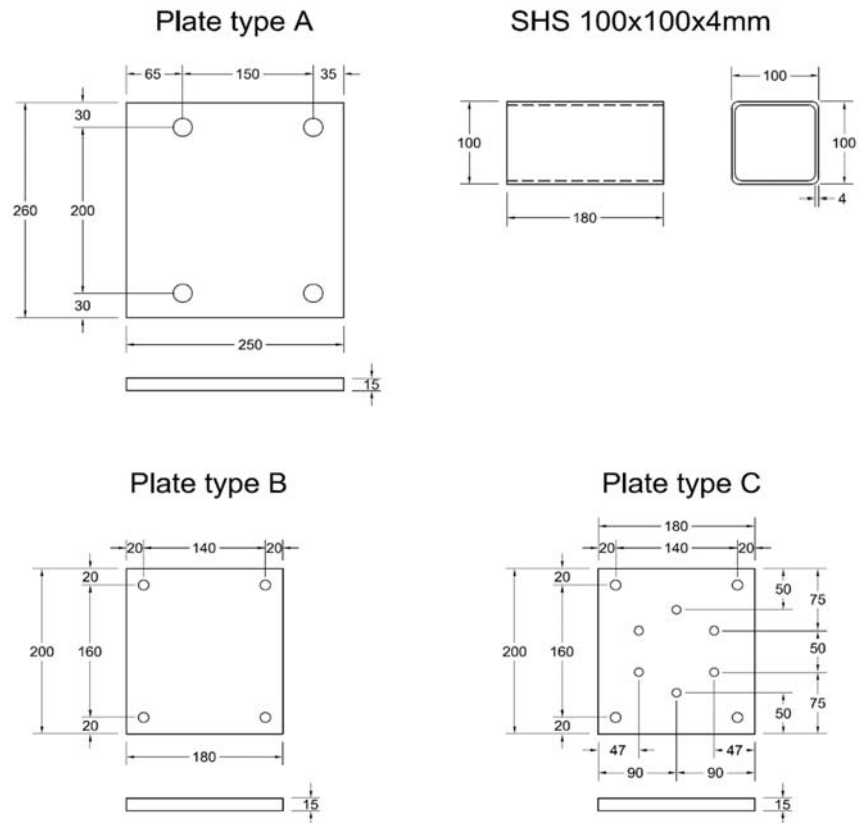


Figure 42: Steel plates details.

### 3.2.5 Testing machine

All samples were tested with a Instron SATEC series 8800 model 300KN static hydraulic universal testing system. The machine has a maximum capacity of 300 kN and can measure displacement data with a maximum precision of  $10^{-3}$  mm. To measure the imposed load on the samples the load cell supplied with the machine was used.



**Figure 43: Testing machine.**

### 3.2.6 Displacement transducers

On each test two rectilinear displacement transducers Gefran PY2 F50 were fixed. The transducers have a double support of the control rod and return spring with a tip of M2.5 thread and stainless-steel ball, with a max stroke of 50mm. They were screwed into the two outermost CLT elements, while the support for the tip was an L-shaped aluminium profile which was attached to the middle element (Figure 46).

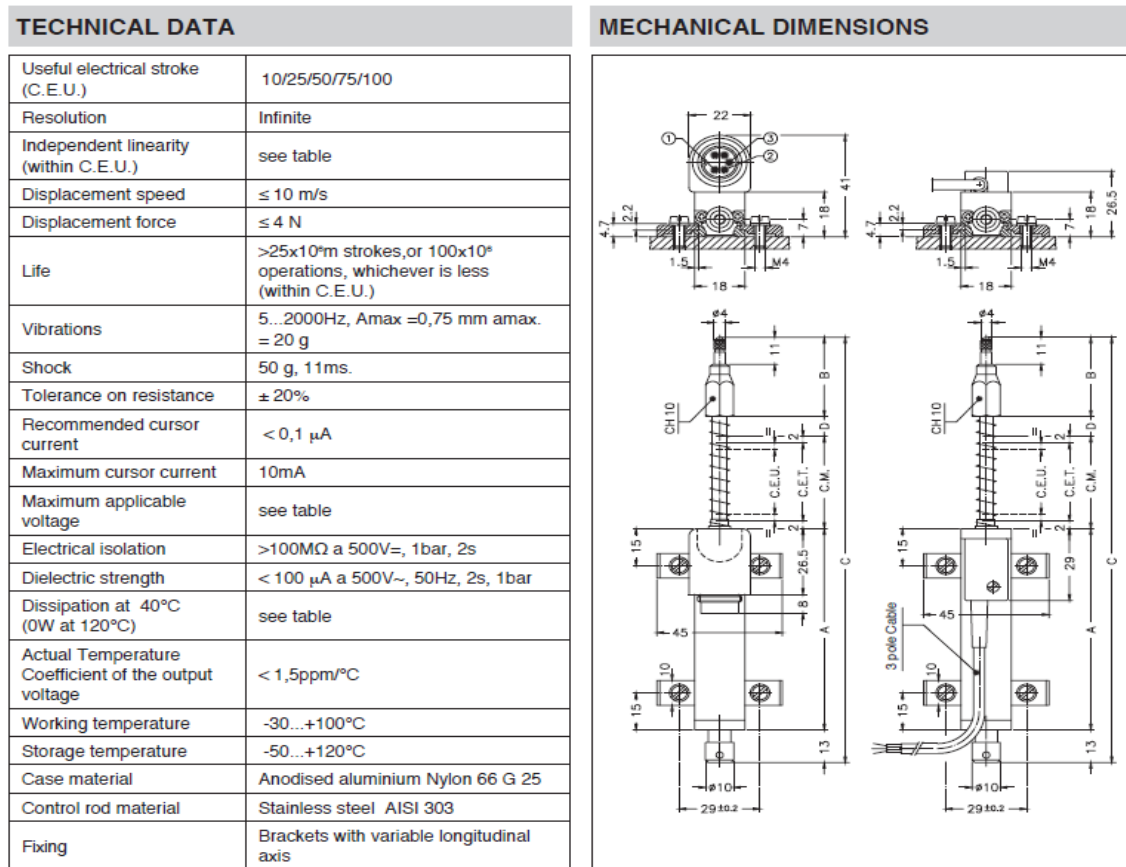


Figure 44: Displacement transducers data from producer.

MECHANICAL / ELECTRICAL DATA						
Model		10	25	50	75	100
Useful electrical stroke (C.E.U.) +1/-0	mm	10	25	50	76	101
Theoretical electrical stroke (C.E.T.) ±1	mm	C.E.U. +1			76	101
Resistance (C.E.T.)	kΩ	1	1	5	5	5
Independent linearity (within C.E.U.)	± %	0.3	0.2	0.1	0.1	0.1
Dissipation at 40° (0W at 120°C)	W	0.2	0.6	1.2	1.8	2.4
Maximum applicable voltage	V	14	25	60	60	60
Mechanical stroke (C.M.)	mm	C.E.U. + 5				
Case length (A)	mm	C.E.U. + 38				
Tip length (B)	mm	32	32	40	40	40
Total length (C)	mm	108	138	196	251	307
Quote (D)	mm	-	-	-	5	11

Figure 45: Displacement transducers data from producer.



**Figure 46: View of the transducers mounted on the specimen.**

### 3.3 Specimen setup

The specimens tested consist of three CLT elements connected to each other along their longer and narrow face through pairs of crossed fully-threaded screws. The screws are inserted, without pre-drilling, with their axes perpendicular to the grain direction of the surface layer and with an angle of 45° to the plane of the panels.



**Figure 47: Specimen set up.**

All the CLT panels employed are 350 mm long (in the grain direction of the outer layer) and 200 mm wide while the thickness varies between 80 mm (3 layers), 100 mm (5 layers) and 120 mm (5 layers) as already seen.

For each specimen, three CLT panels of the same thickness are placed close to each other and lined up to obtain a flat supporting surface. Then two clamps are installed to hold down the specimen while inserting the screws.

In order to keep the right angle to the panel surface, a specifically designed device has been build. It is made by a steel plate with a welded tube that forces the screw to maintain the right angle and the proper position. On the plate surface were drawn guidelines that indicated the right distance from the connection interface and thus the correct positioning.



**Figure 48: Ready made specimen.**

After the assembly of the specimen an identification code was assigned to every configuration. The first letter refers to the screw type: V for VGZ screws by Rothoblaas and W for WT screws by SFS. The following number indicates the nominal diameter of the screw (neglecting tenths of millimetre). Then, for some configurations, one more number is needed to distinguish between specimens with the same type and diameter of the screws but with different length: after a dash, the thickness of the panel is then specified and, consequently, the length of the screws is identified. Finally, a number from 1 to 5 is assigned to each specimen within a configuration to unambiguously identify every single specimen.

In the following table the tested configurations with their specifications are listed.

<b>Name</b>	<b>Screw Type</b>	<b>Diameter [mm]</b>	<b>Panel thickness [mm]</b>	<b>Screw length [mm]</b>
V7-80	VGZ Rothoblaas	7	80	100
V7-100	VGZ Rothoblaas	7	100	140
V7-120	VGZ Rothoblaas	7	120	140
V9	VGZ Rothoblaas	9	120	160
W6	WT SFS	6.5	120	160
W8	WT SFS	8.2	120	160

**Table 6: Screws specifications.**



**Figure 49: A view of all configurations.**



### 3.4 Connection resistance

A fundamental step before the experimental investigation is carried out is the analytical evaluation of the connection resistance. This is done by applying the plastic theory of connections known as Johansen’s theory<sup>42</sup> and implemented in EC5<sup>16</sup>. This operation provides an estimation of the expected forces involved in the tests and is necessary to determine the contribution to the overstrength factor arising from the difference between the actual characteristic strength capacity and the calculated one. Moreover, it is necessary to design the steel holding equipment needed.

#### 3.4.1 Minimum distances

The minimum distances indicated in EC5 refer to solid or glue-laminated timber, and are generally not valid for CLT. This is due to the cross-layered nature of the material that helps to prevent brittle failures such as plug shear and splitting. The reference investigation on this topic is the one by (Blaß & Uibel, 2007)<sup>43</sup> that rely on an experimental programme carried out at Karlsruhe University.

The proposed minimum distances, depending on which face of the panel the screws are inserted, are reported in Table 7. The same values can be found in the ETA document for the Rothoblaas VGZ screws, and in several other documents and manuals.

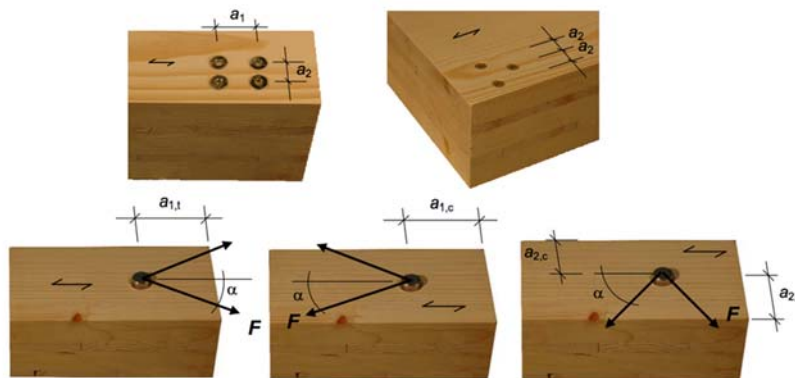
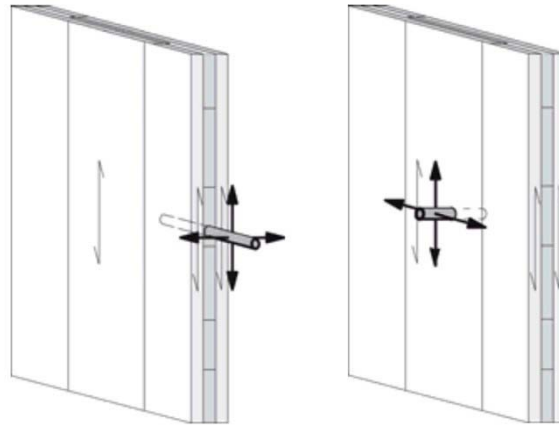


Figure 50: Minimum distances.

	$a_1$	$a_2$	$a_{3,c}$	$a_{3,t}$	$a_{4,c}$	$a_{4,t}$
Lateral face	4d	2.5d	6d	6d	2.5d	6d
Narrow face	10d	3d	7d	12d	5d	6d

Table 7: Minimum distances.

The type of connection employed could be quite complex to categorise since the screws pass through both the lateral face and the narrow one with an angle of 45°. Given that, in any case, the screws cross at least two layers, it seems correct to take in account the provisions for screws inserted in the lateral face of the CLT panels. The greater values proposed for fasteners inserted in the narrow face, in fact, are a consequence of the case in which the connector is inserted through only one layer with its axis parallel to the grain of that layer.



**Figure 51: Narrow and lateral faces.**

In the following the minimum distances for each kind of fastener are reported:

<b>Screw</b>	<b>d</b> [mm]	<b>a<sub>1</sub></b> [mm]	<b>a<sub>3,c</sub></b> [mm]	<b>a<sub>3,t</sub></b> [mm]
VGZ7	7	28	42	42
VGZ9	9	36	54	54
WT-T-6.5	6.5	26	39	39
WT-T-8.2	8.2	32.8	49.2	49.2

**Table 8: Minimum distances for each fastener.**

Each pair of screws is inserted keeping a distance of 100 mm from the upper and the lower narrow face of the specimen. As result, the distance between two pairs of screws in the direction of the grain is 150 mm. By comparing these values with the minimum distances, it is clear that the prescription is well satisfied.

Finally, the minimum distance between two crossed screws should be defined. In the ETA documents by Rothoblaas and SFS this distance is set at 1,5d, and it is mentioned for

crossed screws loaded in shear and in compression/tension. Given the lack of other provisions and considering that the interaction of the crossed screws, exclusively loaded in shear, only occurs in one point (in the interface between the panels), the minimum distance of  $1,5d$  was taken as reference, and a value of 20mm was adopted.

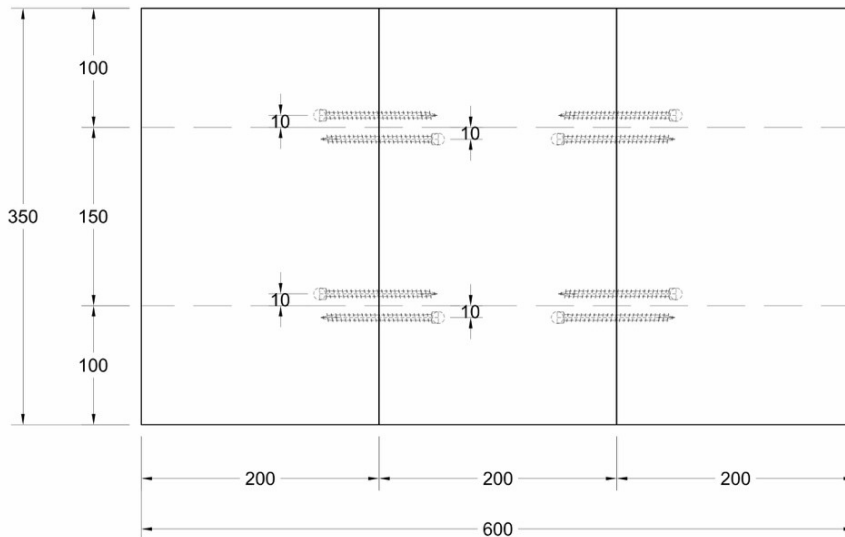


**Figure 52: Distances between the screws.**

### 3.4.2 Embedding strength and withdrawal capacity

Since the wooden elements involved in this connection are CLT panels, some adjustments to the evaluation of the embedding strength and withdrawal capacity of the screw proposed by the code are required

The analytical model prescribed by European standard is built on the assumptions that the employed fasteners are inserted perpendicularly to the direction of the wood grain and that the embedding resistance is constant through the length of the fastener. These hypotheses are not always satisfied in CLT panels due to their layered configuration.

The shear resistance of a fastener inserted in the lateral surface of a CLT panel can be calculated according to a modified Johansen theory that takes into account the variable embedding and withdrawal resistance of each of the crossed layers in accordance with its grain direction. This approach, however, leads to a disproportionate complication of the application of the Johansen theory.

The alternative approach is the one that still considers the original Johansen theory, with the difference of adopting a modified embedding and withdrawal resistance suited to the whole CLT panels.

Due to its greater simplicity and knowing that the results are as reliable as for the first method, the latter approach is usually adopted for design calculations and even included in the product certificates.

The characteristic embedding strength for fully-threaded self-tapping screws inserted in the lateral surface of the panel can be calculated according to the formula proposed by (Blaß and Bejtka, 2006)<sup>44</sup>.

$$f_{h,k} = 0.019 \cdot \rho_{B,k}^{1.24} \cdot d^{-0.3} \quad (11)$$

Where  $d$  is the nominal diameter of the screws in mm and  $\rho_{B,k}$  is the characteristic bulk density of the material in  $\text{kg/m}^3$ . This formulation is valid in case of products with layers of more than 9 mm in thickness. For the tested specimens made by CLT whose strength class of boards is C24, the characteristic density, according to EN 338<sup>41</sup>, is taken as  $\rho_{B,k} = 350 \text{ kg/m}^3$ . The nominal diameter of the screws ranges between 6,5 and 9 mm according to the specific connection configuration tested.

The obtained values of embedding strength are summarised in the following table:

Screw	d [mm]	$f_{h,k}$ [N/mm <sup>2</sup> ]
VGZ 7x100	7	15.13
VGZ 7x140	7	15.13
VGZ 9x160	9	14.03
WT 6.5x160	6.5	15.47
WT 8.2x160	8.2	14.43

**Table 9: Embedding strength**

The characteristic withdrawal resistance of fully-threaded self-tapping screws inserted in the lateral surface of the panel can be calculated according to (Blaß an Uibel, 2007)<sup>43</sup>:

$$F_{ax,k,s} = \frac{31 \cdot d^{0.8} \cdot l_{ef}^{0.9}}{1.5 \cdot \cos^2 \varepsilon + \sin^2 \varepsilon} \quad (12)$$

Where  $d$  is the nominal diameter of the screws in mm,  $l_{ef}$  is the effective screw penetration depth in mm, and  $\varepsilon$  is the screw angle in radians to the grain in the surface layer. In this case, the values of  $l_{ef}$  employed for VGZ screws are calculated as half of the length of the threaded part of the screw minus 5 mm of tolerance for the installation. For the WT screws, the values of  $l_{ef}$  employed should consider the non-threaded portion of the screw

in between the two threaded ones. Therefore, the minimum effective threaded length of the screw is derived by the ETA document without considering any tolerance for the installation. Finally, the value of  $\varepsilon$  is always  $90^\circ$  since the screws are inserted in the lateral surface of the panel perpendicularly to the direction of the grain of the surface layer.

The resulting values of  $F_{ax,k,s}$  shall be compared with the tensile load-bearing capacity of the screw's core cross-section  $F_{tens,k}$  according to the producers' approvals.

The obtained values of withdrawal strength are summarised in the following table:

Screw	$l_{ef}$ [mm]	$F_{ax}$ [N]
VGZ 7x100	40	5067
VGZ 7x140	60	5858
VGZ 9x160	70	8229
WT 6.5x160	65	5934
WT 8.2x160	65	7146

**Table 10: Withdrawal capacity.**

### 3.4.3 Yielding moment of the fasteners

On last component of the Johansen equations has to be defined: the characteristic yielding moment of the employed fastener.

These values are provided by the producers in their technical approvals but it is also possible to calculate them by using the formulations proposed by the standards. Both quantities are reported with the purpose of comparing the results.

According to EC5, the characteristic yielding moment of a cylindrical fastener shall be calculated through the following formula:

$$M_{y,Rk} = 0.3 \cdot f_{u,k} \cdot d_{ef}^{2.6} \quad (13)$$

Where  $f_{u,k}$  is the characteristic tensile strength of the steel in  $N/mm^2$  and  $d_{ef}$  is the effective diameter of the fastener in mm. It should be noted that for a fully-threaded screw, the effective diameter is defined as 1.1 times the core diameter:

In the following table, the results of the calculation of the characteristic yielding moments for the employed fasteners are reported together with the values included in European Technical Approval documents:

Screw	d <sub>core</sub> [mm]	d <sub>def</sub> [mm]	f <sub>uk</sub> [N/mm <sup>2</sup> ]	M <sub>yRk,EC5</sub> [Nmm]	M <sub>yRk,ETA</sub> [Nmm]
VGZ 7x100	4.6	5.06	1000	20319	14174
VGZ 7x140	4.6	5.06	1000	20319	14174
VGZ 9x160	5.9	6.49	1000	38811	27244
WT 6.5x160	4	4.4	990	13987	12700
WT 8.2x160	5.4	5.94	870	26822	19500

**Table 11: Fasteners yielding moment.**

It is worth noting that the values proposed and certified by producers are lower than those calculated according to the standards. Ultimately the more conservative values of the ETA document were adopted.

### 3.4.4 Fasteners shear resistance

Now that every component has been defined, the characteristic load-carrying capacity per shear plane per fastener, can be calculated. The resistance is then taken then as the minimum value found from the following expression, as prescribed by EC5

$$F_{v,Rk} = \min \left\{ \begin{array}{l} f_{h,1,k} \cdot t_1 \cdot d \quad (a) \\ f_{h,2,k} \cdot t_2 \cdot d \quad (b) \\ \frac{f_{h,1,k} t_1 d}{1 + \beta} \cdot \left[ \sqrt{\beta + 2\beta^2 \left[ 1 + \frac{t_2}{t_1} + \left( \frac{t_2}{t_1} \right)^2 \right] + \beta^3 \left( \frac{t_2}{t_1} \right)^2} - \beta \left( 1 + \frac{t_2}{t_1} \right) \right] + \frac{F_{ax,Rk}}{4} \quad (c) \\ 1,05 \cdot \frac{f_{h,1,k} t_1 d}{2 + \beta} \left[ \sqrt{2\beta(1 + \beta) + \frac{4\beta(2 + \beta)M_{y,Rk}}{f_{h,1,k} \cdot d \cdot t_1^2}} - \beta \right] + \frac{F_{ax,Rk}}{4} \quad (d) \\ 1,05 \cdot \frac{f_{h,1,k} t_2 d}{1 + 2\beta} \left[ \sqrt{2\beta^2(1 + \beta) + \frac{4\beta(1 + 2\beta)M_{y,Rk}}{f_{h,1,k} \cdot d \cdot t_2^2}} - \beta \right] + \frac{F_{ax,Rk}}{4} \quad (e) \\ 1,15 \sqrt{\frac{2\beta}{1 + \beta}} \cdot \sqrt{2M_{y,Rk} \cdot f_{h,1,k} \cdot d} + \frac{F_{ax,Rk}}{4} \quad (f) \end{array} \right.$$

Where  $F_{v,Rk}$  is the characteristic load-bearing capacity of a single fastener per shear plane, whilst  $M_{y,Rk}$  is the characteristic yielding moment of the fastener,  $d$  is the fastener diameter,  $f_{h,1,k}$  and  $f_{h,2,k}$  are the characteristic embedding strengths of the two connected timber elements,  $t_1$  and  $t_2$  are the penetration lengths of the screw in each element,  $\beta$  is the ratio between  $f_{h,2,k}$  and  $f_{h,1,k}$  and, finally,  $F_{ax,Rk}$  is the characteristic withdrawal strength. In this case,  $f_{h,1,k}$  and  $f_{h,2,k}$  have the same value, therefore, the factor  $\beta$  becomes equal to 1. Regarding the values of  $t_1$  and  $t_2$ , the screws have been inserted in such a

manner that the middle of their length is exactly within the shear plane and, therefore, this implies that  $t_1$  is equal to  $t_2$ .

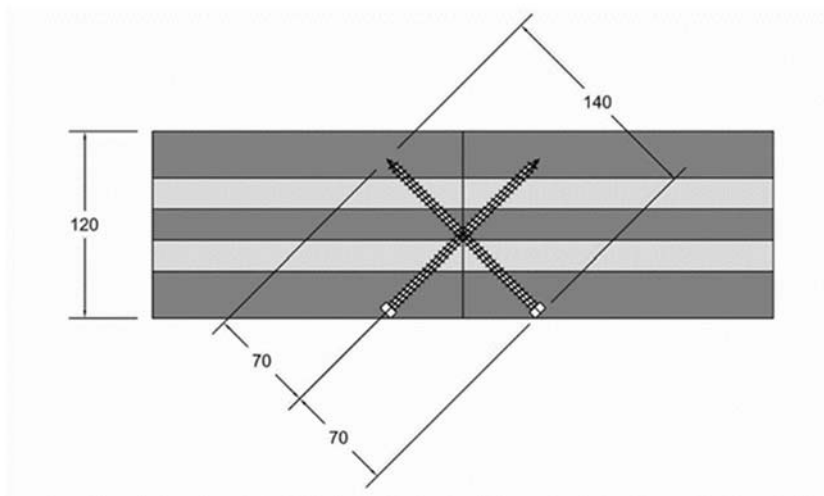


**Figure 53:  $t_1$  and  $t_2$  distances**

The letters next to each expression indicate the possible failure modes that can occur in the connection. Modes a), b), c) are characterized by the failure of the wooden element, while mode d) by the formation of one plastic hinge and modes e) and f) by the formation of two plastic hinges in the fastener.

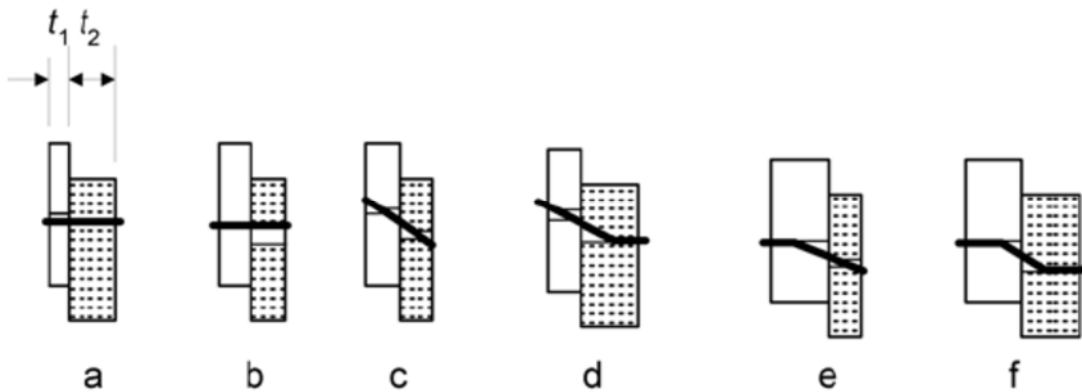


**Figure 54: Possible failure modes according to Johansen's theory.**

A final check should be made on the magnitude of the contribution  $F_{ax,Rk}/4$ . In fact, in the expressions the first term on the right hand side is the load-carrying capacity according to the Johansen yield theory, whilst the second term  $F_{ax,Rk}/4$  is the contribution from the rope effect. The contribution to the load-carrying capacity due to the rope effect should be limited to the 100% of the Johansen part, according to EC5

In the following tables, the data used in the formulas, and the calculated result for each failure mode, are reported for each kind of configuration:

<b>VGZ7-80</b>			<b>VGZ7-100</b>		
$f_{h,1,k} = f_{h,2,k} =$	15.13	N/mm <sup>2</sup>	$f_{h,1,k} = f_{h,2,k} =$	15.13	N/mm <sup>2</sup>
$f_{ax,k} =$	5067	N	$f_{ax,k} =$	5858	N
$M_{y,k} =$	14174	Nmm	$M_{y,k} =$	14174	Nmm
$\beta =$	1	-	$\beta =$	1	-
$t_1 = t_2 =$	50	mm	$t_1 = t_2 =$	70	mm
$R_{v,k}$ mode a)	5295.86	N	$R_{v,k}$ mode a)	7414.21	N
$R_{v,k}$ mode b)	5295.86	N	$R_{v,k}$ mode b)	7414.21	N
$R_{v,k}$ mode c)	3210.41	N	$R_{v,k}$ mode c)	4535.66	N
$R_{v,k}$ mode d)	3156.93	N	$R_{v,k}$ mode d)	4267.99	N
$R_{v,k}$ mode e)	3156.93	N	$R_{v,k}$ mode e)	4267.99	N
$R_{v,k}$ mode f)	3009.51	N	$R_{v,k}$ mode f)	3457.30	N

**Table 12: VGZ7-80 and VGZ7-100 failure modes.**

<b>VGZ7-120</b>			<b>VGZ9</b>		
$f_{h,1,k} = f_{h,2,k} =$	15.13	N/mm <sup>2</sup>	$f_{h,1,k} = f_{h,2,k} =$	14.03	N/mm <sup>2</sup>
$f_{ax,k} =$	5858	N	$f_{ax,k} =$	8229	N
$M_{y,k} =$	14174	Nmm	$M_{y,k} =$	27244	Nmm
$\beta =$	1	-	$\beta =$	1	-
$t_1 = t_2 =$	70	mm	$t_1 = t_2 =$	80	mm
$R_{v,k}$ mode a)	7414.21	N	$R_{v,k}$ mode a)	10103.17	N
$R_{v,k}$ mode b)	7414.21	N	$R_{v,k}$ mode b)	10103.17	N
$R_{v,k}$ mode c)	4535.66	N	$R_{v,k}$ mode c)	6242.11	N
$R_{v,k}$ mode d)	4267.99	N	$R_{v,k}$ mode d)	5942.31	N
$R_{v,k}$ mode e)	4267.99	N	$R_{v,k}$ mode e)	5942.31	N
$R_{v,k}$ mode f)	3457.30	N	$R_{v,k}$ mode f)	5073.94	N

**Table 13: VGZ7-120 and VGZ9 failure modes.**



	<b>W6</b>		<b>W8</b>	
$f_{h,1,k} = f_{h,2,k} =$	15.47	N/mm <sup>2</sup>	$f_{h,1,k} = f_{h,2,k} =$	14.43 N/mm <sup>2</sup>
$f_{ax,k} =$	5934	N	$f_{ax,k} =$	7146 N
$M_{y,k} =$	12700	Nmm	$M_{y,k} =$	19500 Nmm
$\beta =$	1	-	$\beta =$	1 -
$t_1 = t_2 =$	70	mm	$t_1 = t_2 =$	80 mm
$R_{v,k}$ mode a)	8045.02	N	$R_{v,k}$ mode a)	9465.81 N
$R_{v,k}$ mode b)	8045.02	N	$R_{v,k}$ mode b)	9465.81 N
$R_{v,k}$ mode c)	4918.06	N	$R_{v,k}$ mode c)	5830.46 N
$R_{v,k}$ mode d)	4565.75	N	$R_{v,k}$ mode d)	5473.80 N
$R_{v,k}$ mode e)	4565.75	N	$R_{v,k}$ mode e)	5473.80 N
$R_{v,k}$ mode f)	3423.65	N	$R_{v,k}$ mode f)	4379.98 N

**Table 14: W6 and W8 failure modes.**

For all the considered configurations, failure mode f) provides the smallest resistance and, thus, represents the failure mode which occurs in the connection. This failure mode is characterized by the formation of two plastic hinges in the fastener together with the embedding of the wood and is the failure mode that provides the most ductile and dissipative behaviour since it fully exploits the ductility of steel. When designing for earthquake impact one should in fact aim to get at least the formation of one plastic hinge in the fastener, as indicated in the new EC8 draft proposal.

### 3.4.5 Overall connection strength capacity

Once the resistance given for a single fastener has been calculated, it is possible to determine the overall strength capacity of the tested specimen.

As already mentioned, the configuration of the specimens relies on the contribution of 8 screws. For fasteners arranged in a row parallel to the grain inserted in the lateral surface of a CLT panel it is not required to reduce the contribution of each fastener, in function of their spacing, through the coefficient  $n_{ef} \leq n$ . In fact, thanks to the layered configuration of the cross-laminated panels that avoids brittle failures due to cracking, it is possible to adopt  $n_{ef} = n$  regardless of the spacing of the fasteners parallel to the grain, given that the minimum spacing is ensured.

The characteristic overall connection resistance for each of the tested configurations is presented in the following table:

<b>Name</b>	<b>Diameter [mm]</b>	<b>Number of fastener</b>	<b>Failure mode</b>	<b>Connection Strength [kN]</b>
V7-80	7	8	f	24.08
V7-100	7	8	f	27.66
V7-120	7	8	f	27.66
V9	9	8	f	40.59
W6	6.5	8	f	26.57
W8	8.2	8	f	34.05

**Table 15: Connections resistance final values.**

### 3.5 Loading protocol

The machine is controlled through the computer to which it is connected by a software called LabVIEW, which is an integrated development environment that uses a graphical programming syntax. The pre-installed loading protocols, however, have limited option and could not be set to perform cyclic loading procedures. To properly perform the tests a specific loading protocol should have been programmed with LabVIEW. Unfortunately the laboratory personnel was not able to provide this support, and due to the delay accumulated in the making of the samples, there was not enough time for us to learn a new programming language. As a consequence only monotonic test were performed

The testing has been done following the rules of EN 26891:1991<sup>45</sup>. The loading protocol consists in a preliminary cycle that aims for the settling of the specimen and a main part of the test that stops when the ultimate load is reached.

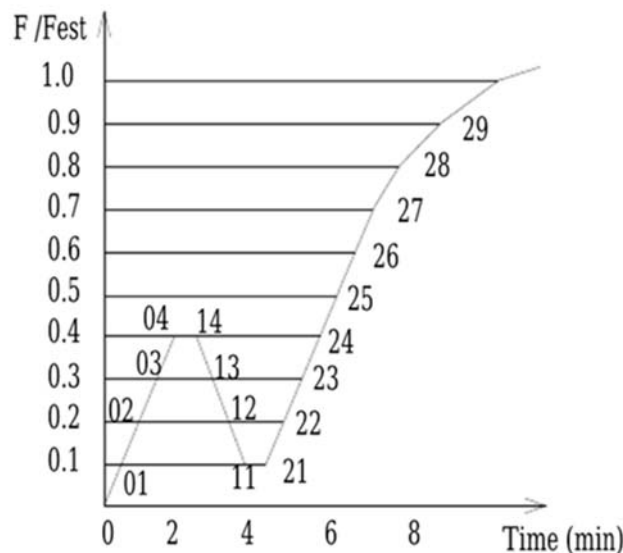
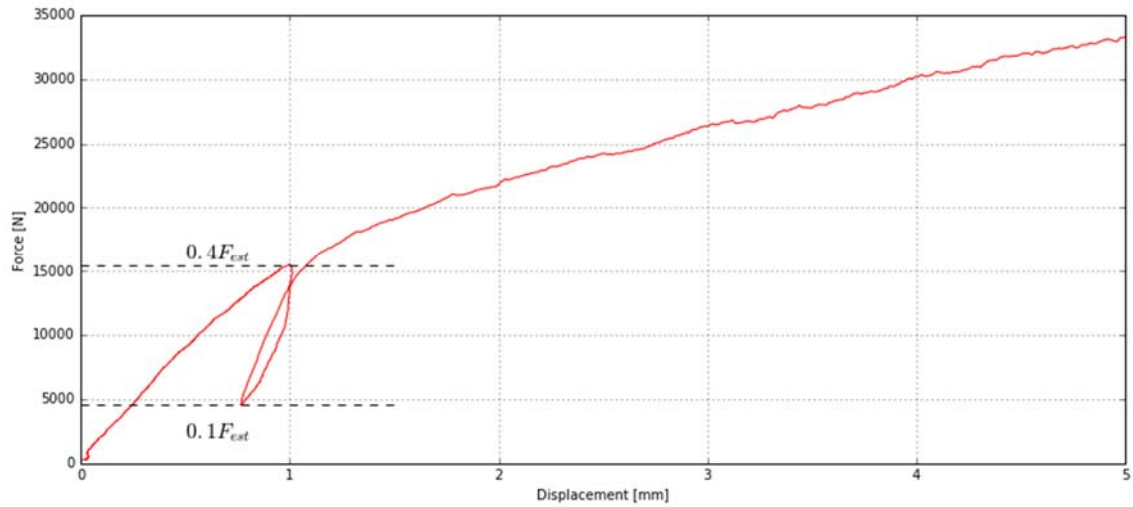


Figure 55: Loading protocol, image from EN26891

In the preliminary cycle the load is applied up to the 40% of  $F_{est}$  (calculated connection resistance) and maintained for 30 seconds, then the load is decreased to 10% of  $F_{est}$  and maintained for 30 seconds more. Under  $0.7 F_{est}$  the load is applied at constant displacement speed that results in an increase of  $0.2 F_{est} (\pm 25\%)$  per minute. Over  $0.7 F_{est}$  the load is applied at constant displacement speed so that the failure or a displacement of 15mm is reached within a total time of 15 minutes. The speed was hence decided so as to achieve the goal displacement of 15mm within the prescribed time. The specimens however showed a deformation capacity much higher than 15mm, and it was therefore

decided to continue the testing until a drop of 20% of  $F_{\max}$  was registered. Due to this some tests lasted up to 30 minutes.



**Figure 56: Detail of the initial part of the loading protocol.**

Because of the limited options available in the program the cycles could not be run in an automated way, but were set manually. The available loading protocol pre-installed in fact did not allow to set the needed options and register the data at once. The test was in fact divided into 3 sub-parts and the data for each sub-cycle was registered. Even though this is not the best way to perform the test, it was the only possible way to follow the prescribed rules from the standard.

Load measures were taken from the loading cell whereas displacement data were recorded by both the machine and the two sensors locally mounted on the specimen.

## 3.6 Test Results

### 3.6.1 Data processing

The outputs from test were exported and saved as txt files through the software that operates the hydraulic press. The sample data, however, is very much influenced by some sort of background noise. This variation in the sampled data with significant peaks, could in part depend on the friction present between the wooden elements, but probably it is due for the most part to some problems with the dampening of the load cell and the frequency of data acquisition. Unfortunately there was not enough time for an in-depth investigation on the nature of such noise, and the personnel of the laboratory was not able to get to the bottom of it. In order to partially solve the problem a moving average with period of 50, was used to smooth out short-term fluctuations and highlight longer-term trends.

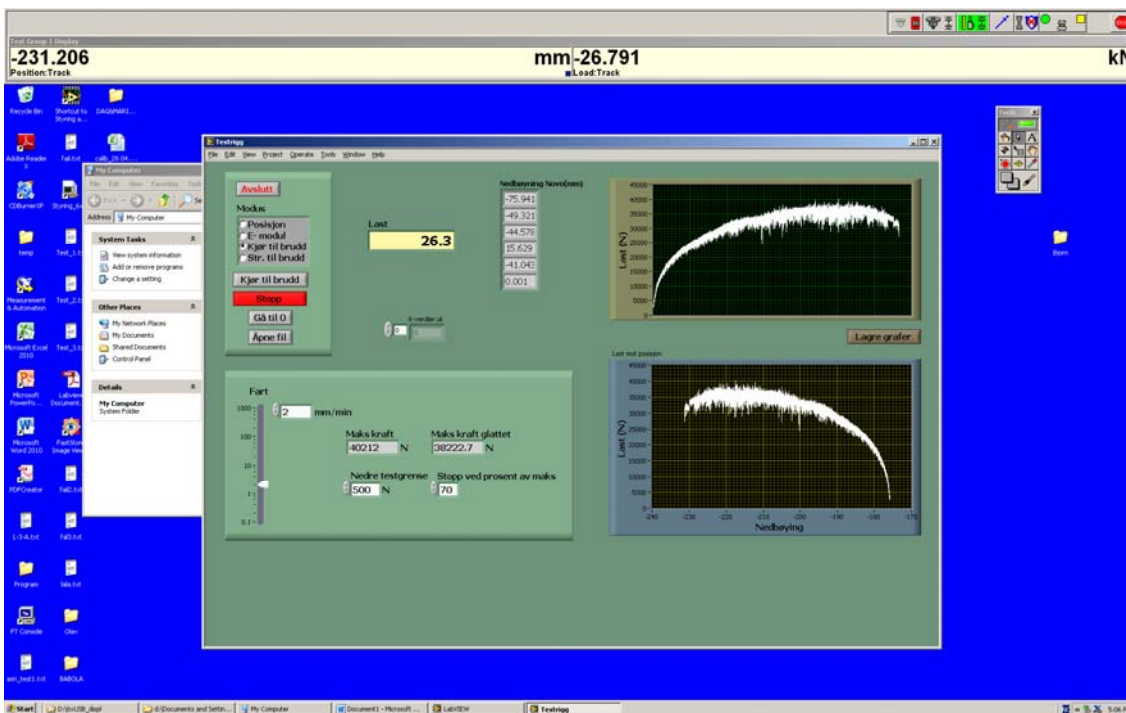


**Figure 57: Screenshot taken from the computer that controls the testing machine, with a detail of the scattering of the load-slip curve.**

The txt files, containing the values of the force and the corresponding measured displacement for each test, were imported and processed through Python. A script was made so as to evaluate all the relevant properties and plot the graphs in an automated way for each configuration.

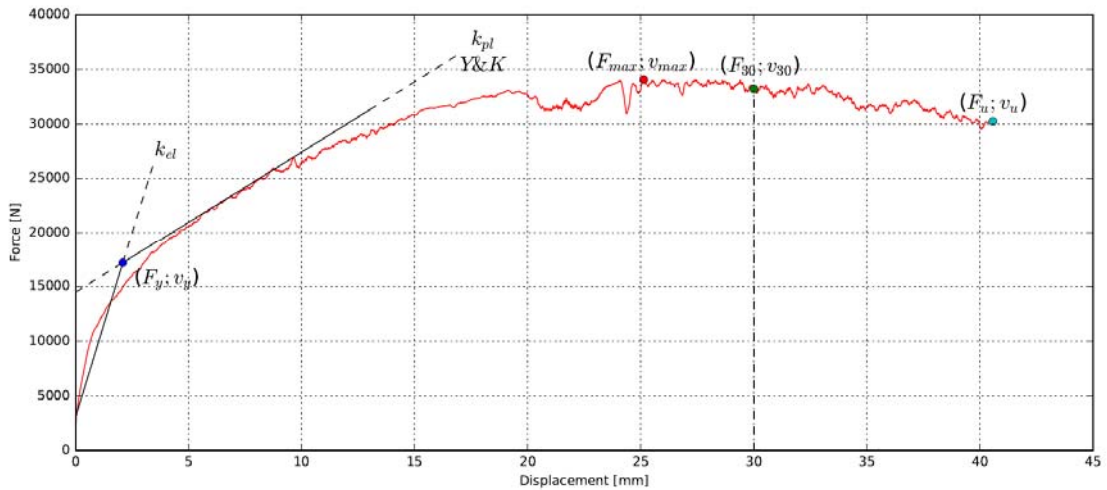


**Figure 58: A view on how the mechanical characteristics was calculated.**

From each set of data, the following mechanical properties were extrapolated:  $k_{el}$  denote the initial stiffness and was derived according EN12512<sup>9</sup>;  $k_{pl}$  represent the plastic stiffness and was derived according the so-called Yasumura & Kaway method<sup>46</sup>. The reason why the Y&K method was preferred to the one given in EN 12512, is that the former fitted the force-displacement curve in a much better way than the latter. Furthermore it is well known and used in the academic field;  $F_y$  indicate the yield force and was found as the intersection point of the initial stiffness and the plastic stiffness;  $v_y$ , indicate instead the yield displacement and was obviously found in the same way as the yield force;  $F_{max}$ , denote the maximum load, while  $v_{max}$ , the corresponding displacement;  $F_u$  and  $v_u$  represent the ultimate load and displacement, and were found according EN 12512 as the load corresponding to failure or 80% of the maximum load, and the relative displacement;  $F_{30}$  is the load corresponding to a displacement of 30mm; finally  $D$  indicate the ductility ratio,  $v_u/v_y$ .

Once that the necessary data from each sample was extrapolated, mean values, 5<sup>th</sup> percentile, 95<sup>th</sup> percentile and standard deviations were derived using EN14358<sup>31</sup> as reference. The expressions used to calculate these values are reported in the following figures taken from the standard. Five specimens were tested for each configuration and, consequently, a  $k_s(n)$  of 2.64 was assumed as prescribed by the standard.

logarithmically normally distributed	normally distributed
$\bar{y} = \frac{1}{n} \sum_{i=1}^n \ln m_i$ (1)	$\bar{y} = \frac{1}{n} \sum_{i=1}^n m_i$ (2)
$s_y = \max \left\{ \sqrt{\frac{1}{n-1} \sum_{i=1}^n (\ln m_i - \bar{y})^2}, 0,05 \right\}$ (3)	$s_y = \max \left\{ \sqrt{\frac{1}{n-1} \sum_{i=1}^n (m_i - \bar{y})^2}, 0,05\bar{y} \right\}$ (4)

percentile	logarithmically normally distributed	normally distributed
5-percentile	$m_k = \exp(\bar{y} - k_s(n)s_y)$ (5)	$m_k = \bar{y} - k_s(n)s_y$ (6)
95-percentile	$m_k = \exp(\bar{y} + k_s(n)s_y)$ (7)	$m_k = \bar{y} + k_s(n)s_y$ (8)

**Figure 59: Image taken from EN14358 that shows how the values were calculated**

Thereafter the values of the overstrength factor was derived according to the procedure proposed in (Jorissen A. & Fragiaco M., 2011)<sup>12</sup>, previously presented in §2.3 that consists in the expression:

$$\gamma_{Rd} = \frac{R_{d,0.95}}{R_{d,0.05}} \cdot \frac{R_{d,0.05}}{R_{d,k}} = \gamma_{sc} \cdot \gamma_{an}$$

### 3.6.2 Results

#### 3.6.2.1 V7-80

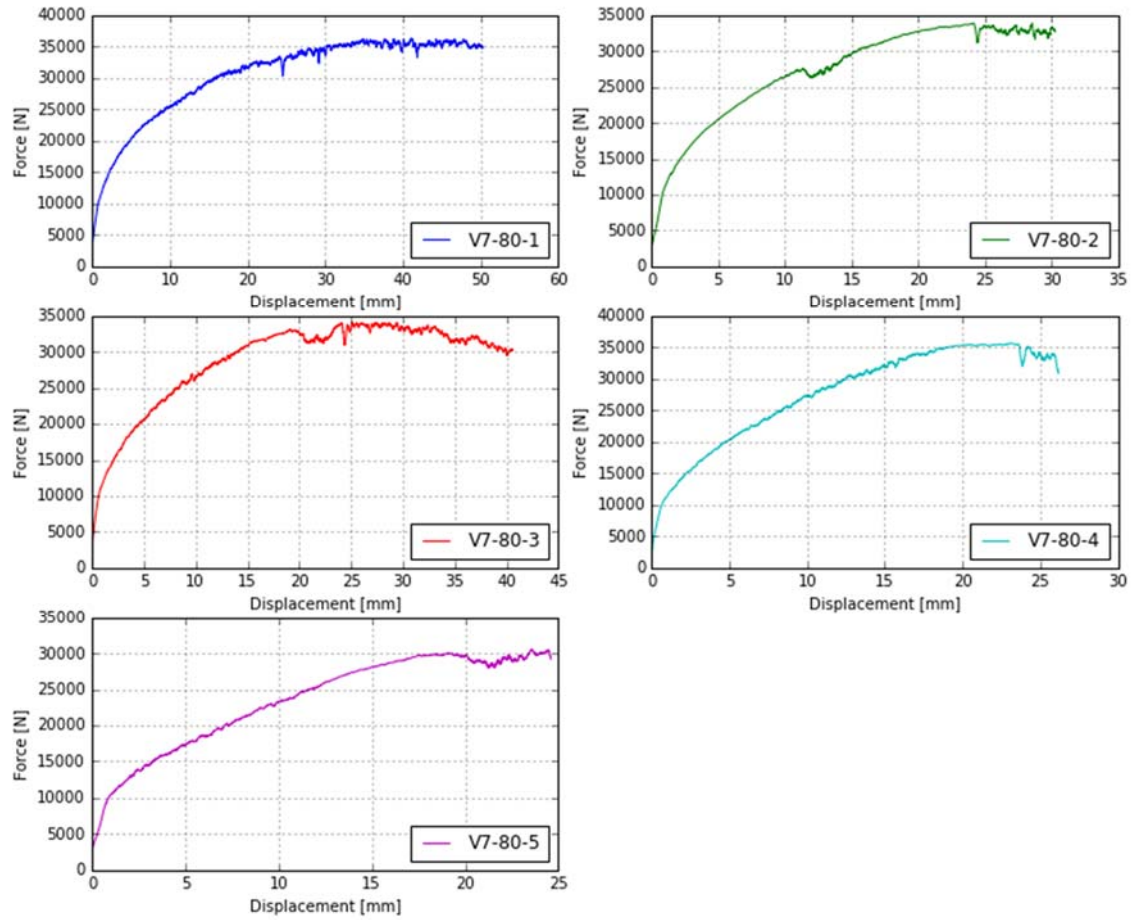


Figure 60: Load-slip curve for each configuration.

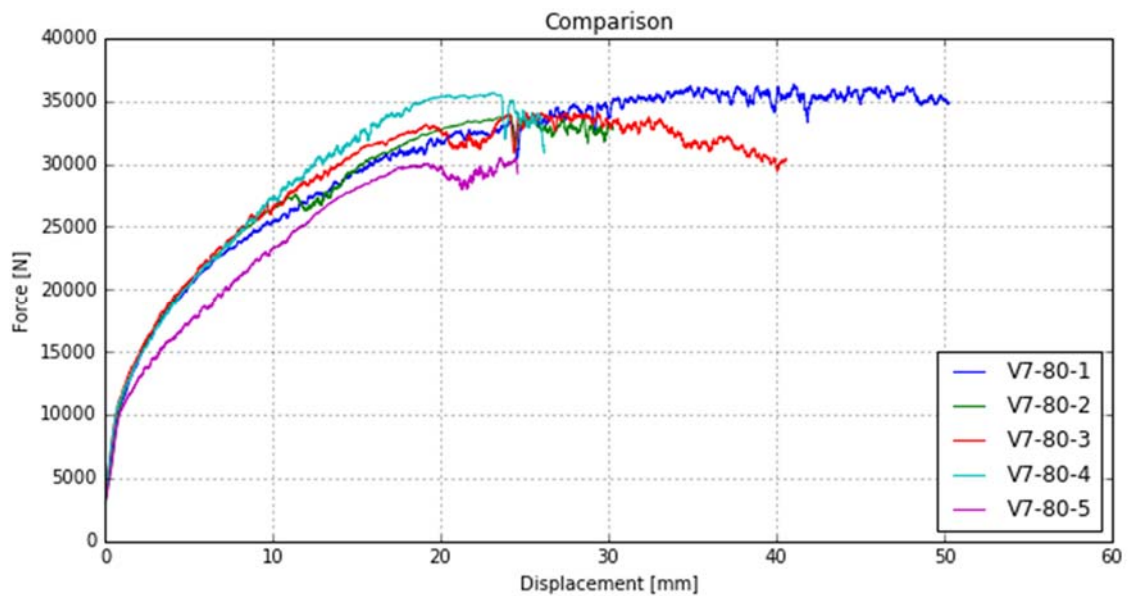


Figure 61: Overlapped load-slip curves.



<b>V7-80</b>						
	<b>1</b>	<b>2</b>	<b>3</b>	<b>4</b>	<b>5</b>	<b>mean</b>
$k_{el}$ [kN/mm]	7.48	9.04	8.53	6.40	7.91	7.87
$k_{pl}$ [kN/mm]	0.69	1.18	1.36	1.30	1.26	1.16
$F_y$ [kN]	21.66	17.94	17.21	17.94	13.73	17.70
$v_v$ [mm]	2.42	1.65	1.63	2.26	1.37	1.87
$F_{max}$ [kN]	36.29	33.89	34.08	36.64	30.50	34.28
$v_{max}$ [mm]	39.61	27.75	23.76	22.66	23.38	27.43
$F_u$ [kN]	34.90	32.80	30.25	30.88	29.22	31.61
$v_u$ [mm]	48.82	29.48	38.87	25.51	23.49	33.23
$F_{30}$ [kN]	35.13	-	33.20	-	-	34.16
D	20.20	17.91	23.79	11.30	17.17	18.07

**Table 16: V7-80 mechanical properties.**

3.6.2.2 V7-100

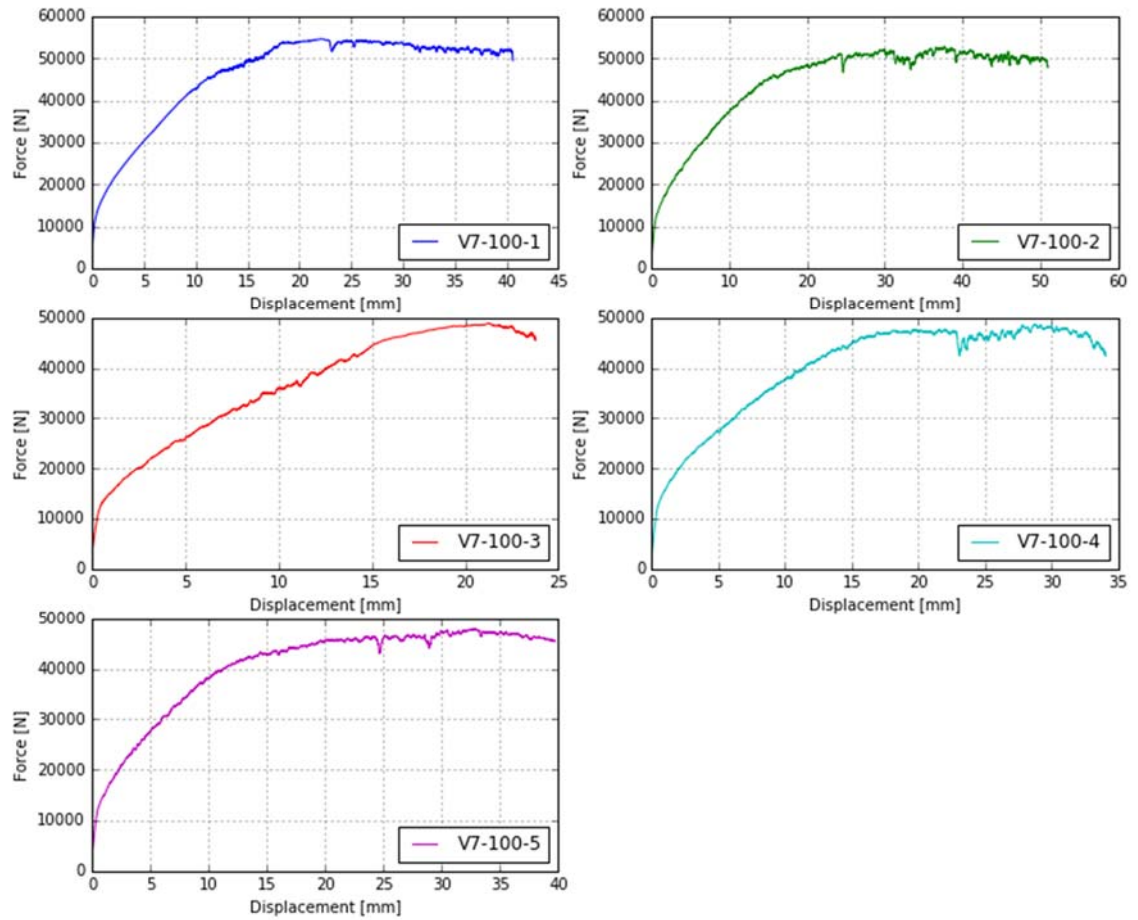


Figure 62: Load-slip curve for each configuration.

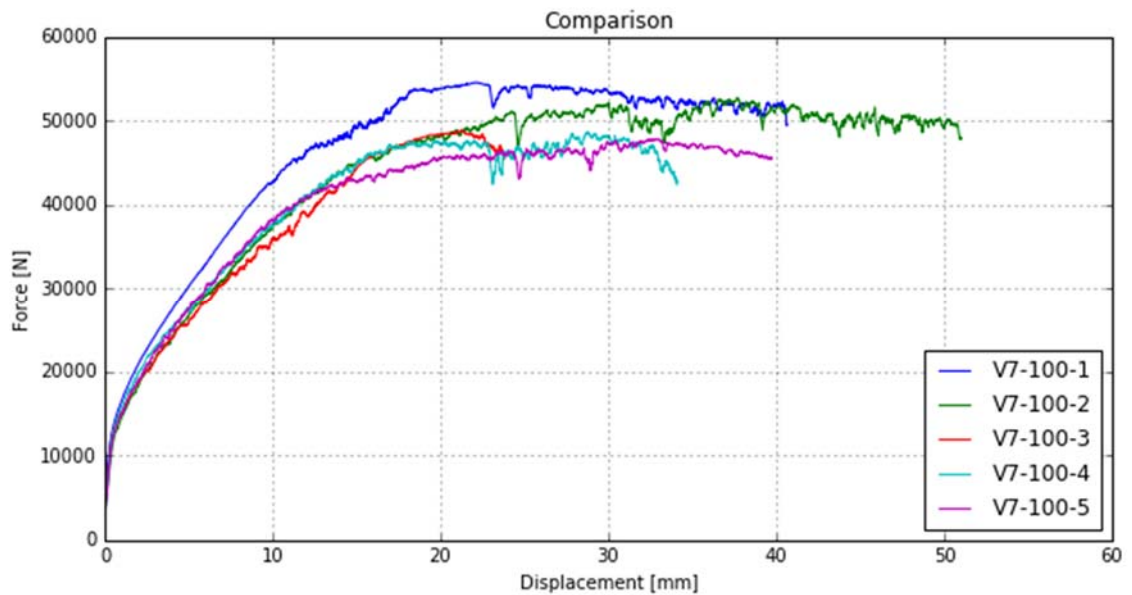


Figure 63: Overlapped load-slip curves.

<b>V7-100</b>						
	<b>1</b>	<b>2</b>	<b>3</b>	<b>4</b>	<b>5</b>	<b>mean</b>
$k_{el}$ [kN/mm]	9.59	7.16	7.71	9.24	9.48	8.64
$k_{pl}$ [kN/mm]	2.11	1.77	2.00	1.97	1.95	1.96
$F_y$ [kN]	29.23	27.55	21.93	23.55	24.58	25.37
$v_v$ [mm]	2.49	3.13	2.22	2.06	2.09	2.40
$F_{max}$ [kN]	54.57	52.73	48.95	48.69	47.86	50.56
$v_{max}$ [mm]	21.09	35.67	20.41	27.81	31.50	27.30
$F_u$ [kN]	49.44	47.89	45.57	42.39	45.43	46.14
$v_u$ [mm]	39.18	49.23	22.88	33.21	38.21	36.54
$F_{30}$ [kN]	52.80	49.08	-	47.81	47.38	49.27
D	15.76	15.72	10.32	16.13	18.26	15.24

**Table 17: V7-100 mechanical properties.**

3.6.2.3 V7-120

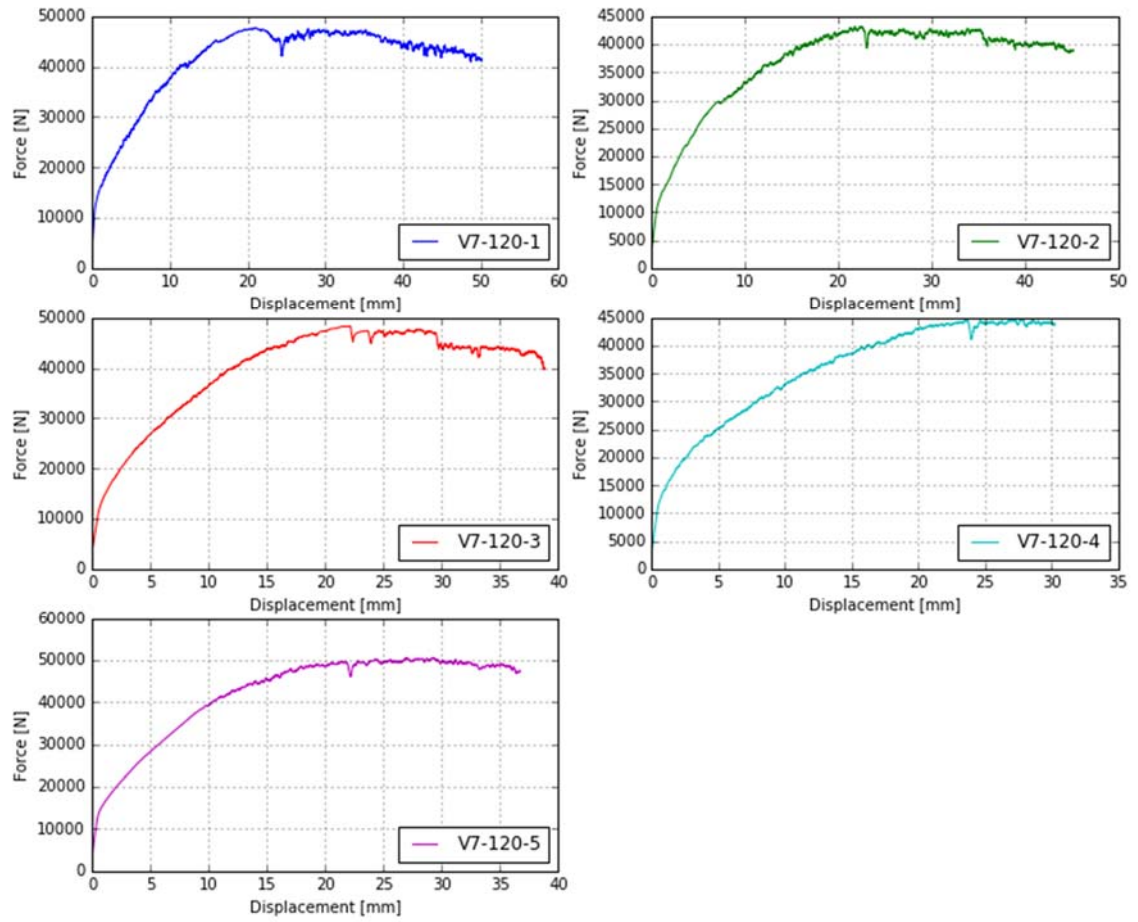


Figure 64: Load-slip curve for each configuration.

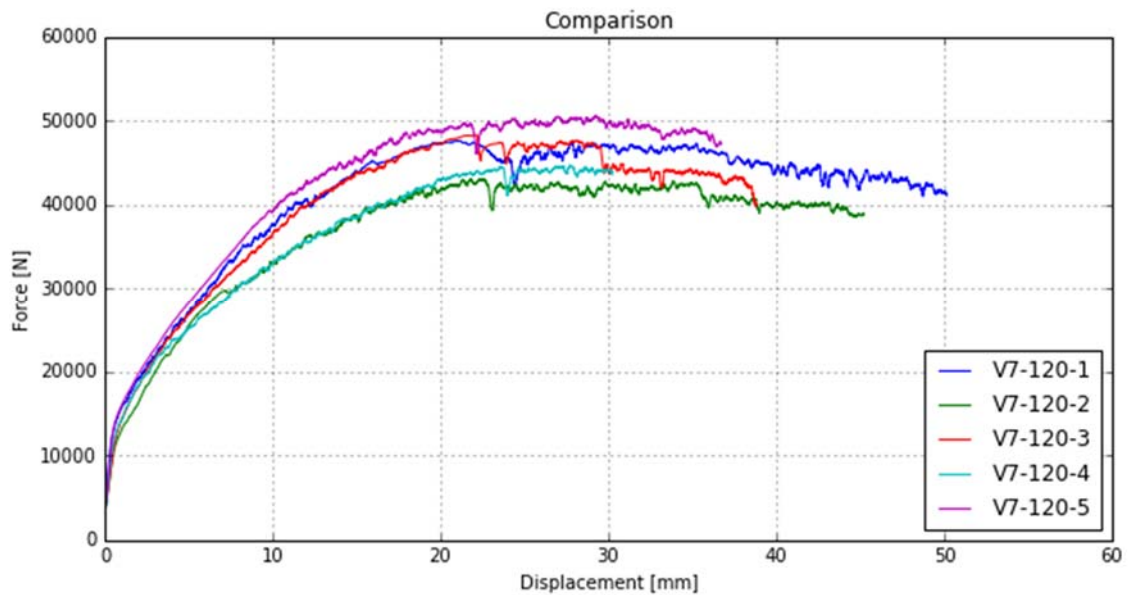


Figure 65: Overlapped load-slip curves.

<b>V7-120</b>						
	<b>1</b>	<b>2</b>	<b>3</b>	<b>4</b>	<b>5</b>	<b>mean</b>
$k_{el}$ [kN/mm]	9.56	12.74	12.65	10.69	9.32	10.99
$k_{pl}$ [kN/mm]	2.03	1.69	2.05	1.55	2.08	1.88
$F_y$ [kN]	24.14	22.40	22.94	22.68	25.68	23.57
$v_v$ [mm]	2.04	1.42	1.43	1.72	2.25	1.77
$F_{max}$ [kN]	47.67	43.10	48.32	44.70	50.61	46.88
$v_{max}$ [mm]	19.83	20.22	20.07	26.16	27.64	22.78
$F_u$ [kN]	41.09	38.80	39.89	43.59	47.20	42.11
$v_u$ [mm]	48.74	43.11	36.26	28.71	35.02	38.37
$F_{30}$ [kN]	47.16	41.92	44.01	-	49.53	45.65
D	23.85	30.31	25.29	16.66	15.56	22.33

**Table 18: V7-120 mechanical properties.**

3.6.2.4 V9

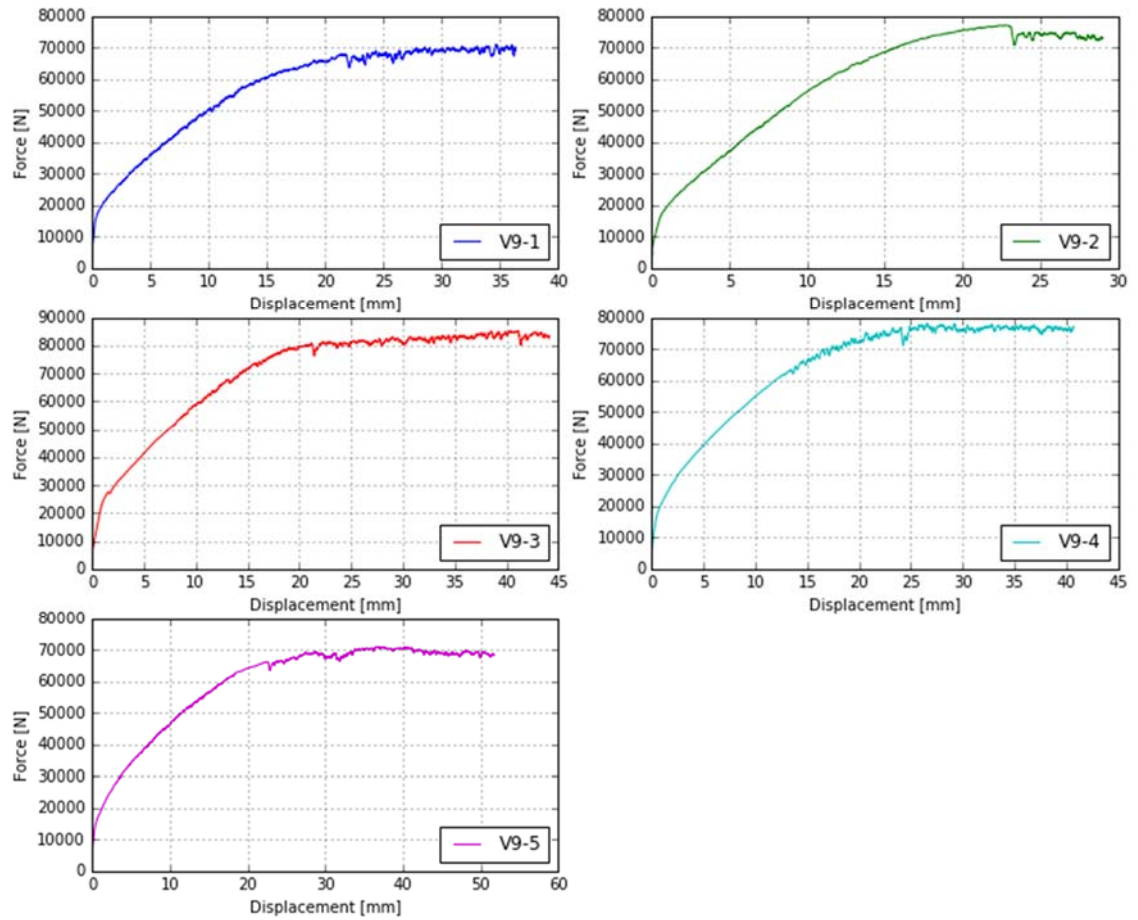


Figure 66: Load-slip curve for each configuration.

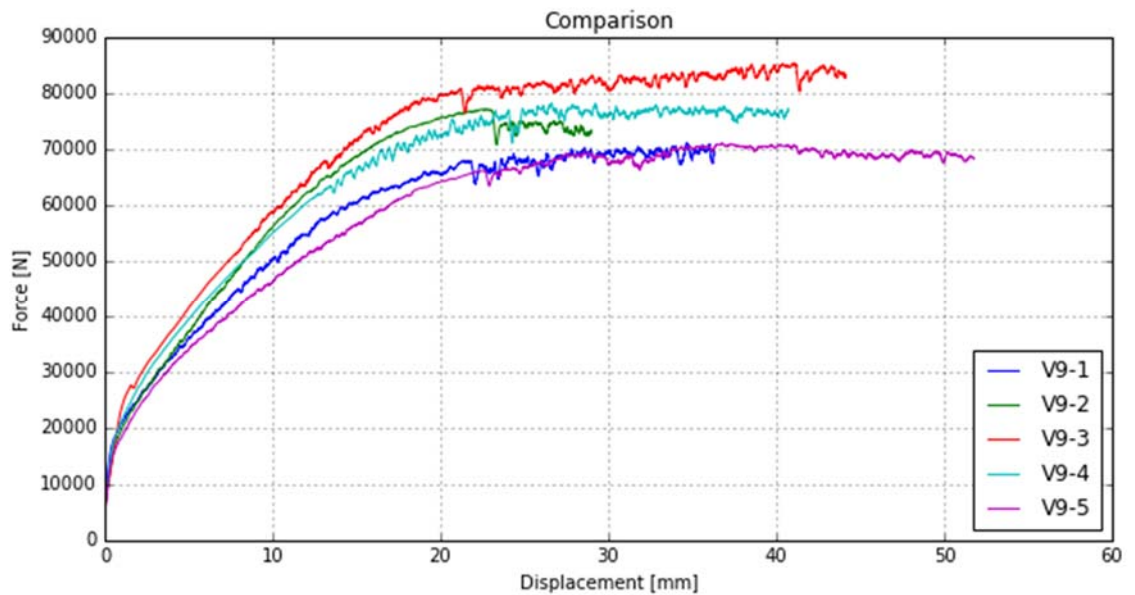


Figure 67: Overlapped load-slip curves.

V9						
	1	2	3	4	5	mean
$k_{el}$ [kN/mm]	8.32	8.28	9.96	10.91	8.39	9.17
$k_{pl}$ [kN/mm]	2.39	3.37	3.05	2.73	1.85	2.68
$F_y$ [kN]	35.10	37.02	41.14	38.85	37.77	37.98
$v_v$ [mm]	3.39	3.57	3.33	2.87	3.67	3.37
$F_{max}$ [kN]	71.07	77.11	85.31	78.15	70.94	76.51
$v_{max}$ [mm]	33.63	21.29	39.66	25.01	35.49	31.02
$F_u$ [kN]	68.93	72.83	82.92	76.89	68.33	73.98
$v_u$ [mm]	35.24	27.34	42.72	39.05	50.55	38.98
$F_{30}$ [kN]	69.74	-	81.82	76.00	68.71	74.06
D	10.39	7.66	12.85	13.59	13.78	11.65

**Table 19: V9 mechanical properties.**

3.6.2.5 W6

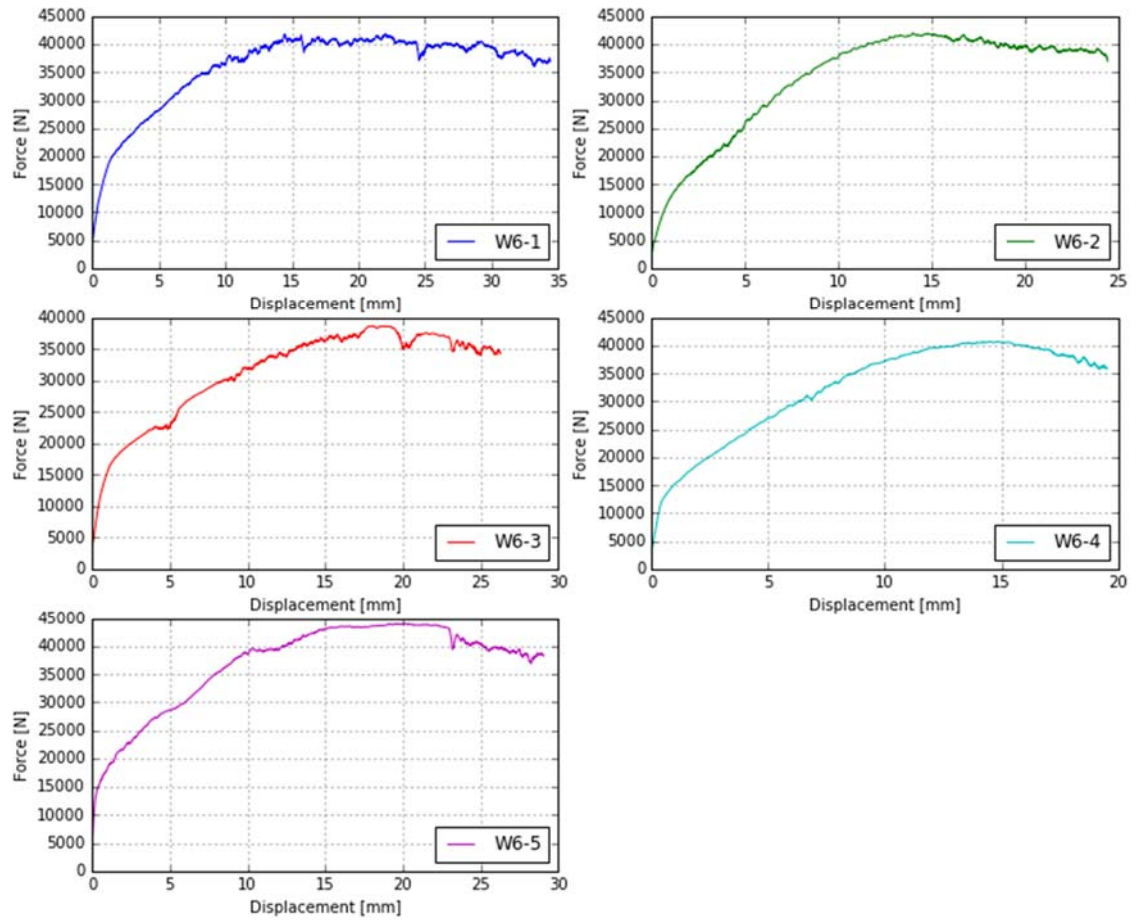


Figure 68: Load-slip curve for each configuration.

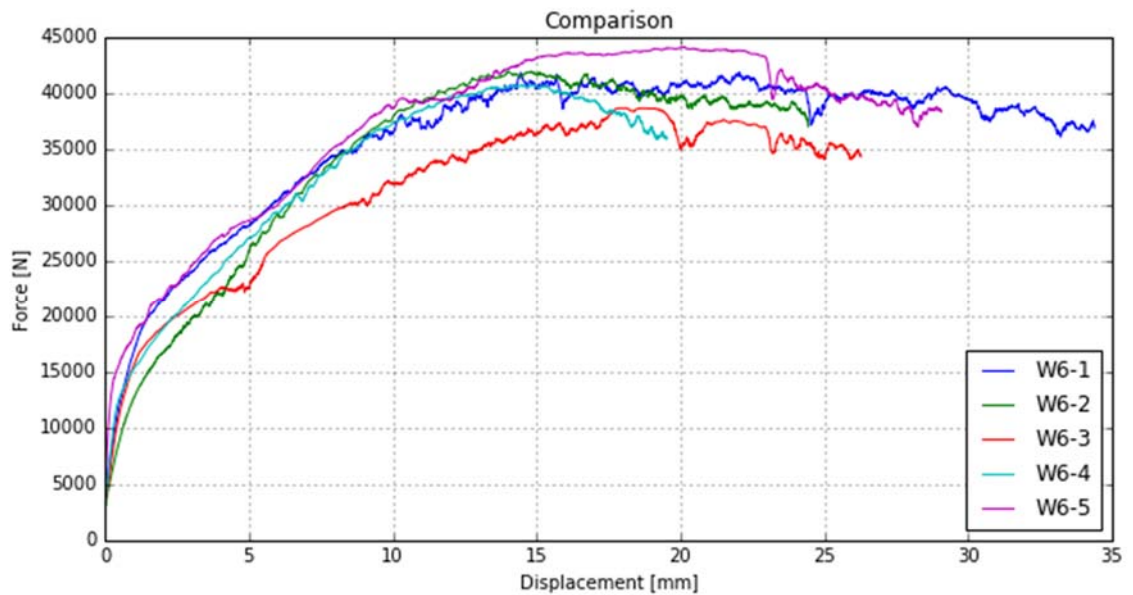


Figure 69: Overlapped load-slip curves.



<b>W6</b>						
	<b>1</b>	<b>2</b>	<b>3</b>	<b>4</b>	<b>5</b>	<b>mean</b>
$k_{el}$ [kN/mm]	12.86	6.40	12.17	9.60	14.68	11.14
$k_{pl}$ [kN/mm]	1.97	2.64	1.62	2.50	1.97	2.14
$F_y$ [kN]	21.74	20.48	19.09	18.31	21.28	20.18
$v_v$ [mm]	1.39	2.64	1.29	1.52	1.16	1.60
$F_{max}$ [kN]	41.83	41.95	38.65	40.73	44.12	41.45
$v_{max}$ [mm]	22.05	13.98	18.10	14.46	20.11	17.74
$F_u$ [kN]	36.89	36.98	34.30	35.81	38.29	36.45
$v_u$ [mm]	34.38	24.44	26.27	19.51	29.05	26.73
$F_{30}$ [kN]	39.48	-	-	-	-	39.48
D	24.74	9.26	20.38	12.82	25.12	18.46

**Table 20: W6 mechanical properties.**

3.6.2.6 W8

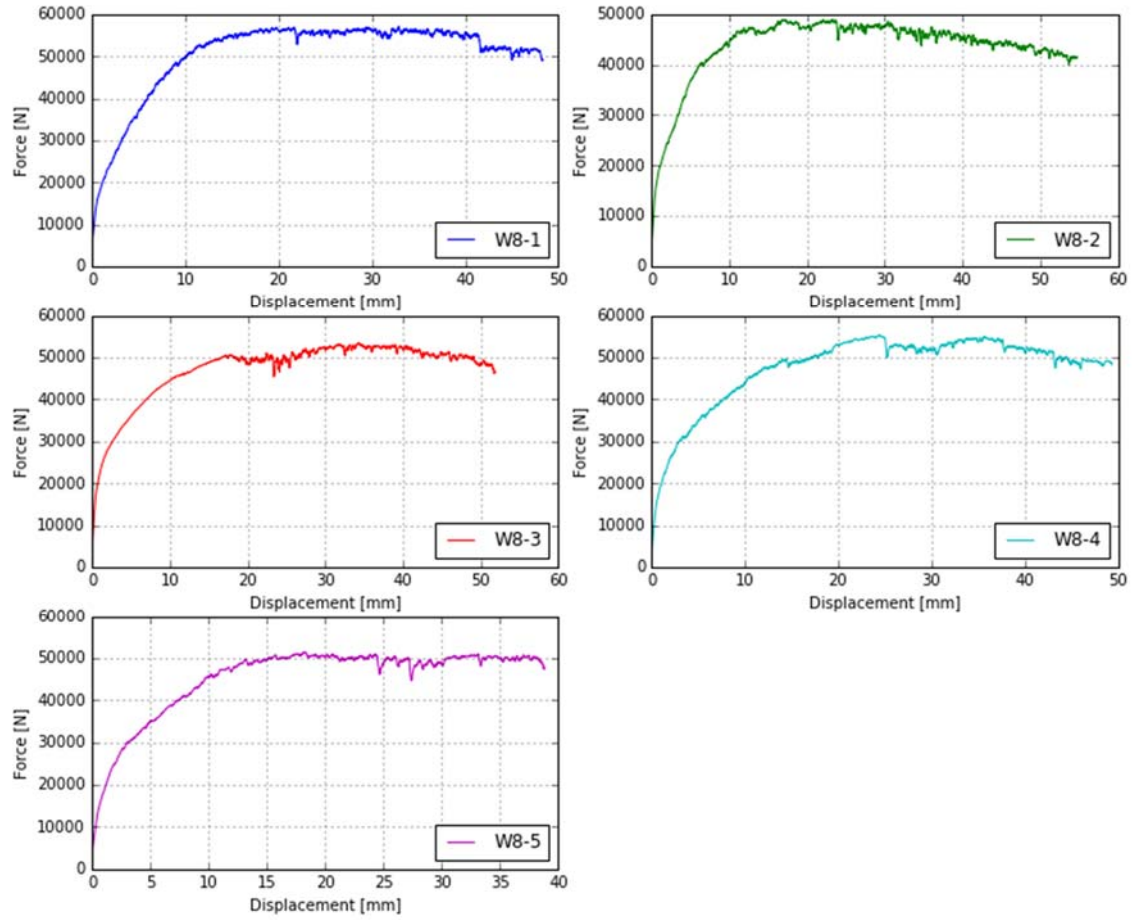


Figure 70: Load-slip curve for each configuration.

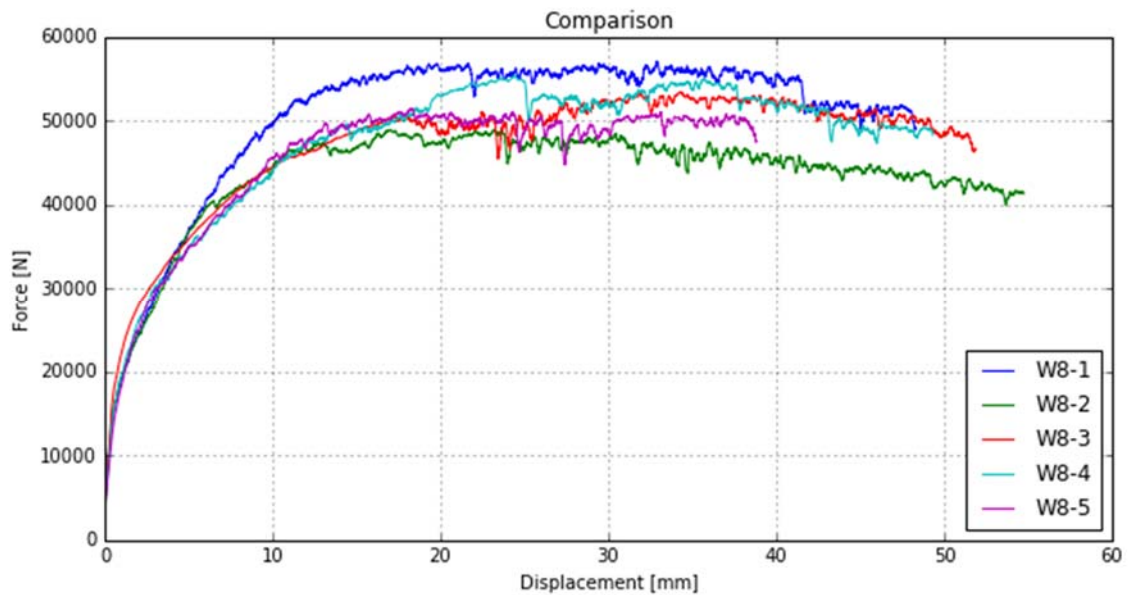


Figure 71: Overlapped load-slip curves.

<b>W8</b>						
	<b>1</b>	<b>2</b>	<b>3</b>	<b>4</b>	<b>5</b>	<b>mean</b>
$k_{el}$ [kN/mm]	10.94	15.11	19.36	13.32	13.13	14.37
$k_{pl}$ [kN/mm]	3.05	2.81	2.02	1.77	2.69	2.47
$F_y$ [kN]	28.46	26.04	28.55	29.32	26.59	27.79
$v_v$ [mm]	2.12	1.44	1.26	1.88	1.71	1.68
$F_{max}$ [kN]	57.03	48.96	53.43	55.37	51.50	53.26
$v_{max}$ [mm]	32.86	23.21	34.24	24.39	18.20	26.58
$F_u$ [kN]	48.96	41.31	46.59	48.31	47.53	46.54
$v_u$ [mm]	48.29	54.72	51.84	49.31	38.80	48.59
$F_{30}$ [kN]	56.21	47.83	51.84	52.03	48.56	51.29
D	22.80	38.03	41.09	26.27	22.69	30.18

**Table 21: W8 mechanical properties.**

3.6.2.7 Overstrength values

	<b>V7-80</b>	<b>V7-100</b>	<b>V7-120</b>	<b>V9</b>	<b>W6</b>	<b>W8</b>	<b>mean</b>
<b>Normal distribution</b>							
F <sub>05</sub> [kN]	28.47	42.87	39.54	61.18	36.36	45.44	-
F <sub>95</sub> [kN]	39.62	56.59	54.22	89.03	46.55	60.11	-
F <sub>v,k</sub> [kN]	24.08	27.66	27.66	40.59	26.57	34.05	-
γ <sub>sc</sub>	1.39	1.32	1.37	1.46	1.28	1.32	1.36
γ <sub>an</sub>	1.18	1.55	1.43	1.51	1.37	1.33	1.40
γ <sub>Rd</sub>	1.65	2.05	1.96	2.19	1.75	1.77	1.89
<b>Lognormal distribution</b>							
F <sub>05</sub> [kN]	28.75	43.45	39.99	62.18	36.62	45.85	-
F <sub>95</sub> [kN]	40.17	56.79	54.78	90.30	46.84	60.58	-
F <sub>v,k</sub> [kN]	24.08	27.66	27.66	40.59	26.57	34.05	-
γ <sub>sc</sub>	1.40	1.31	1.37	1.45	1.28	1.32	1.35
γ <sub>an</sub>	1.19	1.57	1.45	1.53	1.38	1.35	1.41
γ <sub>Rd</sub>	1.67	2.05	1.98	2.22	1.76	1.78	1.91

**Table 22: Overstrength factors results.**

### 3.6.3 Discussion of the results

A visual inspection of the tested specimen has at once allowed to make some preliminary considerations on the results. First, no brittle failures occurred during the testing, moreover every sample reached large deformations before failure, showing therefore a distinctly ductile behaviour. The removal of part of the wood has allowed a closer inspection, that confirmed the formation of plastic hinges in the fasteners. In both the inspected samples the screws had formed two clearly visible plastic hinges, that confirmed the failure mode predicted by Johansen’s theory. All the tested samples reached, in fact, an ultimate displacement greater than 19 mm, with an average value of 37 mm.



**Figure 72: Yielded screws after testing.**

Even though some mechanical properties, such as stiffness, ultimate load and ductility ratio, should be evaluated from cyclic tests, the outcomes extrapolated from the monotonic ones, give anyway a first indication of such properties. For example, all configurations show pretty high values for the ductility ratio, ranging from the minimum mean value of 11.65 obtained from the V9 configuration, to the maximum mean value of 30.18 obtained from the W8 configuration. This fact confirms the reason why the vertical connection between wall element for CLT buildings is recognized as the most ductile one,

and is indicated as the connection devoted to dissipative behaviour for building designed in high ductility class in the draft proposal for the new section 8 of Eurocode 8.

The goal of the research was, however, to assess the value of the overstrength factor for a typical vertical connection between CLT panels, and to compare the results with the outcomes from previous investigation on similar kind of connections. Several researches have been carried out on lap joint and spline joint connections between CLT elements, but none regarding the OSF was found on the configuration tested within this programme, even though it is easily implementable.

From the presented results is clear that the difference between the adoption of a normal or a log-normal distribution does not have a great influence on the final results. A comparison between the two shows that the difference is never greater than 1.5%. Since the reference standard<sup>31</sup> explicitly states that strength parameters should be assumed as logarithmically normally distributed, unless analysis of the data shows that a normal distribution is more appropriate, the log-normal distribution was chosen.

The term  $\gamma_{sc}$ , defined as the ratio between  $F_{95}$  and  $F_{05}$ , which accounts for the scatter of the connection strength properties, have values ranging between 1.28 and 1.45, with a mean value of 1.35. The results are in accordance with those found by previous studies on similar kinds of configurations<sup>32 33</sup>. The mean value for the OSF found in (Gavric et al, 2012)<sup>33</sup> is in fact 1.356, practically the same value found within this investigation. The OSF found by 1.2 was instead 1.63, so a little higher. For instance, in (Gavric et al, 2013)<sup>39</sup> the authors, propose a more conservative value of 1.6 for screwed connections between panels, with respect to the value of 1.3 proposed for angular brackets and hold-down loaded in shear and tension.

The term  $\gamma_{an}$ , defined instead as the ratio between  $F_{05}$  and  $F_{v,k}$ , which accounts for the accuracy of the analytical formulas used to predict the connection resistance, have values ranging between 1.18 and 1.57, with a mean value of 1.4. These high values confirm that the design model provide conservative predictions of the resistance. Even though there is common agreement that this contribution should be taken into account in the calculation of the final value of the OSF, most of the researches do not report these values, and calculate  $\gamma_{Rd}$  with the only contribution of  $\gamma_{sc}$ . The researches who report these values are: (Jorissen A. & Fragiacommo M., 2011)<sup>12</sup> that derive a mean  $\gamma_{an}$  of 1.18; (Schick et al, 2013)<sup>35</sup> that derive instead an average  $\gamma_{an}$  of 1.43, and (Gavric et al, 2015)<sup>34</sup> that derive a mean  $\gamma_{an}$  of 1.8. (Gavric et al, 2015)<sup>34</sup> seem to point out though that the predictions tend

to be more conservative for brittle types of failures, as a  $\gamma_{an}$  of 1.35 was found when a ductile failure mode was achieved. It should anyway be pointed out anyway that the kind of connection tested in all of the above-mentioned works are very different from those tested here, and furthermore in 1.6 a slightly different approach is used, as previously explained in §2.3.

The total values for the overstrength factors, given by the product of the two contributions, range from a minimum of 1.65 to a maximum of 2.22 with an average value of 1.9.

## 4 CONCLUSIONS

The preparation of the work on this thesis can be divided into two main phases. The first phase consisted in a survey of the existing literature. To begin with, an extended investigation of the research treating the evaluation of the from experimental investigation was carried out. From here the research continued in the study of how the current regulatory framework treats the subject, and then a comparison was made with how the evaluation of the OSF is carried out for other structural materials. The second phase consisted in the planning, execution and data analysis of the experimental testing programme. At first the size of the specimens was decided, then the design of the connections and of the equipment was carried out. The wooden panels were first gathered from different places, then cut into the final size, and finally the specimens were assembled. Once the tests were performed, the data was analysed, and thereafter the conclusions that were drawn have been reported with some suggestions for future works.

The draft of the new version of chapter 8 of EC8 proposes a value of 1.3 for the OSF  $\gamma_{Rd}$  for CLT structures. The outcomes of this research seem to confirm this value; however a clarification should be made, this value seems reasonable only under two circumstances:

- When the resistance of the dissipative connection is evaluated through experimental tests, and not through the Johansen's equations.
- If both the dissipative and the non-dissipative element that appear in the equation are connections.

In both these cases it seems reasonable to neglect the fact that the European yielding model gives conservative values for the evaluation of the connection resistance. In the



first case it is obvious, since the resistance is evaluated directly from tests. In the second case, if both the elements are connection, it seems reasonable to assume that both will be overdesigned by approximately the same quantities. For the latter sentence to be true, however, some other circumstance should be checked. In fact, since the resistance of a connection system is given by the minimum of the resistance values that represent all the potential failure modes that could happen in the connection, it should be checked that the models used to predict the occurrence of brittle failure modes, such as the resistance of net steel part of the connector or pull-through/withdrawal resistance of the fastener, are as conservative (or more conservative) than the models used to assess the resistance of the dissipative connection system, i.e. ductile failure modes expressions in Johansen's equations.

If the last sentence is not true, then the only way to have the mathematical certainty that the equation  $R_{b,Rd} \geq \gamma_{Rd} \cdot R_{d,Rd}$  will be satisfied, is to adopt an overstrength factor that includes the contribution of the accuracy of the analytical formulas used to predict the connection resistance (the term  $\gamma_{an}$ ) and thus adopting higher values for  $\gamma_{Rd}$ . The results from this experimental programme indicate that the value for the OSF that consider such contribution should be taken as 1.9.

Unfortunately, as already mentioned, we were not able to perform cyclic tests, but since the problems met will be addressed in the near future by the university, and since the necessary equipment has already been built, future upcoming thesis works could use the job done here as reference and perform the cyclic tests. In addition, future works could investigate the approach to the matter with the adoption of the Monte Carlo method. This could in fact be a possible alternative approach that could be used to confirm the adoption of lower values for the overstrength factor, as already done for other structural materials. The use of structural reliability analysis with limit state functions through the Monte Carlo method is in fact widely used for other structural materials, such as steel and concrete.

# 5 REFERENCES

1. Franch, M. G. (2007). *The Sofie Project*.
2. Ceccotti, A., Follesa, M., Lauriola, M. & Sandhaas, C. (2006). *Sofie project–test results on the lateral resistance of cross-laminated wooden panels*. Proceedings of the First European Conference on Earthquake Engineering and Seismicity.
3. Ceccotti, A. (2008). New technologies for construction of medium-rise buildings in seismic regions: the XLAM case. *Structural Engineering International*, 18 (2): 156-165.
4. Dujic, B., Strus, K., Zarnic, R. & Ceccotti, A. (2010). *Prediction of dynamic response of a 7-storey massive XLam wooden building tested on a shaking table*. Proceedings of the world conference on timber engineering WCTE, Riva del Garda, Italy.
5. Paulay, T. & Priestley, M. J. N. (1992). *Seismic design of reinforced concrete and masonry buildings*. New York: Wiley.
6. *EN 1998-1: Eurocode 8: Design of structures for earthquake resistance – Part 1: General rules, seismic actions and rules for buildings*. (2004). CEN.
7. Bisch, P., Carvalho, E., Degee, H., Fajfar, P., Fardis, M., Franchin, P., Kreslin, M., Pecker, A., Pinto, P. & Plumier, A. (2012). Eurocode 8: seismic design of buildings worked examples. *Luxembourg: Publications Office of the European Union*.
8. Gioncu, V. (2000). Framed structures. Ductility and seismic response: General Report. *Journal of Constructional Steel Research*, 55 (1): 125-154.
9. *EN 12512:2001. Timber structures – Test methods – Cyclic testing of joints made with mechanical fasteners*. (2004). CEN.
10. Stehn, L. & Björnfort, A. (2002). *Comparison of different ductility measures for a nailed steel-to-timber connection*. World conference on timber engineering: 12/08/2002-15/08/2002: Penerbitan Publications. Paper 4.4. 2: 155-162 pp.
11. Malo, K., Siem, J. & Ellingsbø, P. (2011). Quantifying ductility in timber structures. *Engineering Structures*, 33 (11): 2998-3006.
12. Jorissen, A. & Fragiacomio, M. (2011). General notes on ductility in timber structures. *Engineering Structures*, 33 (11): 2987-2997.
13. Muñoz, W., Mohammad, M., Salenikovich, A. & Quenneville, P. (2008). Determination of yield point and ductility of timber assemblies: in search for a harmonised approach. *Engineered Wood Products Association*.
14. Pozza, L. (2013). *Ductility and behaviour factor of wood structural systems*: PhD thesis, University of Padova (I).
15. Ceccotti, A., Massari, M. & Pozza, L. (2016). Procedures for seismic characterization of traditional and modern wooden building types. *International Journal for Quality Research*, 10 (1).

16. *EN 1995-1-1: Eurocode 5: Design of timber structures - Part 1-1: General - Common rules and rules for buildings.* (2004). CEN.
17. Follesa, M., Fragiaco, M. & Lauriola, M. P. (2011). *A proposal for revision of the current timber part (Section 8) of Eurocode 8 Part 1.* 44th CIB-W18 Meeting, Alghero.
18. *SIA 265:2012: Holzbau.* (2012). Schweizerischer Ingenieur- und Architektenverein.
19. NZS 3604:2011 - Timber-framed buildings. (2011).
20. *NZS 3603:1993.TIMBER STRUCTURES STANDARD.* (1996). Standards New Zealand.
21. Carradine, D. (2014). Guiding multi-storey timber buildings. *Build.*
22. *CSA 086-14. Engineering design in wood.* (2016). Canadian Standard Association.
23. *EC8- New Chapter 8 (2017-02-01) - draft proposal.* (2017).
24. Mitchell, D. & Paultre, P. (1994). Ductility and overstrength in seismic design of reinforced concrete structures. *Canadian Journal of Civil Engineering*, 21 (6): 1049-1060.
25. Humar, J. & Rahgozar, M. (1996). Concept of overstrength in seismic design. *Proceedings of the 11th WCEE. IAEE, Acapulco, Mexico, Paper (639).*
26. Mazzolani, F., Landolfo, R. & Della Corte, G. (2009). Eurocode 8 provisions for steel and steel-concrete Composite structures: comments, critiques, improvement proposals and research needs. *Atti del convegno finale del progetto ReLUIS-DPC05-08.*
27. Elghazouli, A. (2008). Seismic design of steel-framed structures to Eurocode 8. *Moment*, 1 (2.0): 1.5-2.0.
28. Galasso, C., Maddaloni, G. & Cosenza, E. (2014). Uncertainly analysis of flexural overstrength for capacity design of RC beams. *Journal of Structural Engineering*, 140 (7): 04014037.
29. Somja, H., Nofal, S., Hjiij, M. & Degee, H. (2013). Effect of the steel material variability on the seismic capacity design of steel-concrete composite structures: a parametric study. *Bulletin of Earthquake Engineering*, 11 (4): 1099-1127.
30. Sam R. Leslie, G. A. M., Mark P. Staiger. (2009). *Overstrength Factors for Seismic Design of Steel Structures.*
31. *EN 14358:2016. Timber structures - Calculation of characteristic 5-percentile values and acceptance criteria for a sample.* (2016). CEN.
32. Fragiaco, M., Dujic, B. & Sustersic, I. (2011). Elastic and ductile design of multi-storey crosslam massive wooden buildings under seismic actions. *Engineering Structures*, 33 (11): 3043-3053.
33. Gavric, I., Fragiaco, M. & Ceccotti, A. (2012). Strength and deformation characteristics of typical X-lam connections. *Proceedings of WCTE.*
34. Gavric, I., Fragiaco, M. & Ceccotti, A. (2015). Cyclic behaviour of typical metal connectors for cross-laminated (CLT) structures. *Materials and Structures*, 48 (6): 1841-1857.

35. Schick, M., Vogt, T. & Seim, W. (2013). *Connections and anchoring for wall and slab elements in seismic design*. Meeting.
36. Vogt, T., Hummel, J., Schick, M. & Seim, W. (2014). Experimentelle Untersuchungen für innovative erdbebensichere Konstruktionen im Holzbau. *Bautechnik*, 91 (1): 1-14.
37. Brühl, F., Schänzlin, J. & Kuhlmann, U. (2014). Ductility in Timber Structures: Investigations on Over-Strength Factors. In *Materials and Joints in Timber Structures*, pp. 181-190: Springer.
38. Köhler, J. (2007). *Reliability of timber structures*: vdf Hochschulverlag AG.
39. Gavric, I., Fragiaco, M. & Ceccotti, A. (2013). *Capacity seismic design of X-LAM wall systems based on connection mechanical properties*. Meeting forty-six of the Working Commission W18-Timber Structures, CIB, International Council for Research and Innovation: Timber Scientific Publishing-KIT Holzbau und Baukonstruktionen. 285-298 pp.
40. *EN 16351: Timber structures - Cross laminated timber*. (2015). CEN.
41. *EN 338: Structural timber. Strength classes*. (2016). CEN.
42. Johansen, K. (1949). *Theory of timber connections*. International Association of Bridge and Structural Engineering. 249-262 pp.
43. Blaß, H. J. & Uibel, T. (2007). Tragfähigkeit von stiftförmigen Verbindungsmitteln in Brettsperholz.
44. Blaß, H. J., Bejtka, I. & Uibel, T. (2006). Tragfähigkeit von Verbindungen mit selbstbohrenden Holzschrauben mit Vollgewinde.
45. *EN 26891: Timber structures; Joints made with mechanical fasteners; General principles for the determination of strength and deformation characteristics*. (1991). CEN.
46. Yasumura, M. & Kawai, N. (1998). *Estimating seismic performance of wood-framed structures*. Proceedings of.



Norges miljø- og biovitenskapelig universitet  
Noregs miljø- og biovitenskapelige universitet  
Norwegian University of Life Sciences

Postboks 5003  
NO-1432 Ås  
Norway